Dissertation

submitted to the

Combined Faculties of the Natural Sciences and Mathematics

of the Ruperto-Carola-University of Heidelberg, Germany

for the degree of

Doctor of Natural Sciences

Put forward by

Dipl.-Phys. Karsten Joho

born in: Eberbach

Oral examination: February 08, 2013

Transient noise spectra in mesoscopic systems

Referees: Prof. Andreas Komnik
Prof. Andreas Mielke

Transiente Rauschspektren in mesoskopischen Systemen: Im Zentrum der vorliegenden Arbeit steht das zeitabhängige elektronische Quantenrauschen in Nanostrukturen. Die beiden hierbei betrachteten, grundlegenden Modelle der mesoskopischen Physik sind exakt lösbar und stellen gleichzeitig effektive Beschreibungen experimentell realisierbarer Systeme dar. Diese bestehen aus einem Quantenpunkt, der über den quantenmechanischen Tunneleffekt an zwei Elektroden gekoppelt ist. Im einen Fall wird die Elektron-Elektron Wechselwirkung vollständig vernachlässigt, während sie im anderen auf spezielle Weise Berücksichtigung findet. Anhand dieser Modelle wird unter Verwendung des Schwinger-Keldysh Formalismus exemplarisch aufgezeigt, wie das Stromrauschen nach abrupter Änderung eines Systemparameters seinem stationären Zustand zustrebt und in welcher Hinsicht sich dieses Verhalten qualitativ von der zeitlichen Entwicklung des Stromes unterscheidet. Überdies werden erste Schritte zur Behandlung eines verwandten Problems – das des zeitabhängigen Wärmerauschens – vorgestellt.

Transient noise spectra in mesoscopic systems: The focus of this thesis is on the time-dependent electronic quantum noise in nanostructures. Both basic models of mesoscopic physics considered in this context are exactly solvable and constitute effective descriptions of experimentally realizable systems. They consist of a quantum dot that is coupled via quantum tunneling to two electrodes. In one case, the electron-electron interaction is completely neglected, whereas in the other, it is taken into account in a specific manner. On the basis of these models, it is shown by means of the Schwinger-Keldysh formalism how the current noise approaches its steady state after an abrupt change of a system parameter and in what respect this behavior differs qualitatively from the time evolution of the current itself. Moreover, the first steps toward the treatment of a related problem – the time-dependent heat noise – are presented.

Contents

Chapter 1

Introduction

Condensed matter physics has always been a thriving research field whose objective is the characterization of states of matter consisting of many particles whose mutual interactions are responsible for their strong cohesion. In this sense, it encompasses systems ranging from liquids via soft matter such as polymers and liquid crystals to crystalline and amorphous solids, trying to explain their material properties of electric, magnetic, mechanical and thermal nature, to name only a few.

In the past decades, the focus of a considerable part of this branch of the scientific community moved toward nanometer-sized electronic devices driven by the enormous technical progress in fabricating such tiny structures. The tremendous growth of this emergent field – for which the term 'mesoscopic physics' has been coined – even allowed to enter a regime where the peculiar effects of the quantum realm come into play. There are plenty of systems in which these may become manifest including semiconductor heterostructures, carbon nanotubes and other molecular conductors. The observation of single electron tunneling signatures followed by the implementation of single electron transistors and Cooper pair boxes figure among the most spectacular advances in this area. Another important milestone was the detection of the mesoscopic Kondo effect in non-equilibrium, a generic many body effect which has a direct counterpart in bulk solids. Up to date, these accomplishments have attracted an increased interest of many researchers to explore quantum transport characteristics extensively – partly in pursuit of getting control about such systems to achieve the ultimate goal of a quantum computer.

Apart from the current flowing in an electric circuit, the most prominent accompanying feature is noise resulting from random fluctuations of manifold origins. If the system is coupled to a reservoir at finite temperature, there is always a contribution from thermal fluctuations, called Johnson-Nyquist noise after its discoverers. Other significant types of noise comprise shot noise, which is associated with the granularity of charge carriers and flicker noise, which originates from the presence of a large range of relaxation times e.g. due to impurities in a sample. Although undesirable in most applications, noise can reveal valuable information about the current carrying excitations. For instance, the fractional charge of quasiparticles in the fractional quantum Hall regime or the charge of Cooper pairs in superconductors can be recovered in the Fano factor, which is the ratio of the shot noise to electric current. In case of the aforementioned examples, this quantity has been determined in seminal experimental works performed by de Picciotto et al. [1997] and Saminadayar et al. [1997] as well as Jehl et al. [2000], respectively.

Nowadays, in addition to the measurement of current-voltage characteristics and noise in nanoscale devices, even higher cumulants in a non-equilibrium steady state situation can be accessed as well (Basset et al. [2012], Ubbelohde et al. [2012]). The corresponding theoretical tool to gain the information about all current cumulants is referred to as full counting statistics (FCS) and was developed and successfully tested on many free as well as interacting systems during the last 20 years (Levitov et al. [1996], Levitov and Lesovik [1993], Nazarov [1999]). However, in preparative non-equilibrium, where certain parameters are changed rapidly, only the current has been extensively addressed so far both experimentally and theoretically (Gustavsson et al. [2006], Schmidt et al. [2008]). A notable exception has been work on transient current fluctuations at equal times (Feng et al. [2008]). At the moment, much effort is invested by several research groups to access the FCS in these situations, but has not been successful even for the simplest models available.

Instead of following this route, we tackle the theoretically challenging task of analytically determining the transient finite-frequency current noise spectrum as a reaction to the instantaneous switching-on of the tunneling coupling for two exactly solvable models fundamental to mesoscopic physics: the resonant level model (RLM), which is equivalent to the non-interacting Anderson impurity model (AIM) (Anderson [1961]), and the Majorana resonant level model (MRLM), which corresponds to a special parameter constellation of the interacting resonant level model (IRLM) and can be mapped onto the Kondo model at the Toulouse point (Emery and Kivelson [1992]). Both are considered in a two-terminal setup describing a quantum dot that consists of one single electronic level coupled to two electronic reservoirs at different chemical potentials. Experimentally, the noise spectrum can directly be registered and is related to measurable quantities like the conductivity. A connection between these quantities is provided by the fluctuation-dissipation theorem whose formal derivation basically relies on the restrictive condition of linear response though. As the generalization of the fluctuation-dissipation theorem to arbitrary non-equilibrium settings has not been established so far, it is thus interesting to investigate this regime, which makes our approach also valuable from this perspective.

The appropriate theoretical framework to deal with this issue is provided by quantum field theory as its formalism of second quantization is especially apt when one has to describe a non-relativistic system composed of many degrees of freedom. Since the presented work is concerned with electrons propagating through a nanostructure – a generic non-equilibrium situation, the analytical method of choice is the Schwinger-Keldysh formalism. We would like to point out that, besides their relevance to practical setups, our calculations may serve as a benchmark for various numerical simulational methods such as the density-matrix renormalization group (DMRG), the functional renormalization group (FRG), the scattering-states numerical renormalization group, or the Monte Carlo technique, which have already been applied to some models closely related to those to be treated below (Branschädel et al. [2010], Carr et al. [2011], Andergassen et al. [2011], Schmitt and Anders [2010], Schmidt et al. [2008]).

The thesis is structured as follows. In Chapter 2, after the introduction of the central models along with a short review of the basic non-equilibrium Schwinger-Keldysh formalism, we provide the corresponding Green's functions that are useful when computing the temporal evolution of transport quantities. Chapter 3 constitutes the main part and is devoted to our results, namely the analysis of transient current noise in the respective models. In particular, we provide a comprehensive analysis of the zero-temperature case to extract the effects due to shot noise

only. In addition, the influence of thermal fluctuations is addressed for the RLM. Besides the current noise, we also present first steps toward the solution of a related problem – the transient heat noise spectrum. We close this thesis by a summary of our findings.

Chapter 2

Non-equilibrium quantum dynamics of characteristic models for mesoscopic systems

This chapter presents the basic theoretical tools taken to investigate transient quantum noise accompanying electronic transport in nanostructures, which is a generic non-equilibrium problem. After an outline of the general significance of quantum dots in the vast field of mesoscopic physics we describe the practical relevance of our chosen models to common experimental setups and specify the respective Hamilton and current operators. To deal with such non-equilibrium settings, we aim at applying a formalism according to Schwinger and Keldysh which is outlined subsequently following standard textbook references such as Rammer [2007] and Mahan [1990]. Furthermore, we provide all relevant Green's functions which, for our purposes, prove to be beneficial to extract quantum transport quantities in the transient regime. As a convention, we henceforth set the units $\hbar = k_B = e = 1$ unless otherwise stated.

2.1 Quantum dots as a paradigm for basic nanoelectronic devices

Quantum dots are separated regions in metallic nanostructures in which the motion of electrons is highly confined, typically to geometrical dimensions on the order of tens of nanometers in all three spatial directions. Today, these effectively zero-dimensional objects can routinely be manufactured in many laboratories worldwide. There are various strategies for their fabrication including the selective deformation of carbon nanotubes or the control of the motion of charge carriers in two-dimensional electron gases by gate electrodes in semiconductor heterostructures. On account of the confinement-induced discrete electronic level structure of a quantum dot, the term 'artificial atom' is often synonymously used in the literature. These dot-lead structures are often operated in a quantum coherent regime meaning that the phase coherence length is much greater than their typical diameter. Quantum dots have therefore become an ideal testing ground for the realization of quantum mechanical models. There are indeed many ideas to harness their potential for applications. In particular, they are promising candidates for the implementation of quantum bits, which form the basis of a quantum computer, a device which can solve certain problems more efficiently than its classical counterpart. On a level below this ultimate goal, quantum dot arrays may also serve as a quantum simulator which allows

for a treatment of problems in many areas of physics which are hard to attack analytically or numerically.

In this work, we primarily focus on the quantum transport properties of quantum dots in situations where the quantum mechanical effects are dominant. Their knowledge is of paramount importance for electric circuitry on microprocessors which will inevitably enter the quantum coherent regime in the course of the advancing miniaturization of these devices during the next decades. Consequently, it is appropriate to study models which are elementary and relevant to nanoelectronics, thus remaining analytically solvable and, at the same time, describing the essential physics in realistic experimental setups.

Our models of interest to be treated below are the resonant level model (RLM) and the Majorana resonant level model (MRLM) both of which assume two separate electronic reservoirs at chemical potentials μ_L and μ_R as well as temperatures Θ_L and Θ_R that can exchange particles through quantum tunneling events via a quantum dot. Furthermore, we require that this dot can host only one electron. In the former model, the lead electrons are treated as non-interacting fermions (Fermi liquids), whereas in the latter, depending on the system realization, they are one-dimensional (1D) interacting fermions (Luttinger liquids) and, in addition, perceive a Coulomb repulsion with an electron on the dot if one starts with a resonant level in a Luttinger liquid (Komnik and Gogolin [2003a]), and non-interacting Fermi liquids in the case of the Toulouse point of the Kondo model (Schiller and Hershfield [1998]).

A typical realization of the RLM is a quantum dot on the basis of semiconductor materials in the regime in which electronic correlations on the dot are negligible. Alternatively, one can think of quantum dots in the deep Kondo limit, the transport properties of which are dominated by the resonant level physics (Goldhaber-Gordon et al. [1998], Cronenwett et al. [1998], Glazman [2000]). An example of the former case is a semiconductor heterostructure in which a quasi-two-dimensional electron gas is located at the interface between two types of semiconductors like GaAs and AlGaAs, which have similar lattice constants but different energy gaps. Appropriate top gates guarantee the separation of an island, forming the quantum dot, from two outer regions that host two-dimensional macroscopic electron gases satisfying the condition of a Fermi liquid. Another strategy starts with a nanowire grown on top of a semiconducting material by molecular beam epitaxy, which is then contacted by metallic leads usually resulting in the formation of tunneling barriers between the individual components. Besides the source-drain voltage that drives the current, additional gate electrodes can be used to tune the dot level energy and the tunneling coupling. In such setups, the criterion of single occupancy is justified if the quantum dot is sufficiently small to achieve an appreciable size quantization and if the spin degeneracy of the energy levels is lifted, for instance by applying a strong external magnetic field so that transport can occur effectively only through one level. The last condition can equivalently be fulfilled by a large on-dot repulsion between electrons. A schematic of such a structure is depicted in Fig. 2.1 while the involved energy scales are illustrated in Fig. 2.2.

In contrast, the MRLM can be relevant in dot-lead structures, in which the conduction electrons are strongly correlated and form Luttinger liquids, a specialty in one spatial dimension (Bockrath et al. [1999], Egger and Gogolin [1997]). From an experimental point of view, there are several realizations of systems, in which the motion of the delocalized conduction electrons is effectively confined to one dimension. One has to be aware of the fact that a necessary con-

dition to observe metallic behavior is the suppressed tendency to the appearance of a Peierls instability. This means that an upper bound on the transition temperature to an insulating regime should be at sufficiently small temperature. To enumerate only a few examples of real systems where these criteria can be fulfilled, we cite semiconductor heterostructures, where the motion of electrons is confined to 1D by an appropriate gating, Bechgaard salts, single-wall carbon nanotubes (SWNTs), certain elongated organic compounds and the edge states of two-dimensional systems in the fractional quantum Hall regime. As an example, we want to concentrate on single-wall carbon nanotubes which are wrapped graphene sheets. These are composed of carbon atoms that are arranged in a honeycomb lattice, which can be illustrated as two intertwined Bravais sublattices, or equivalently as a Bravais lattice with a diatomic basis. There are several possibilities of cutting and wrapping the graphene sheets. Among them are two achiral ways, namely the wrapping around an armchair edge and around a zigzag edge. In the former case, they are called zigzag nanotubes and are semiconducting, whereas in the latter, they are called armchair nanotubes and show metallic behavior. These properties were predicted theoretically (Mintmire et al. [1992], Hamada et al. [1992], Saito et al. [1992]) and later verified in experiments (Wildöer et al. [1998], Odom et al. [1998]). The latter situation allowing for electronic transport is of special interest to us. In these SWNTs, the interacting conduction electrons can only move along one direction. Having a linear dispersion in leading approximation, the low-temperature properties of the electron liquid can be modeled by a Luttinger liquid as will be discussed later. Experimentally, using an atomic force microscope (AFM) or a scanning tunneling microscope (STM), the structure of these SWNTs can be perturbed in such a way to separate a small island mimicking a quantum dot. In Fig. 2.4, we illustrate a resonant level setup composed of an armchair nanotube, the corresponding energy level diagram would be similar to Fig. 2.2 apart from the fact that the Fermi edge of a Luttinger liquid is smeared out even at zero temperature. Such a setup is thus well suited to probe the physics of the *interacting resonant level model*. A calculation shows that an electron on the dot senses a Coulomb repulsion less than the interaction between conduction electrons. In practice, it could thus be quite realistic to reach even the parameter constellation corresponding to the *Majorana resonant level model*. However, at the moment of writing, it seems to be rather involved to tune the tunneling coupling parameters by external manipulation. More promising candidates are electrons confined by appropriate gating in semiconductor heterostructures or even fermionic gases trapped in optical (lattice) potentials. Future progress will decide which setups make it possible to test our predictions on transient noise in the Majorana resonant level model.

2.2 Resonant level model

The resonant level model to be discussed first can be seen as a variant of the Anderson impurity model in which the on-dot interaction of electrons is negligible. As the system under consideration is then purely non-interacting, i.e. charge carriers are non-interacting both in the leads *and* the dot region, the spin degree of freedom is consequently irrelevant and therefore we suppress the corresponding index of fermion operators. Moreover, we assume that the dot can only be occupied by at most one single electron at a time.

We want to address in more detail the justification of neglecting interactions in the electrodes. Considering the very large number of conduction electrons in a bulk metal, it may seem hopeless at first sight to take into account interactions adequately. However, in the case of macroscopic 2D or 3D electron gases, it was shown by Landau in 1956 that there exists a formulation

in terms of non-interacting fermionic quasiparticles which are in one-to-one correspondence with the original electrons, meaning that they carry the same quantum numbers apart from a renormalization of certain parameters such as an effective mass. The conceptual framework of identifying these quasiparticles in terms of original fermions is provided by Landau's Fermi liquid theory. At this point, it is important to remark that this approach is essentially based on an adiabaticity assumption concerning the switch-on process of the interactions between particles. Later, we will encounter a case where this assumption is not acceptable anymore. In our setup, we are interested in tunneling processes from metallic leads to the localized level on a quantum dot. In most cases, this tunneling contact can be regarded as structureless, since only the isotropic s-wave scattering processes are relevant, which enables the mapping to a one-dimensional field theory (Ludwig and Affleck [1994]).

2.2.1 Hamilton operator

Under the above requirements, the Hamilton operator reads

$$H_{\mathrm{RLM}} = H_0 + H_D + H_T \,. \tag{2.1}$$

The first term on the rhs specifies the contribution of the lead electrons, which can be written down as an effective Hamiltonian for one-dimensional non-interacting electrons,

$$H_0 = \sum_{\alpha=L,R} \sum_k (\epsilon_{k,\alpha} - \mu_\alpha) c^\dagger_{k,\alpha} c_{k,\alpha} \,, \tag{2.2}$$

with $c_{k,\alpha}$ denoting the annihilation operator of an electron with momentum k in lead α kept at chemical potential μ_α. A further ingredient is the dot Hamiltonian, which describes the single dot level and is given by

$$H_D = \Delta d^\dagger d \,. \tag{2.3}$$

In addition, we consider tunneling processes between the leads and the dot region, represented by the corresponding Hamiltonian

$$H_T = \sum_{\alpha=L,R} \gamma_\alpha \left[\psi^\dagger_\alpha(x=0) d + \mathrm{H.c.} \right] , \tag{2.4}$$

where γ_α is the tunneling amplitude and d and ψ_α are the annihilation operators of dot and lead electrons, respectively. In most of the calculations presented below only fields at the tunneling point are involved (which means $x = 0$), therefore we suppress the spatial coordinate.

2.2.2 Current operator

We define the operator of the total current through the constriction as

$$\hat{I}(t) = \frac{\hat{I}_L(t) - \hat{I}_R(t)}{2} \tag{2.5}$$

where the operator for the current between an individual lead α and the dot is given by the intuitive formula

$$\hat{I}_\alpha(t) = \mathrm{i}\gamma_\alpha(t) \left[\psi^\dagger_\alpha(t) d(t) - \mathrm{H.c.} \right] . \tag{2.6}$$

It can be derived from the Heisenberg equation of motion for the particle number operator of lead α. Anticipating the sudden switching on of tunneling we consider later, we already included an explicitly time-dependent tunneling amplitude $\gamma(t)$. For reasons of clarity, we always assume a symmetric coupling $\gamma_L(t) = \gamma_R(t) = \gamma(t)$. The asymmetric case can be treated as well, but the main physical effects to be discussed in this thesis are unaffected by its concrete choice. For later use, we define the hybridization constant Γ expressible in terms of the tunneling amplitude γ and the electronic density of states of the leads ρ_0, which is assumed to be energy independent for the rest of this thesis. This seemingly crude approximation is often called the wide flat band limit. For the RLM, we take the convention $\Gamma = 2\pi\rho_0\gamma^2$.

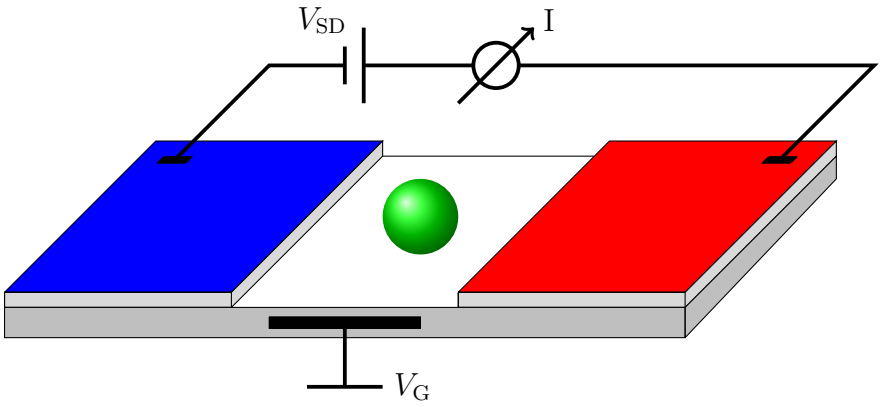

Figure 2.1: Realization of the RLM setup on the basis of a semiconductor heterostructure. The blue and red areas represent the left and right electrodes kept at different chemical potentials μ_L and μ_R, their difference being the source-drain voltage V_{SD}. The green sphere emphasizes the localized quantum dot. For clarity, only the gate voltage V_{G} controlling the dot energy is indicated.

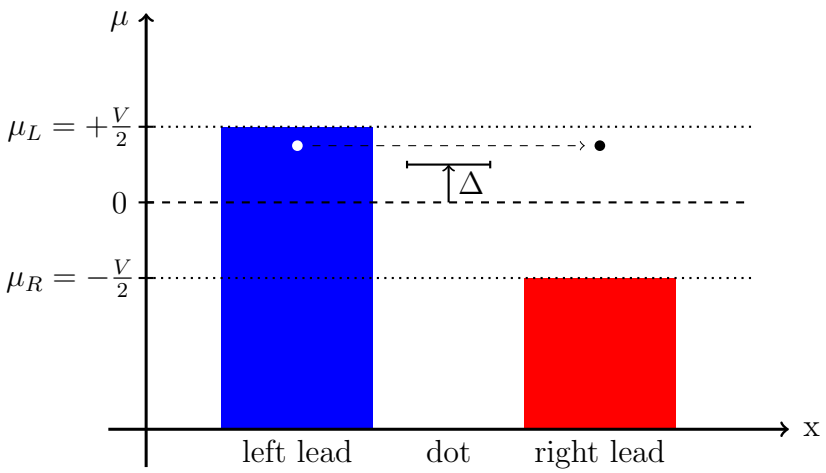

Figure 2.2: Schematic drawing of the resonant level setup in energy space for the case of zero temperature. The shaded areas represent the filled Fermi seas of the electrodes. An electron from the left lead can tunnel to an unoccupied state of the right lead.

2.3 Majorana resonant level model

In this section, we give the basic steps of the derivation of the MRLM which is an extension of the RLM that effectively describes interacting systems. This model can have quite different origins: the interacting resonant level model and the Kondo model. To prevent the presentation from becoming overloaded, we restrict to the former model as a starting point and only add some comments concerning the latter model. Readers who are interested in more detailed information about the alternative way could consult for example Gogolin et al. [1998].

We thus keep the two-terminal setup from the last section with the modification that a resonant level is now sandwiched between two electrodes in the Luttinger liquid phase which is characterized by one-dimensional interacting electrons. In addition, we take into account a capacitive dot-lead coupling representing the Coulomb repulsion between an electron on the resonant level and lead electrons at the dot-lead boundary. Since we include the electron-electron interaction explicitly, at first glance, this seems to be a major complication since the Hamiltonian now becomes quartic in terms of fermionic creation and annihilation operators. However, compared to higher dimensions and under some additional assumptions to be specified below, the Hamiltonian of one-dimensional interacting electrons can be mapped – via the bosonization technique – to a Hamiltonian of one-dimensional non-interacting bosonic degrees of freedom.

Before proceeding, we want to give a short review of the crucial role of interactions depending on the spatial dimension of the physical system. Unlike its higher dimensional counterparts, a one-dimensional interacting fermion gas is an intrinsically strongly correlated system, regardless of the interaction strength between the constituent particles. Even in case of arbitrarily weak, finite interaction, this fundamental difference excludes the applicability of naive perturbation theory. The breakdown of Fermi liquid theory can qualitatively be understood as follows. In contrast to 2D or 3D, the Fermi surface in 1D is not connected, reducing to a finite set of points. If we are only concerned about the physics at sufficiently low energy, an excitation of a certain energy unambiguously determines its wave number up to the sign, whereas in higher dimensions, it can belong to any wavenumber between zero and the Fermi momentum k_F. This kinematic restriction ties together electrons and holes giving rise to new quasiparticles which behave as effective bosonic degrees of freedom. Furthermore, we are entitled to linearize the spectrum in the vicinity of the Fermi points and, additionally, extend it to negative infinity filling all states with negative energies, which does not influence the low-energy physics either (see Fig. 2.3). The resulting, by now famous model is termed 'Luttinger liquid'. Under the above assumptions, the Hamiltonian acquires a quadratic structure in terms of bosonic excitations thus allowing for an exact solution even in non-equilibrium.[1] Indeed, the Hamiltonian is similar to the one describing harmonic modes of a 1D string, one of the simplest examples of a non-interacting problem in physics. To sum up, at low energy, the formulation in terms of individual fermions loses its meaning since these combine to form soundwave-like eigenmodes, which can be considered as non-interacting to a good approximation. A more detailed presentation of the transformation can be found in the vast literature about the subject (see e.g. Sénéchal [1999], von Delft and Schoeller [1998]). At this point, we only want to present the resulting bosonic

[1] Actually, this is only true for certain kinds of scattering events. For instance, at half-filling of a band, we have to include Umklapp-scattering events, which leads to a sine-Gordon type Hamiltonian.

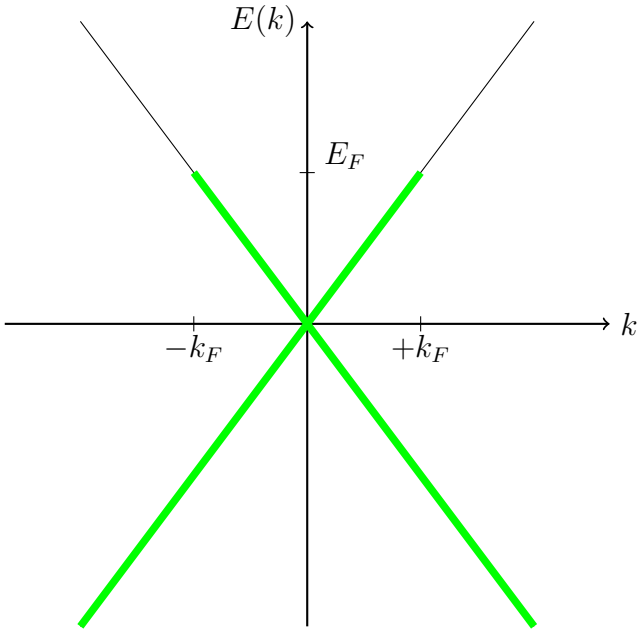

Figure 2.3: Dispersion relation of the Luttinger liquid model: The thick green line represents the Fermi sea. E_F and k_F denote the Fermi energy and the Fermi momentum, respectively.

Hamiltonian

$$H_0\left[\phi_L,\phi_R\right]=\frac{1}{4\pi}\sum_{\alpha=L,R}\int dx\,\left[\partial_x\phi_\alpha(x)\right]^2+\frac{V}{2}\int dx\,\left[\rho_L(x)-\rho_R(x)\right], \tag{2.7}$$

where we already included the contribution due to the voltage between the left and right leads in our two-terminal setup. The connection of the original fermionic operator $\psi_\alpha(x)$ to the fermionic density operator $\rho_\alpha(x)$ and the bosonic operator $\phi_\alpha(x)$ is provided by

$$\rho_\alpha(x)=\psi_\alpha^\dagger(x)\psi_\alpha(x)=\frac{\partial_x\phi_\alpha(x)}{2\pi\sqrt{g}} \tag{2.8}$$

together with the relation at the dot-lead boundary

$$\psi_\alpha(x=0)=\frac{\eta_\alpha}{\sqrt{2\pi a_0}}\mathrm{e}^{\mathrm{i}\phi_\alpha(x=0)/\sqrt{g}}, \tag{2.9}$$

where $g=1/\sqrt{1+\frac{U}{\pi v_F}}$ is the conventional Luttinger liquid parameter with U being the bare interparticle interaction strength. The different cases $g=1$, $g>1$ and $g<1$ correspond to absent, attractive and repulsive electron-electron interactions, respectively. η_α is the Klein factor to ensure the correct anti-commutation relations between the fermionic dot and lead operators and a_0 is the lattice constant of an underlying lattice model.

2.3.1 Hamilton operator

After this short digression, we now turn to the Hamiltonian of the IRLM which is given by

$$H_{\mathrm{IRLM}}=H_K+H_T+H_C, \tag{2.10}$$

where

$$H_K = \Delta d^\dagger d + H_0\left[\phi_L, \phi_R\right] \tag{2.11}$$

is again the kinetic part describing the localized dot level and 1D interacting fermions modeled by the Luttinger liquids, and

$$H_T = \sum_{\alpha=L,R} \gamma_\alpha \left[\psi_\alpha^\dagger(x=0)d + \text{H.c.}\right] \tag{2.12}$$

is the usual tunneling part. The additional term (Komnik and Gogolin [2003b,a], Komnik [2009])

$$H_C = \lambda_C\, d^\dagger d \sum_{\alpha=L,R} \psi_\alpha^\dagger(x=0)\psi_\alpha(x=0) \tag{2.13}$$

is responsible for the Coulomb repulsion. In a general non-equilibrium setting, this model has not been solved exactly so far. To proceed further, we can apply Eqs. (2.8) and (2.9) along with the spin operators written in terms of the local fermion

$$S_x = \frac{1}{2}(d^\dagger + d), \quad S_y = \frac{\mathrm{i}}{2}(d - d^\dagger), \quad S_z = d^\dagger d - \frac{1}{2} \tag{2.14}$$

to the respective parts of the IRLM Hamiltonian to obtain

$$H_C = \frac{\lambda_C}{2\pi\sqrt{g}} S_z \sum_{\alpha=L,R} \partial_x \phi_\alpha(x)\Big|_{x=0}, \tag{2.15}$$

$$H_T = \sum_{\alpha=L,R=\pm} \frac{\eta_\alpha}{\sqrt{2\pi a_0}} \left[\gamma_\alpha \mathrm{e}^{-\mathrm{i}\phi_\alpha/\sqrt{g}} S_- + \gamma_\alpha^* S_+ \mathrm{e}^{\mathrm{i}\phi_\alpha/\sqrt{g}}\right], \tag{2.16}$$

where we neglected contributions that do not alter the model dynamics. This transformation shows that the capacitive coupling corresponds to a coupling between S_z and the electron density in an associated Kondo problem. We then construct even/odd field operators $\phi_\pm = (\phi_L \pm \phi_R)/\sqrt{2}$ and apply the Emery-Kivelson rotation (Emery and Kivelson [1992]) to the Hamiltonian according to $H' = U^\dagger H U$, where

$$U = \mathrm{e}^{\mathrm{i}S_z\phi_+(0)/\sqrt{2g}}. \tag{2.17}$$

This finally leads to

$$H_K' + H_C' = H_K + \left[\frac{\lambda_C}{\pi\sqrt{2g}} - \sqrt{\frac{2}{g}}\right] S_z \partial_x \phi_+(x)\Big|_{x=0} \tag{2.18}$$

$$H_T' = \sum_{\alpha=L,R=\pm} \frac{\eta_\alpha}{\sqrt{2\pi a_0}} \left[\gamma_\alpha \mathrm{e}^{-\mathrm{i}\alpha\phi_-/\sqrt{2g}} S_- + \gamma_\alpha^* S_+ \mathrm{e}^{\mathrm{i}\alpha\phi_-/\sqrt{2g}}\right], \tag{2.19}$$

with the spin raising/lowering operators $S_\pm = S_x \pm \mathrm{i}S_y = d^\dagger, d$. Remarkably, one can refermionize the bosonic Hamiltonian at the special value of the interaction parameter $g = 1/2$ (Komnik and Gogolin [2003b,a]). To this end, one defines the following operator that obviously obeys fermionic anti-commutation relations,

$$\psi_\pm = \mathrm{e}^{\mathrm{i}\phi_\pm}/\sqrt{2\pi a_0}, \tag{2.20}$$

so that the particle density operator can be expressed as $\psi_\pm^\dagger(x)\psi_\pm(x) = \partial_x\phi_\pm(x)/(2\pi)$. These steps allow to recast the Hamiltonian into the form (Komnik and Gogolin [2003a])

$$H = H_0\left[\psi_\pm\right] + (\lambda_C - 2\pi)2S_z\psi_+^\dagger\psi_+ + \Delta S_z + S_+(\gamma_L\psi_- + \gamma_R\psi_-^\dagger) + (\gamma_L\psi_-^\dagger + \gamma_R\psi_-)S_-. \tag{2.21}$$

The special choice $\lambda_C = 2\pi$ ($= 2\pi v_F$ if the Fermi velocity of the lead electrons $v_F \neq 1$) evidently leads to a Hamiltonian purely quadratic in fermionic operators. After the above series of transformations and the subsequent decomposition of the conventional fermionic operators ψ_- and d into its Majorana components through $\psi_- = (\xi + \mathrm{i}\eta)/\sqrt{2}$ and $d = (a + \mathrm{i}b)/\sqrt{2}$, the resulting model is called the *Majorana resonant level model (MRLM)* and possesses an exact solution (Schiller and Hershfield [1998, 1996]). Its Hamiltonian can be written down in the following way

$$H_{\mathrm{MRLM}} = H_K\left[\xi, \eta, a, b\right] + H_T'\left[\xi, \eta, a, b\right], \tag{2.22}$$

where

$$H_K\left[\xi, \eta, a, b\right] = \mathrm{i}\Delta ab + \mathrm{i}\int dx\left[\eta(x)\partial_x\eta(x) + \xi(x)\partial_x\xi(x) + V\xi(x)\eta(x)\right] \tag{2.23}$$

governs the dynamics of free lead Majorana fields $\eta(x)$ and $\xi(x)$ and local dot Majorana fermions a and b, whereas

$$H_T'\left[\xi, \eta, a, b\right] = -\mathrm{i}\left[\gamma_+ b\xi(x=0) - \gamma_- a\eta(x=0)\right] \tag{2.24}$$

is an interaction term modeling couplings between lead and local dot Majorana fermions. Here, we introduced the coupling constants $\gamma_\pm = \gamma_L \pm \gamma_R$.

As already mentioned, the MRLM can have an entirely different origin. One can start from the Kondo model which constitutes an effective theory of the AIM in the limit of infinite on-dot interactions. In this model, the quantum dot has only a spin degree of freedom which interacts with the delocalized electrons from the surrounding conductor via a Heisenberg-type coupling. Historically, this model in equilibrium was used to explain the puzzle of a resistance minimum at low temperature observed in certain bulk metals with embedded impurities, which remained unsolved for a long time (Kondo [1964]). In a two-terminal non-equilibrium setup, one can find a mapping to the MRLM according to a similar procedure as in the IRLM case to identify a parameter set that allows for an exact solution (Schiller and Hershfield [1998, 1996]). This special point is named Toulouse limit (Toulouse [1969]) after the person who first solved the analogous problem in equilibrium.

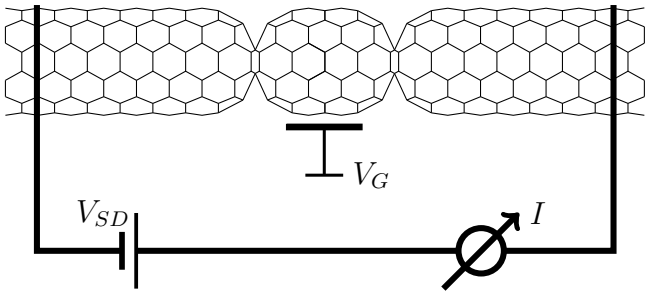

Figure 2.4: Possible realization of the MRLM setup: an armchair nanotube is locally deformed (e.g. by an STM tip) to isolate a central region which mimics a quantum dot.

2.3.2 Current operator

We take our operator for the total current through the constriction in Majorana fermion representation (Komnik [2009])

$$\hat{I}(t) = -\frac{\mathrm{i}}{2}\left[\gamma_+(t)b(t)\eta(t) + \gamma_-(t)a(t)\xi(t)\right] \tag{2.25}$$

with special emphasis on the time dependence of the tunneling coupling. For the rest of this thesis, we also specialize to symmetric coupling in this case and therefore have to impose the condition $\gamma_-(t) = 0$, and we denote $\gamma_+(t) = \gamma(t)$ to alleviate notation. For the MRLM, we also define a hybridization related to the tunneling coupling via $\Gamma = \gamma^2/2$ using $\rho_0 = 1/(2\pi)$. It has to be noticed that the splitting of the current into left and right contributions is only reasonable in our derivation starting from the resonant tunneling setup between Luttinger liquids. In the Kondo picture this is not meaningful since this model describes the scattering of conduction electrons off a local impurity, in which tunneling between the electrodes is a single-stage process (electrode-electrode jump with a spin-flip of the impurity), while electron transmission in the Luttinger set-up is a two-stage process (electrode-dot-electrode). One further difference concerns the interpretation of the dot energy in the Kondo case as a local magnetic field. Thus the dot magnetization in the Kondo picture corresponds to the dot occupation in the Luttinger setup.

2.4 Schwinger-Keldysh technique

2.4.1 General formalism

We briefly want to motivate the inadequacy of the ordinary equilibrium Green's function technique and the necessity of extending this formalism for systems that are perturbed out of equilibrium. In general, probing condensed matter almost inevitably requires the knowledge of correlation functions a.k.a. Green's functions. As an example, one could be interested in a process where an electron is injected into the system and one then wants to monitor its subsequent evolution. In an interacting system, this electron usually becomes 'dressed' with other particles or excitations to form new entities, generally called quasiparticles. Thus, we are forced to evaluate a quantity like the two-point correlator, which, in second quantization, reads

$$G(\lambda, t; \lambda', t') = -\mathrm{i}\langle T[c_H(\lambda, t)c_H^\dagger(\lambda', t')]\rangle \tag{2.26}$$

and represents the *time-ordered* expectation value of two creation/annihilation operators at certain times, taken with respect to the complete Hamiltonian of the system. Here, the index λ subsumes all quantum numbers relevant to the specific problem, and the operators are chosen to be in the Heisenberg representation of quantum mechanics, where the temporal dynamics is entirely incorporated in the operators. A generalization of the discussion to an arbitrary n-point Green's function is self-explanatory. If the system Hamiltonian splits into two parts $H = H_0 + V$, where H_0 is diagonalizable, whereas the spectrum of H is not necessarily known, it proves to be advantageous to switch to the interaction representation, where the corresponding operators are defined in the following way,

$$O_I(t) = U(t) O_H(x,t) U^\dagger(t) \tag{2.27}$$

with the unitary operator $U(t) = \mathrm{e}^{\mathrm{i}H_0 t}\mathrm{e}^{-\mathrm{i}Ht}$. The time evolution of the quantum states is then governed by the operator V alone, obeying the differential equation

$$\mathrm{i}\partial_t |\psi(t)\rangle_I = V_I(t)|\psi(t)\rangle_I. \tag{2.28}$$

By solving this equation, it can be shown that the evolution of the state between two different times t and t' is determined by the $\mathcal{S}$ matrix defined as $\mathcal{S}(t,t') = U(t)U^\dagger(t')$, which fulfills

$$\mathcal{S}(t,t') = T\exp\left[-\mathrm{i}\int_t^{t'} V_I(s)ds\right]. \tag{2.29}$$

The Gell-Mann-Low theorem states that the quantum state at time t of a physical system governed by H is related to an eigenstate $|\phi_0\rangle$ of H_0 in the following way,

$$|\psi(t)\rangle = \mathcal{S}(t,-\infty)|\phi_0\rangle, \tag{2.30}$$

which is a rigorously proven mathematical identity for an adiabatic switching-on of the perturbation V (Molinari [2007]), which is often a realistic assumption. Putting all pieces together, we can rewrite Eq. (2.26) as

$$\begin{aligned} G(\lambda,t;\lambda',t') &= -\mathrm{i}\langle\phi_0|\mathcal{S}(-\infty,t)T[c_I(\lambda,t)\mathcal{S}(t,t')c_I^\dagger(\lambda',t')\mathcal{S}(t',-\infty)]|\phi_0\rangle \\ &= -\mathrm{i}\langle\phi_0|\mathcal{S}(-\infty,+\infty)T[c_I(\lambda,t)c_I^\dagger(\lambda',t')\mathcal{S}(+\infty,-\infty)]|\phi_0\rangle. \end{aligned} \tag{2.31}$$

The next crucial step carried out for systems in equilibrium leads to

$$G^{\mathrm{eq}}(\lambda,t;\lambda',t') = -\mathrm{i}\frac{\langle\phi_0|T[c_I(\lambda,t)c_I^\dagger(\lambda',t')\mathcal{S}(+\infty,-\infty)]|\phi_0\rangle}{\langle\phi_0|\mathcal{S}(+\infty,-\infty)|\phi_0\rangle}. \tag{2.32}$$

The transition from Eq. (2.31) to Eq. (2.32) is justified by the following, useful theorem of equilibrium quantum field theory which says that the states in the infinite future and the infinite past are proportional to each other up to a phase factor, thus obeying

$$|\psi(+\infty)\rangle = \mathrm{e}^{\mathrm{i}\alpha}|\phi_0\rangle. \tag{2.33}$$

Eq. (2.33) relies on the condition that V is also turned off adiabatically in the remote future, which is often justified e.g. in scattering experiments at particle colliders. If we instead consider

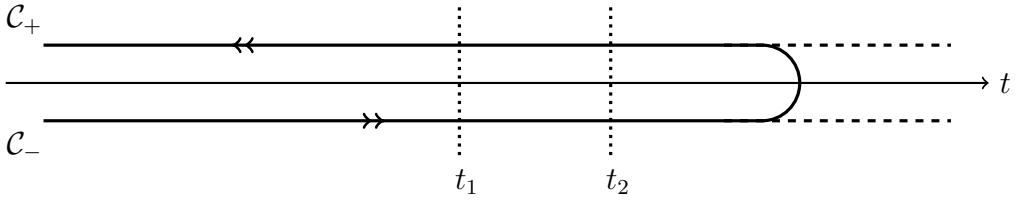

Figure 2.5: Schwinger-Keldysh time contour: Equivalent approaches: $\mathcal{C} = \mathcal{C}_- \cup \mathcal{C}_+$ is the full contour consisting of a forward branch $\mathcal{C}_-$ and a backward branch $\mathcal{C}_+$. In contrast to the Schwinger contour (thick line), Keldysh extended the path to $t = +\infty$ (dashed lines).

a system that remains out of equilibrium, this relation is definitely not applicable anymore. We thus face the problem of the presence of some operators being time-ordered as introduced above and some being ordered in the reversed sense. Especially in a perturbative expansion of the $\mathcal{S}$ matrix, one has to carefully keep track of this complication. As a remedy, Schwinger and Keldysh invented similar and completely equivalent techniques independently from each other by introducing time contours $\mathcal{C}$ which enlarge the conventional time path back to the infinite past (see Fig. 2.5). The slight difference between the two approaches lies in the turning point of the time loop, which has to be chosen to be greater than the maximum measuring time $\max(t, t')$, and is either taken to be finite (Schwinger) or infinite (Keldysh). This freedom is a consequence of the unitary time evolution of quantum mechanics. In this thesis, we choose the latter option, extending the contour to infinity. This approach enables one to rewrite the Green's function in the concise form

$$G(\lambda, t; \lambda', t') = -\mathrm{i}\langle\phi_0|T_{\mathcal{C}}[c_I(\lambda, t)c_I^\dagger(\lambda', t')\mathcal{S}_{\mathcal{C}}(-\infty, -\infty)]|\phi_0\rangle, \tag{2.34}$$

where $T_{\mathcal{C}}$ denotes the *contour-ordering* operator, that places an operator at a certain point on the contour to the right of those located at a later point in the sense indicated by the arrow in Fig. 2.5, and $\mathcal{S}_{\mathcal{C}}$ is the extension of the ordinary $\mathcal{S}$ matrix to Keldysh space defined as

$$\mathcal{S}_{\mathcal{C}}(-\infty, -\infty) = T_{\mathcal{C}}\ \mathrm{e}^{-\mathrm{i}\int_{\mathcal{C}} ds\ V_I(s)}. \tag{2.35}$$

In the previous formula, we use the shorthand notation

$$\int_{\mathcal{C}} ds\, V_I(s) = \int_{-\infty}^{+\infty} ds_-\, V_I(s_-) + \int_{+\infty}^{-\infty} ds_+\, V_I(s_+). \tag{2.36}$$

This passage from the integration along the time contour $\mathcal{C}$ to the integration along the real time axis is usually referred to as *Keldysh disentanglement*. We would like to emphasize that contour ordering means that some operators may appear to the left of others although occurring at an earlier *real* time. As a consequence, in contrast to equilibrium, where the knowledge of the *time-ordered* Green's function alone is sufficient, there are additional types of Green's functions. For the two-point correlator considered above, this means that one has four possibilities of attributing the two times to different branches. It is thus useful to go over to a matrix notation in which the Green's function is defined in the following way

$$\hat{G}(t, t') = \begin{pmatrix} G^{--}(t, t') & G^{-+}(t, t') \\ G^{+-}(t, t') & G^{++}(t, t') \end{pmatrix}, \tag{2.37}$$

its components being given by

$$\begin{aligned} G^{--}(\lambda,t;\lambda',t') &= -\mathrm{i}\langle T[c_H(\lambda,t)c_H^\dagger(\lambda',t')]\rangle, \\ G^{-+}(\lambda,t;\lambda',t') &= \pm\mathrm{i}\langle[c_H^\dagger(\lambda',t')c_H(\lambda,t)]\rangle, \\ G^{+-}(\lambda,t;\lambda',t') &= -\mathrm{i}\langle[c_H(\lambda,t)c_H^\dagger(\lambda',t')]\rangle, \\ G^{++}(\lambda,t;\lambda',t') &= -\mathrm{i}\langle\tilde{T}[c_H(\lambda,t)c_H^\dagger(\lambda',t')]\rangle. \end{aligned} \tag{2.38}$$

Here, $\tilde{T}$ represents the anti-time-ordering operator and the upper/lower sign refers to the case of a fermionic/bosonic operator. The four aforementioned Green's functions are normally called *time-ordered*, *lesser*, *greater* and *anti-time-ordered* in the order from top to bottom. At this point, we have the general formalism at hand to treat concrete problems.

2.4.2 Application to switch-on processes in resonant level setups

In this work, we intend to study the models introduced above in a *preparative* non-equilibrium situation, which means that some parameters are changed rapidly at some time $t = t_0$. These resonant level setups are particularly appropriate to study such switch-on processes due to their appealing mathematical simplicity, but nonetheless describing realistic setups. In the following, we assume that the system has adiabatically reached a state $|\psi(t_0)\rangle$ with leads at different chemical potentials but still uncoupled to the dot, so that formula (2.30) can be used for our non-equilibrium setting. As already announced, at a certain time $t = t_0$, we apply the tunneling Hamiltonian H_T with the coupling constant fulfilling $\gamma(t) = \gamma f(t-t_0)\theta(t-t_0)$, where $f(t-t_0)$ encodes the specific increase of the coupling. Thus, having a completely known system at t_0, we can rewrite Eq. (2.31) as

$$\begin{aligned} G(\lambda,t;\lambda',t') &= -\mathrm{i}\langle\psi(t_0)|\mathcal{S}(t_0,t)T[c_I(\lambda,t)\mathcal{S}(t,t')c_I^\dagger(\lambda',t')\mathcal{S}(t',t_0)]|\psi(t_0)\rangle \\ &= -\mathrm{i}\langle\psi(t_0)|T_{\mathcal{C}}[c_I(\lambda,t)c_I^\dagger(\lambda',t')\mathcal{S}_{\mathcal{C}_0}(t_0,t_0)]|\psi(t_0)\rangle. \end{aligned} \tag{2.39}$$

The effective integration path $\mathcal{C}_0$ begins and ends at t_0, which is depicted in Fig. 2.6. Without loss of generality, we take $t_0 \equiv 0$ to unburden notation for the rest of this thesis. To be specific,

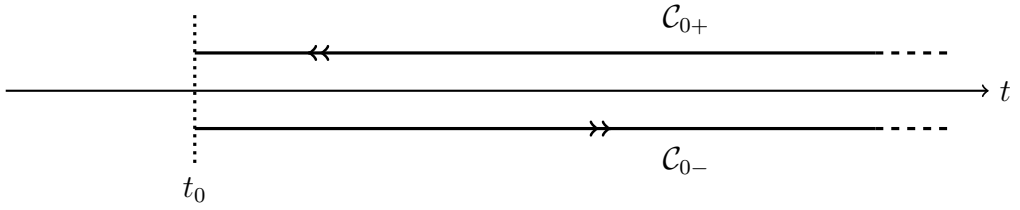

Figure 2.6: Effective Keldysh time contour $\mathcal{C}_0 = \mathcal{C}_{0-} \cup \mathcal{C}_{0+}$ in case of switch-on processes starting at time t_0.

let us consider the simplest way of implementing a switch-on process: the instantaneous jump of the tunneling coupling from zero to a constant finite value, i.e. $\gamma(t) = \gamma\theta(t)$ – in the following

referred to as a *sudden* switch-on process. Although seeming rather artificial, we note that such a choice simplifies the problem tremendously while the conclusions drawn for the behavior at large times remain unaffected. Unless stated otherwise, we keep this restriction throughout this work.

2.5 Green's functions for the RLM

As outlined above, in order to compute transport quantities, we need the Green's functions obtained by expansion of the $\mathcal{S}$ matrix. We adopt the general definition of the Keldysh time-ordered Green's functions from Section 2.4

$$G_{\zeta\zeta'}(t,t') = -\mathrm{i}\left\langle T_{\mathcal{C}}\psi_{\zeta}(t)\psi^{\dagger}_{\zeta'}(t')\right\rangle \tag{2.40}$$

$$= -\mathrm{i}\left\langle T_{\mathcal{C}}\psi_{\zeta}(t)\psi^{\dagger}_{\zeta'}(t')\mathcal{S}_{\mathcal{C}}\right\rangle_{0} \tag{2.41}$$

and the definition of the $\mathcal{S}$ matrix

$$\mathcal{S}_{\mathcal{C}} = T_{\mathcal{C}}\,\mathrm{e}^{-\mathrm{i}\int_{\mathcal{C}} dt\, H_T(t)}. \tag{2.42}$$

where ζ and ζ' specify the respective dot and lead operators. Here, we use a compact notation which treats both operators on equal footing, which means that we identify $d \equiv \psi_d$ and, for later use, we define the dot Green's function $D(t,t') \equiv G_{dd}(t,t')$. The average in Eq. (2.40) is taken with respect to the coupled system, while the average in Eq. (2.41) is performed with respect to the uncoupled one.

2.5.1 Free lead and dot Green's functions

In case of strict isolation of the quantum dot from the leads, the evaluation of the correlation functions – then termed *free* Green's functions[2] – is straightforward. Formally, they are obtained by setting $\mathcal{S}_{\mathcal{C}} = \mathbb{1}$ in Eq. (2.41). The free lead Green's function in Fourier-Keldysh space then reads (Caroli et al. [1971], Meir and Wingreen [1992])

$$\hat{g}_{\alpha\alpha'}(\omega) = 2\pi\mathrm{i}\rho_0\delta_{\alpha\alpha'}\begin{pmatrix} n_\alpha - 1/2 & n_\alpha \\ n_\alpha - 1 & n_\alpha - 1/2\end{pmatrix}, \tag{2.43}$$

where $n_\alpha(\omega) = n_F(\omega - \mu_\alpha)$ represents the Fermi-Dirac distribution function of the respective lead electrode α with chemical potential μ_α. The free dot Green's function is given by

$$\hat{D}_0(t,t') = \mathrm{e}^{-\mathrm{i}\Delta(t-t')}\begin{pmatrix} -\mathrm{i}[\theta(t-t')(1-n_0) - \theta(t'-t)n_0] & \mathrm{i}n_0 \\ -\mathrm{i}(1-n_0) & -\mathrm{i}[\theta(t'-t)(1-n_0) - \theta(t-t')n_0]\end{pmatrix}, \tag{2.44}$$

where n_0 denotes the initial population of the quantum dot.

[2] In our terminology, *free* refers to a dot-lead system without tunneling coupling, while *full* characterizes a coupled system.

2.5.2 Relations between different types of full Green's functions

The next, somewhat tedious task is to evaluate the various *full* Green's functions for our problem of the sudden switching on of the tunneling coupling. To achieve that, we make extensive use of the following general relation for the RLM case

$$G^{\eta\eta'}_{\zeta\zeta'}(t,t') = g^{\eta\eta'}_{\zeta\zeta'}(t,t') - \sum_{\kappa=L,R}\sum_{\sigma=\pm}\sigma\cdot\int_{-\infty}^{+\infty} ds\,\gamma(s)\left[g^{\eta\sigma}_{\zeta\kappa}(t,s)G^{\sigma\eta'}_{d\zeta'}(s,t') + g^{\eta\sigma}_{\zeta d}(t,s)G^{\sigma\eta'}_{\kappa\zeta'}(s,t')\right], \tag{2.45}$$

where the upper indices indicate the branch of the Keldysh contour ($-/+$ for the forward/ backward branch) and the lower ones specify the lead/dot operators. This formula is derived by expansion of the $\mathcal{S}$ matrix and subsequent re-exponentiation, which is sketched in the following. One starts with Eq. (2.41) and expresses the $\mathcal{S}$ matrix using the series representation of the exponential function. Rearrangement of terms then leads to

$$\begin{aligned} G_{\zeta\zeta'}(t,t') = &-\mathrm{i}\left\langle T_{\mathcal{C}}\psi_\zeta(t)\psi^\dagger_{\zeta'}(t')\right\rangle_0 \\ &+\left\langle T_{\mathcal{C}}\psi_\zeta(t)\psi^\dagger_{\zeta'}(t')\sum_{n=1}^{\infty}\frac{(-\mathrm{i})^{n+1}}{n!}\prod_{i=1}^{n}\int ds_i\,\gamma(s_i)\sum_{\kappa=L,R}\left[\psi^\dagger_\kappa(s_i)d(s_i)+d^\dagger(s_i)\psi_\kappa(s_i)\right]\right\rangle_0 . \end{aligned} \tag{2.46}$$

In this form, we are in a position to apply Wick's theorem, paying attention to the fact that we have to multiply by (-1) when interchanging fermionic operators. There are n ways to pair $\psi_\zeta(t)$ and $\psi^\dagger_{\zeta'}(t')$ with the other operators. Since interchanging two indices $i \leftrightarrow j$ does not change the integral we obtain

$$\begin{aligned} G_{\zeta\zeta'}(t,t') = &-\mathrm{i}\left\langle T_{\mathcal{C}}\psi_\zeta(t)\psi^\dagger_{\zeta'}(t')\right\rangle_0 - \sum_{\kappa=L,R}\int d\tau\left\langle T_{\mathcal{C}}\psi_\zeta(t)\psi^\dagger_\kappa(\tau)\right\rangle_0 \\ &\times\left\langle T_{\mathcal{C}}\psi^\dagger_{\zeta'}(t')d(\tau)\sum_{n=1}^{\infty}\frac{\gamma(\tau)(-\mathrm{i})^{n+1}}{(n-1)!}\prod_{i=1}^{n-1}\int ds_i\,\gamma(s_i)\left(\psi^\dagger_\kappa(s_i)d(s_i)+d^\dagger(s_i)\psi_\kappa(s_i)\right)\right\rangle_0 \\ &-\sum_{\kappa=L,R}\int d\tau\left\langle T_{\mathcal{C}}\psi_\zeta(t)d^\dagger(\tau)\right\rangle_0 \\ &\times\left\langle T_{\mathcal{C}}\psi^\dagger_{\zeta'}(t')\psi_\kappa(\tau)\sum_{n=1}^{\infty}\frac{\gamma(\tau)(-\mathrm{i})^{n+1}}{(n-1)!}\prod_{i=1}^{n-1}\int ds_i\,\gamma(s_i)\left(\psi^\dagger_\kappa(s_i)d(s_i)+d^\dagger(s_i)\psi_\kappa(s_i)\right)\right\rangle_0 . \end{aligned} \tag{2.47}$$

After carrying out the re-exponentiation, we immediately find Eq. (2.45). To access the stationary and transient noise results, it is helpful to make use of the compact Keldysh matrix notation. The above relation can then be written in the following way. From now on, we also

take into account both the left and right indices, so that it follows

$$\hat{G}_{\zeta\zeta'} = \hat{g}_{\zeta\zeta'} + \gamma \sum_{\kappa=L,R} \left(\hat{g}_{\zeta\kappa}\hat{\sigma}_3\hat{G}_{d\zeta'} + \hat{g}_{\zeta d}\hat{\sigma}_3\hat{G}_{\kappa\zeta'} \right), \tag{2.48}$$

or, equivalently,

$$\hat{G}_{\zeta\zeta'} = \hat{g}_{\zeta\zeta'} + \gamma \sum_{\kappa=L,R} \left(\hat{G}_{\zeta\kappa}\hat{\sigma}_3\hat{g}_{d\zeta'} + \hat{G}_{\zeta d}\hat{\sigma}_3\hat{g}_{\kappa\zeta'} \right), \tag{2.49}$$

where $\hat{\sigma}_3 = \mathrm{diag}(1,-1)$ is the third Pauli matrix and products represent integrations over the internal time variables. In Eqs. (2.48) and (2.49), we note that we need to insert the third Pauli-matrix twice in order to keep track of the corresponding signs on the forward/backward contour in the transition from contour integration to ordinary integration.

2.5.3 Dyson equation for full dot Green's function

We can also combine the two formulas Eq. (2.48) and Eq. (2.49) for various choices of ζ and ζ' to obtain the following equations

$$\hat{D} = \hat{D}_0 + \gamma^2 \hat{D}_0\hat{\sigma}_3(\hat{g}_{RR} + \hat{g}_{LL})\hat{\sigma}_3\hat{D}, \tag{2.50}$$

$$\hat{G}_{\alpha\alpha} = \hat{g}_{\alpha\alpha} + \gamma^2 \hat{g}_{\alpha\alpha}\hat{\sigma}_3\hat{D}_0\hat{\sigma}_3\hat{G}_{\alpha\alpha}, \tag{2.51}$$

with $\alpha \in (L,R)$. In quantum field theory, such types of self-consistent integral equations for full Green's functions are known as Dyson equations. In our case, it proves to be advantageous to concentrate on one species of full Green's functions meaning that we express all other types in terms of the *full* dot Green's function $D(t,t')$ and the *free* lead and dot Green's functions $g_{\alpha\alpha'}(t,t')$ and $D_0(t,t')$. The Dyson equation for the full dot Green's function in matrix notation reads

$$\hat{D}(t,t') = \hat{D}_0(t,t') + \int dt_1 \int dt_2\, \hat{D}_0(t,t_1)\hat{\sigma}_3\hat{\Sigma}_+(t_1,t_2)\hat{\sigma}_3\hat{D}(t_2,t'), \tag{2.52}$$

where, for later use, we defined the even/odd tunneling self-energy as

$$\hat{\Sigma}_\pm(t,t') = \gamma(t)\gamma(t')\left[\hat{g}_{LL}(t,t') \pm \hat{g}_{RR}(t,t')\right]. \tag{2.53}$$

We note that the self-energy in case of a sudden switch-on process contains a step function which effectively restricts the integration range to the interval $(0,+\infty)$.
In general, the above conventional representation is not unique. We can indeed find equivalent formulations by applying a unitary transformation. A special choice which is commonly used leads to the triagonal representation, which is discussed in Appendix B. According to a widely accepted terminology, the transformed Green's functions are then named *retarded*, *advanced* and *Keldysh* Green's functions. Although the numerical implementation is straightforward in the conventional representation for the stationary case, the benefit drawn from such a transformation resides in the fact that the Dyson equations for the retarded and advanced parts simplify considerably and can be solved immediately as shown next.
Returning to our problem, the Dyson equation for the retarded Green's function acquires the following well-known structure

$$D^R(t,t') = D_0^R(t-t') + \int_{-\infty}^{\infty} dt_1 \int_{-\infty}^{\infty} dt_2\, D_0^R(t-t_1)\Sigma^R(t_1-t_2)D^R(t_2,t'), \tag{2.54}$$

and is solvable by iterations. For $t, t' \geq 0$, its general solution for an arbitrary switching function $\gamma(t)$ reads

$$D^R(t,t') = -\mathrm{i}\theta(t-t')\mathrm{e}^{-\mathrm{i}\Delta(t-t')}\mathrm{e}^{-\int_{t'}^{t} ds\,\gamma^2(s)}. \tag{2.55}$$

To access its advanced counterpart, we make use of the general relation

$$G^R(t,t') = \left[G^A(t',t)\right]^*, \tag{2.56}$$

which immediately leads to

$$D^A(t,t') = +\mathrm{i}\theta(t'-t)\mathrm{e}^{-\mathrm{i}\Delta(t-t')}\mathrm{e}^{+\int_{t'}^{t} ds\,\gamma^2(s)}. \tag{2.57}$$

In the special case of a sudden switch-on process characterized by a Heaviside step function $\gamma(t) = \gamma\theta(t)$, we have

$$D^R(t,t') = -\mathrm{i}\theta(t-t')\mathrm{e}^{-\mathrm{i}\Delta(t-t')}\mathrm{e}^{-\Gamma(t-t')} = D^R(t-t') \tag{2.58}$$

and

$$D^A(t,t') = +\mathrm{i}\theta(t'-t)\mathrm{e}^{-\mathrm{i}\Delta(t-t')}\mathrm{e}^{+\Gamma(t-t')} = D^A(t-t'). \tag{2.59}$$

These functions are insensitive to the initial dot occupation, which is reflected in the fact that they are solely dependent on the time difference, which is indeed a remarkable property as we have not considered a time-translation invariant system. These retarded and advanced Green's functions were calculated in earlier works (see Wingreen et al. [1993], Jauho et al. [1994]).
The remaining task is to compute the lesser and greater Green's functions $D^{-+}(t,t')$ and $D^{+-}(t,t')$, which is achieved by using the respective versions of the Langreth theorem (Langreth [1976])

$$D^{+-} = (1 + D^R\Sigma^R)D_0^{+-}(1 + D^A\Sigma^A) + D^R\Sigma^{+-}D^A, \tag{2.60}$$

$$D^{-+} = (1 + D^R\Sigma^R)D_0^{-+}(1 + D^A\Sigma^A) + D^R\Sigma^{-+}D^A, \tag{2.61}$$

where again integration over the internal time variables is implied. Depending on the initial system preparation, one of these expressions simplifies tremendously. For an initially empty dot $D_0^{-+}(t,t') = 0$, whereas for an initially occupied dot we have $D_0^{+-}(t,t') = 0$. To be specific, if we prepare the resonant level system in a state with an empty dot level at the beginning and insert all necessary quantities into Eq. (2.61), we arrive at the result

$$D^{-+}(t,t') = \frac{\mathrm{i}\Gamma}{2\pi}\int d\omega \frac{[n_R(\omega) + n_L(\omega)]}{(\omega-\Delta)^2 + \Gamma^2} \times \left(\mathrm{e}^{\mathrm{i}\omega(t'-t)} - \mathrm{e}^{\mathrm{i}\omega t'}\mathrm{e}^{-\mathrm{i}\Delta t}\mathrm{e}^{-\Gamma t} - \mathrm{e}^{-\mathrm{i}\omega t}\mathrm{e}^{\mathrm{i}\Delta t'}\mathrm{e}^{-\Gamma t'} + \mathrm{e}^{\mathrm{i}\Delta(t'-t)}\mathrm{e}^{-\Gamma(t+t')}\right) \tag{2.62}$$

and immediately find $D^{+-}(t,t')$ using the general relation $D^{+-} = D^{-+} + D^R - D^A$. As announced, these functions constitute the starting point for the derivation of all other needed Green's functions.

2.5.4 Full mixed Green's functions

A Green's function is denoted as mixed if it is specified by both a dot index d and an index $\alpha \in (L, R)$ representing one of the leads.

Mixed greater and lesser Green's functions

We note the following, basic relations

$$\begin{aligned} G^R &= G^{--} - G^{-+} = G^{+-} - G^{++} \\ G^A &= G^{--} - G^{+-} = G^{-+} - G^{++}. \end{aligned} \tag{2.63}$$

Using Eq. (2.45) together with the relations of Eq. (2.63), we obtain after some algebra

$$G^{-+}_{\alpha d}(t,t') = -\mathrm{i}\pi\rho_0\gamma D^{-+}(t,t') + \gamma \int dt_1\, g^{-+}_{\alpha\alpha}(t,t_1) D^A(t_1,t'), \tag{2.64}$$

$$G^{+-}_{d\alpha}(t,t') = +\mathrm{i}\pi\rho_0\gamma D^{+-}(t,t') + \gamma \int dt_1\, D^R(t,t_1) g^{+-}_{\alpha\alpha}(t_1,t'). \tag{2.65}$$

Thus, we conclude for the differences

$$G^{-+}_{dL}(t,t') - G^{-+}_{dR}(t,t') = G^{+-}_{dL}(t,t') - G^{+-}_{dR}(t,t') = \gamma \int dt_1\, D^R(t,t_1) \left[g^{-+}_{LL}(t_1,t') - g^{-+}_{RR}(t_1,t') \right], \tag{2.66}$$

$$G^{-+}_{Ld}(t,t') - G^{-+}_{Rd}(t,t') = G^{+-}_{Ld}(t,t') - G^{+-}_{Rd}(t,t') = \gamma \int dt_1 \left[g^{-+}_{LL}(t,t_1) - g^{-+}_{RR}(t,t_1) \right] D^A(t_1,t'), \tag{2.67}$$

where we made additional use of the identity

$$g^{-+}_{LL}(\omega) - g^{-+}_{RR}(\omega) = g^{+-}_{LL}(\omega) - g^{+-}_{RR}(\omega) = 2\pi\mathrm{i}\rho_0 \left[n_L(\omega) - n_R(\omega) \right]. \tag{2.68}$$

Mixed advanced and retarded Green's functions

As these kinds of Green's functions are also needed in subsequent derivations we determine them here. We start from the identities of Eq. (2.63) and obtain the relations

$$G^A_{d\alpha}(t,t') = +\mathrm{i}\pi\rho_0\gamma D^A(t,t'), \tag{2.69}$$

$$G^R_{d\alpha}(t,t') = -\mathrm{i}\pi\rho_0\gamma D^R(t,t'). \tag{2.70}$$

2.5.5 Full lead Green's functions

To access the full lead Green's functions, we could either opt for the strategy of solving the corresponding Dyson equation. For our purposes, it is preferable to calculate it by expressing them through the already known quantities: the full dot Green's functions and the free lead

Green's functions. Thereby, we use again Eq. (2.45) along with Eqs. (2.63) and (2.70) and obtain

$$\begin{aligned} G^{\eta\eta'}_{\alpha\beta} &= g^{\eta\eta'}_{\alpha\beta}(t,t')\delta_{\alpha\beta} + \gamma \int dt_1 \left[g^{\eta-}_{\alpha\alpha}(t,t_1) G^{-\eta'}_{d\beta}(t_1,t') - g^{\eta+}_{\alpha\alpha}(t,t_1) G^{+\eta'}_{d\beta}(t_1,t') \right] \\ &= g^{\eta\eta'}_{\alpha\beta}(t,t')\delta_{\alpha\beta} + \pi^2 \rho_0^2 \gamma^2 D^{\eta\eta'}(t,t') \\ &\quad + \mathrm{i}\pi\rho_0\gamma^2 \left(\int dt_1 g^{\eta\eta'}_{\alpha\alpha}(t,t_1) D^A(t_1,t') - \int dt_1 D^R(t,t_1) g^{\eta\eta'}_{\alpha\alpha}(t_1,t') \right), \end{aligned} \tag{2.71}$$

with $\alpha, \beta \in (L,R)$. This immediately entails the fairly surprising result that

$$G^{\eta\eta'}_{LL} + G^{\eta\eta'}_{RR} - G^{\eta\eta'}_{LR} - G^{\eta\eta'}_{RL} = g^{\eta\eta'}_{LL} + g^{\eta\eta'}_{RR}. \tag{2.72}$$

Lead self-energy

The lead self-energy is given by $\hat{\Sigma}_{L,R}(t,t') = \gamma(t)\gamma(t')\hat{D}_0(t,t')$. For retarded and advanced parts, we then have explicity

$$\begin{aligned} \Sigma^R(t,t') &= \gamma(t)\gamma(t') D^R_0(t,t') = -\mathrm{i}\gamma^2 \theta(t)\theta(t')\theta(t-t') \mathrm{e}^{-\mathrm{i}\Delta(t-t')}, \\ \Sigma^A(t,t') &= \gamma(t)\gamma(t') D^A_0(t,t') = +\mathrm{i}\gamma^2 \theta(t)\theta(t')\theta(t'-t) \mathrm{e}^{-\mathrm{i}\Delta(t-t')}. \end{aligned} \tag{2.73}$$

In addition, we point out that the lead self-energy Σ^{-+}/Σ^{+-} vanishes provided that the dot is initially unpopulated/populated.

2.6 Green's functions for the MRLM

Our task is now to calculate the various Green's functions for the MRLM to be in a position to access its non-equilibrium dynamics. To begin with, we briefly want to outline the demonstration of the free Green's functions, which can be deduced analogously to the last Section. After that, we provide all relevant full Green's functions.

2.6.1 Free lead and dot Majorana Green's functions

To calculate the free Green's functions of the lead Majorana fields, we make use of the decomposition into conventional fermionic operators

$$\xi = \frac{1}{\sqrt{2}}(\psi^\dagger_- + \psi_-), \quad \eta = \frac{\mathrm{i}}{\sqrt{2}}(\psi^\dagger_- - \psi_-), \tag{2.74}$$

which entails

$$\hat{g}_{\xi\xi}(t-t') = -\mathrm{i}\left\langle T_{\mathcal{C}} \xi(t)\xi(t') \right\rangle_0 = -\frac{\mathrm{i}}{2}\left[\left\langle T_{\mathcal{C}} \psi_-(t)\psi^\dagger_-(t') \right\rangle_0 + \left\langle T_{\mathcal{C}} \psi^\dagger_-(t)\psi_-(t') \right\rangle_0 \right]. \tag{2.75}$$

In Fourier space, we therefore have the relation

$$g^{kl}_{\xi\xi}(t-t') = \int \frac{d\omega}{2\pi} e^{-\mathrm{i}\omega(t-t')} \frac{1}{2}\left[g^{kl}_{\psi_-\psi_-}(\omega) - g^{lk}_{\psi_-\psi_-}(-\omega) \right], \tag{2.76}$$

where $g^{kl}_{\psi_-\psi_-}(\omega)$ are free Green's functions of conventional fermions and are given by the components of Eq. (2.43). Using the property of the Fermi function $n_F(\omega) = 1 - n_F(-\omega)$ and introducing left and right Fermi functions $n'_L(\omega) = n_F(\omega - V)$ and $n'_R(\omega) = n_F(\omega + V)$, we get (Schiller and Hershfield [1998], Komnik and Gogolin [2003a])

$$\hat{g}_{\xi\xi}(\omega) = \frac{\mathrm{i}}{2} \begin{pmatrix} n'_L(\omega) + n'_R(\omega) - 1 & n'_L(\omega) + n'_R(\omega) \\ n'_L(\omega) + n'_R(\omega) - 2 & n'_L(\omega) + n'_R(\omega) - 1 \end{pmatrix}, \tag{2.77}$$

where we used the convention $\rho_0 = 1/(2\pi)$. The primes indicate that, instead of choosing the electrodes' real chemical potentials $\mu_{L,R} = \pm V/2$, we have to insert effective ones $\mu'_{L,R} = \pm V$ into the Fermi-Dirac distribution functions (Komnik and Gogolin [2003a]). Analogously, one can easily show that

$$\hat{g}_{\eta\eta}(\omega) = \hat{g}_{\xi\xi}(\omega). \tag{2.78}$$

Additionally, one obtains for the mixed lead Majorana Green's function

$$\hat{g}_{\xi\eta}(\omega) = \frac{1}{2}\left[n'_L(\omega) - n'_R(\omega) \right] \begin{pmatrix} 1 & 1 \\ 1 & 1 \end{pmatrix}, \tag{2.79}$$

whose components are all equal, and which satisfy

$$\hat{g}_{\eta\xi}(\omega) = -\hat{g}_{\xi\eta}(\omega). \tag{2.80}$$

Since we need it later, we calculate the free retarded Green's function for the lead Majoranas.

$$\hat{g}^R_{\xi\xi}(t,t') = -\mathrm{i}\left\langle \{\xi(t), \xi(t')\} \right\rangle \theta(t-t') = -\frac{\mathrm{i}}{2}\int \frac{d\omega}{2\pi} e^{-\mathrm{i}\omega(t-t')}\theta(t-t') = -\frac{\mathrm{i}}{2}\delta(t-t')\theta(t-t'). \tag{2.81}$$

In a similar fashion as above, we start from the decomposition of the local b Majorana fermion

$$b = -\frac{\mathrm{i}}{\sqrt{2}}(d - d^\dagger), \tag{2.82}$$

which directly implies

$$D^{(0)-+}_{bb}(t,t') = -\mathrm{i}\left\langle b(t)b(t') \right\rangle_0 = -\frac{\mathrm{i}}{2}\left[\left\langle d(t)d^\dagger(t') \right\rangle_0 + \left\langle d^\dagger(t)d(t') \right\rangle_0 \right] = -\frac{\mathrm{i}}{2}\mathrm{e}^{\pm\mathrm{i}\Delta(t-t')}. \tag{2.83}$$

The upper/lower sign in the exponent of Eq. (2.83) applies to an initially unoccupied/occupied dot. We can also transform to Fourier space, which yields

$$D^{(0)-+}_{bb}(\omega) = -\mathrm{i}\pi\delta(\omega \pm \Delta). \tag{2.84}$$

For the retarded component, we then obtain

$$D^{(0)R}_{bb}(t-t') = -\mathrm{i}\left\langle \{b(t), b(t')\} \right\rangle_0 \theta(t-t') = -\mathrm{i}\theta(t-t')\cos\left[\Delta(t-t')\right], \tag{2.85}$$

which, in Fourier space, reads

$$D^{(0)R}_{bb}(\omega) = \frac{\omega}{\omega^2 - \Delta^2}. \tag{2.86}$$

2.6.2 Dyson equation and full dot Majorana Green's function

In analogy with the RLM case, it is easiest to write down the Dyson equation for the retarded dot Green's function of the b Majorana fermions. The restriction to the sudden switching scenario then leads to (Komnik [2009])

$$\begin{aligned} D^R_{bb}(t,t') &= D^{(0)R}_{bb}(t-t') + \int_{-\infty}^{\infty} dt_1 \int_{-\infty}^{\infty} dt_2\, D^{(0)R}_{bb}(t-t_1)\Sigma^R(t_1,t_2)D^R_{bb}(t_2,t') \\ &= D^{(0)R}_{bb}(t-t') + \gamma^2 \int_0^{\infty} dt_1 \int_0^{\infty} dt_2\, D^{(0)R}_{bb}(t-t_1) g^R_{\xi\xi}(t_1-t_2) D^R_{bb}(t_2,t'), \end{aligned} \tag{2.87}$$

with the retarded self-energy

$$\Sigma^R(t,t') = \gamma(t)\gamma(t') g^R_{\xi\xi}(t,t') \tag{2.88}$$

and the constituent free Green's functions

$$D^{(0)R}_{bb}(t,t') = -\mathrm{i}\theta(t-t')\cos\left[\Delta(t-t')\right], \quad g^R_{\xi\xi}(t,t') = -\frac{\mathrm{i}}{2}\delta(t-t')\theta(t-t'). \tag{2.89}$$

With the definition of the integral equation kernel

$$\begin{aligned} \Gamma\, K(t-t_2) &= \gamma^2 \int_0^{\infty} dt_1\, D^{(0)R}_{bb}(t,t_1) g^R_{\xi\xi}(t_1,t_2) \\ &= -\Gamma\, \theta(t-t_2)\cos\left[\Delta(t-t_2)\right], \end{aligned} \tag{2.90}$$

the Dyson equation then reads

$$D^R_{bb}(t,t') = D^{(0)R}_{bb}(t-t') + \Gamma \int_0^t dt_2\, K(t-t_2) D^R_{bb}(t_2,t'). \tag{2.91}$$

Owing to its retarded nature, the full dot Green's function $D^R_{bb}(t,t')$ can be written as

$$D^R_{bb}(t,t') = -\mathrm{i}\theta(t-t') f(t,t'), \tag{2.92}$$

with

$$f(t,t') = \cos\left[\Delta(t-t')\right] - \Gamma \int_{t'}^{t} d\tau\, \cos\left[\Delta(t-\tau)\right] f(\tau,t'). \tag{2.93}$$

Thus, the remaining task is to solve the following equation for $f(t,t')$. This is a Volterra integral equation of the second kind solvable by means of the Laplace transformation. It is an equation of the form

$$f(t,t') = f^{(0)}(t-t') - \Gamma \int_{t'}^{t} d\tau\, f^{(0)}(t-\tau) f(\tau,t'). \tag{2.94}$$

One can show by iterations that the solution must be of the translationally invariant form $f(t,t') = f(t-t')$. In a sense, the Laplace transformation defined as

$$F(s) = \int_0^{\infty} e^{-st} f(t), \;\; s \in \mathbb{C} \tag{2.95}$$

generalizes the Fourier transformation. The image function of $f^{(0)}(t) = \cos(\Delta t)$ is given by $F^{(0)}(s) = s/(s^2 + \Delta^2)$. In image space, the integral equation thus reduces to an algebraic equation that can be solved straightforwardly, so that

$$F(s) = \frac{s}{s^2 + \Delta^2 + \Gamma s}. \tag{2.96}$$

Computation of the original yields

$$f(t) = \frac{e^{-\frac{\Gamma t}{2}}}{2\Omega'} \left[\left(\Omega' - \frac{\Gamma}{2} \right) e^{\Omega' t} + \left(\Omega' + \frac{\Gamma}{2} \right) e^{-\Omega' t} \right] \tag{2.97}$$

with $\Omega' = \sqrt{(\Gamma/2)^2 - \Delta^2}$.
To calculate the lesser Green's function $D_{bb}^{-+}(t, t')$, we start from the matrix Dyson equation in the conventional representation for our choice $\gamma_- = 0$,

$$\hat{D}_{bb}(t, t') = \hat{D}_{bb}^{(0)}(t, t') + \int_0^\infty dt_1 \int_0^\infty dt_2 \, \hat{D}_{bb}^{(0)}(t, t_1) \hat{\Sigma}(t_1, t_2) \hat{D}_{bb}(t_2, t'). \tag{2.98}$$

The self-energy matrix $\hat{\Sigma}(t, t')$ is connected to the free ξ Majorana Green's function via

$$\hat{\Sigma}(t, t') = \gamma(t)\gamma(t')\hat{\sigma}_3 \hat{g}_{\xi\xi}(t, t')\hat{\sigma}_3. \tag{2.99}$$

Later, we shall also need the retarded and advanced self-energies given by

$$\Sigma^R(t, t') = -\mathrm{i}\Gamma\delta(t - t')\theta(t - t') = -\Sigma^A(t', t). \tag{2.100}$$

Stationary case

In the steady state, all Green's functions only depend on the time difference $t - t'$. This allows for a transformation to Fourier space. After that, we can solve the matrix equation for $\hat{D}_{bb}$,

$$\hat{D}_{bb}(\omega) = \left[1 - \gamma^2 \hat{D}_{bb}^{(0)}(\omega)\sigma_3 \hat{g}_{\xi\xi}(\omega)\sigma_3 \right]^{-1} \hat{D}_{bb}^{(0)}(\omega). \tag{2.101}$$

Time-dependent case

In order to compute $D_{bb}^{-+}(t, t')$ in a general transient scenario, we follow the recipe of the RLM calculation by applying the version of the Langreth formula Eqs. (2.60) and (2.61),

$$\begin{aligned} D^{-+}(t, t') &= \left[(1 + D^R\Sigma^R) D^{(0)-+} (1 + \Sigma^A D^A) \right](t, t') + \left[D^R \Sigma^{-+} D^A \right](t, t') \\ &= D^{(0)-+}(t, t') + \left[D^R \Sigma^R D^{(0)-+} \right](t, t') + \left[D^{(0)-+} \Sigma^A D^A \right](t, t') \\ &\quad + \left[D^R \Sigma^R D^{(0)-+} \Sigma^A D^A \right](t, t') + \left[D^R \Sigma^{-+} D^A \right](t, t'), \end{aligned} \tag{2.102}$$

where, as usual, multiple time integrations are implicitly assumed. This expression has to be evaluated term by term. Compared with the RLM, the calculation here is more involved. This complication arises because neither for an empty nor for an occupied quantum dot does one of the free Majorana Green's functions $D_{bb}^{(0)-+}$ or $D_{bb}^{(0)+-}$ vanish.

2.6.3 Full mixed Majorana Green's functions

To derive all required relations, we use the standard definition of the $\mathcal{S}$ matrix

$$\begin{aligned}\mathcal{S}_{\mathcal{C}} &= T_{\mathcal{C}} \exp\left[-\mathrm{i}\int_{\mathcal{C}} ds\, V_I(s)\right] \\ &= T_{\mathcal{C}} \exp\left[-\int_{\mathcal{C}} ds\, \gamma(s) b(s) \xi(s)\right].\end{aligned} \tag{2.103}$$

We proceed along the lines of the RLM case to deduce the mixed Green's functions by expansion of the $\mathcal{S}$ matrix followed by re-exponentiation. As we will see later, the necessary Green's functions to calculate current and noise in the MRLM are those listed in the following. As a result, we obtain

$$\begin{aligned}\hat{G}_{b\eta}(t,t') &= -\mathrm{i}\gamma \int_{\mathcal{C}} ds \left[\hat{D}_{bb}(t,s)\hat{g}_{\xi\eta}(s,t') - \hat{G}_{b\xi}(t,s)\hat{g}_{b\eta}(s,t')\right] \\ &= -\mathrm{i}\gamma \int_{\mathcal{C}} ds\, \hat{D}_{bb}(t,s)\hat{g}_{\xi\eta}(s,t'),\end{aligned} \tag{2.104}$$

where, in the last line, we used the fact that $\hat{g}_{b\eta}$ vanishes as it describes tunneling in the case of an uncoupled dot-lead system. We have already shown that all components of the matrix $\hat{g}_{\xi\eta}$ are equal. Performing the Keldysh disentanglement, this leads to the further simplification

$$\begin{aligned}G^{lm}_{b\eta}(t,t') &= -\mathrm{i}\gamma \int_0^\infty ds \left[D^{l-}_{bb}(t,s) g^{-m}_{\xi\eta}(s,t') - D^{l+}_{bb}(t,s) g^{+m}_{\xi\eta}(s,t')\right] \\ &= -\mathrm{i}\gamma \int_0^\infty ds \left[\left(D^{l-}_{bb}(t,s) - D^{l+}_{bb}(t,s)\right) g^{-k}_{\xi\eta}(s,t')\right] \\ &= -\mathrm{i}\gamma \int_0^\infty ds\, D^{R}_{bb}(t,s) g^{-k}_{\xi\eta}(s,t').\end{aligned} \tag{2.105}$$

We thus arrive at the conclusion that all components of $\hat{G}_{b\eta}(t,t')$ are identical. We can now carry out an analogous calculation, giving

$$\hat{G}_{\eta b}(t,t') = \mathrm{i}\gamma \int_{\mathcal{C}} ds\, \hat{g}_{\eta\xi}(t,s)\hat{D}_{bb}(s,t') \tag{2.106}$$

with its components

$$G^{lm}_{\eta b}(t,t') = \mathrm{i}\gamma \int_0^\infty ds\, g^{-+}_{\eta\xi}(t,s) D^{A}_{bb}(s,t'). \tag{2.107}$$

We can draw the same conclusion that all components of $\hat{G}_{\eta b}(t,t')$ are equal. This directly implies that the corresponding retarded and advanced Green's functions vanish, that is,

$$G^{R}_{b\eta}(t,t') = G^{R}_{\eta b}(t,t') = G^{A}_{b\eta}(t,t') = G^{A}_{\eta b}(t,t') = 0. \tag{2.108}$$

2.6.4 Full lead Majorana Green's functions

Since we assume symmetric coupling, which means that the η Majorana field does not couple to the local Majoranas, we immediately anticipate that we have the identification

$$\hat{G}_{\eta\eta}(t,t') = \hat{g}_{\eta\eta}(t,t'), \tag{2.109}$$

which is confirmed by an explicit calculation. In fact, starting from

$$\hat{G}_{\eta\eta}(t,t') = \hat{g}_{\eta\eta}(t,t') + \mathrm{i}\gamma \int_{\mathcal{C}} ds\, \hat{G}_{\eta b}(t,s)\hat{g}_{\xi\eta}(s,t'), \tag{2.110}$$

it follows that

$$G^{lm}_{\eta\eta}(t,t') = g^{lm}_{\eta\eta}(t,t') + \mathrm{i}\gamma \int ds\, \left[g^{l-}_{\eta\xi}(t,s)G^{-m}_{b\eta}(s,t') - g^{l+}_{\eta\xi}(t,s)G^{+m}_{b\eta}(s,t')\right] = g^{lm}_{\eta\eta}(t,t'). \tag{2.111}$$

The last equality of Eq. (2.111) results from the fact that the second summand vanishes due to the identities Eqs. (2.79), (2.105) and (2.107) deduced previously.

Chapter 3

Transient noise spectra in resonant tunneling structures

This chapter is devoted to the main results of this thesis, namely the transient current noise evolution in the setups introduced in Chapter 2 with a clear emphasis on the resonant level model, for which the problem is solved both at zero and finite temperature. In addition, the transient current noise at zero temperature is then calculated for the Majorana resonant level model to test if the results also hold true in case of a simple interacting model. This confirmation provides the basis to investigate further more complicated models which, however, is beyond the scope of this thesis. We conclude this chapter with the presentation of preliminary steps to tackle the problem of transient heat noise in the resonant level model.

3.1 Transport properties of mesoscopic systems

The complete information for the characterization of the charge transport through nanostructures is incorporated in the probability distribution $P(Q)$ of the charge passing through a given region in a fixed time interval. This information is equivalently encoded in the Full Counting Statistics, hereafter abbreviated by FCS, which is indeed the characteristic function of $P(Q)$. Its successive derivatives provide all relevant transport quantities: the current, the noise, the skewness and all higher cumulants of the probability distribution. It is thus advantageous to compute or measure the cumulant generating function (CGF). To date only the CGF for a steady state situation is available in many cases though. To the best of our knowledge, even for the non-interacting resonant level model, the time-dependent CGF has not been successfully attacked so far. Instead, in this thesis, we directly pursue the exact calculation of the transient finite frequency quantum noise in case of the sudden switching on of the tunneling coupling for both a non-interacting and an interacting model. Not only can this be considered as a first step toward the establishment of the complete time-dependent FCS, but quantum noise in its own right can reveal new signatures not contained in the current. Before proceeding with the main topic of this thesis, namely transient current noise, we first calculate transport quantities of interest that are more easily accessible. These are the dot occupation and the current which we want to compare with the noise evolution, calculated later.

3.2 Currents in the RLM and the MRLM

3.2.1 Transient current in the RLM

In this section, we want to apply the Green's function formalism to calculate the evolution of the transient current after an abrupt switching on of the tunneling coupling with the electrodes kept at fixed chemical potential difference $\mu_L - \mu_R = V > 0$ (see Schmidt et al. [2008]).

Left and right currents

The current operator is defined as follows

$$\hat{I}_\alpha(t) = -\frac{d\hat{Q}_\alpha(t)}{dt} = \mathrm{i}\left[\hat{Q}_\alpha, H\right] = \mathrm{i}\gamma(t)\left[\psi_\alpha^\dagger(t)d(t) - d^\dagger(t)\psi_\alpha(t)\right] = \mathrm{i}\gamma\theta(t)\left[\psi_\alpha^\dagger(t)d(t) - d^\dagger(t)\psi_\alpha(t)\right], \tag{3.1}$$

where $\hat{Q}_\alpha$ is the charge operator for lead α. Taking the expectation value, we obtain

$$I_\alpha(t) = \left\langle \hat{I}_\alpha(t)\right\rangle = \mathrm{i}\gamma(t)\left[\left\langle\psi_\alpha^\dagger(t)d(t)\right\rangle - \left\langle d^\dagger(t)\psi_\alpha(t)\right\rangle\right] = \gamma(t)\left[G_{d\alpha}^{-+}(t,t) - G_{\alpha d}^{-+}(t,t)\right]. \tag{3.2}$$

Thus, the calculation reduces to two lesser Green's functions at equal times determined by Eqs. (2.64) and (2.65), yielding

$$I_\alpha(t) = 2i\pi\rho_0\gamma^2 D^{-+}(t,t')\Big|_{t=t'} + \gamma^2\left\{\int dt_1\left[D^R(t,t_1)g_{\alpha\alpha}^{-+}(t_1,t') - g_{\alpha\alpha}^{-+}(t,t_1)D^A(t_1,t')\right]\right\}\Big|_{t=t'}. \tag{3.3}$$

After insertion of the respective functions, we obtain the following result valid for $t > 0$,

$$I_\alpha(t) = -\frac{\Gamma^2}{2\pi}\int d\omega\ \frac{n_L(\omega)+n_R(\omega)}{(\omega-\Delta)^2+\Gamma^2}\left\{1 + \mathrm{e}^{-2\Gamma t} - 2\mathrm{e}^{-\Gamma t}\cos\left[(\omega-\Delta)t\right]\right\}$$
$$+ \frac{1}{2\pi}\int d\omega\, n_\alpha(\omega)\left\{\frac{2\Gamma^2}{(\omega-\Delta)^2+\Gamma^2} - 2\Gamma\mathrm{e}^{-\Gamma t}\frac{\Gamma\cos\left[(\omega-\Delta)t\right] - (\omega-\Delta)\sin\left[(\omega-\Delta)t\right]}{(\omega-\Delta)^2+\Gamma^2}\right\}. \tag{3.4}$$

For equal hybridizations $\Gamma = \Gamma_L = \Gamma_R$, the left and right currents are obviously related by symmetry,

$$I_R(V,t) = -I_L(-V,t). \tag{3.5}$$

For the sudden switching on of the tunneling, the left current has a discontinuity at $t = 0$, which is equal to the limit of infinite voltage, and is given by

$$I_L(0) = \int\frac{d\omega}{2\pi}\frac{\Gamma^2}{(\omega-\Delta)^2+\Gamma^2} = \frac{\Gamma}{2} = \lim_{V\to+\infty} I_L(t), \tag{3.6}$$

This physically counterintuitive result can be explained by the fact that we used the wide flat band limit throughout our calculations: Each electron in the left band can populate the initially unoccupied dot with equal probability and the infinite bandwidth implies that there are electrons with arbitrarily high energies, which leads to an immediate onset of the left current.

Total current

The total transient current through the dot-lead structure then follows as (Schmidt et al. [2008])

$$I(V,t) = \frac{1}{2}\left[I_L(V,t) - I_R(V,t)\right] = \frac{1}{2}\left[I_L(V,t) - I_L(-V,t)\right]. \tag{3.7}$$

Inserting the respective Green's functions yields the compact formula

$$I(V,t) = \frac{1}{2\pi}\int d\omega\left[n_L(\omega) - n_R(\omega)\right]\mathcal{T}(\omega,t) \tag{3.8}$$

with the time-dependent transmission coefficient

$$\mathcal{T}(\omega,t) = \frac{\Gamma^2 - \Gamma e^{-\Gamma t}(\Gamma\cos\left[(\omega-\Delta)t\right] - (\omega-\Delta)\sin\left[(\omega-\Delta)t\right])}{(\omega-\Delta)^2+\Gamma^2} \tag{3.9}$$

for the case of an initially empty dot. The factor $n_L(\omega) - n_R(\omega)$ in Eq. (3.8) reflects the fact that contributions to the total current can only come from those electrons having an energy between the two Fermi edges since an electron from the left lead can tunnel only to an empty state in the right lead. The observed exponential damping accompanied by oscillations of the current is due to the time-dependent effective transmission coefficient and can be illustrated by an intuitive picture. At first, when the dot is decoupled from the leads, its spectral function is represented by a Dirac δ-function. Sudden switching on of the tunneling coupling provokes the onset of the current. The hybridization Γ then defines a measure of an escape rate of electrons, which therefore determines the speed of approaching the steady state and appears as the damping constant. Obviously, this quantity also characterizes the width of the spectral function in this new steady state, which has a Lorentzian profile centered around the dot level energy. This profile can be made plausible if one considers that only lead electrons with exactly the same energy as the dot level are perfectly transmitted through the constriction. All other electrons have probability amplitudes smaller than unity to jump to the dot and then to pass to the other lead or to return to the original lead. The available paths for an electron to attain the right reservoir leads to a quantum mechanical interference phenomenon, which is analogous to that of a double-barrier structure such as a Fabry-Pérot interferometer in the limit of vanishing length. The intermediate oscillations result from the fact that, initially, after the abrupt switching on of the tunneling, electrons from both leads attempt to occupy the dot with probability amplitudes $\propto \mathrm{e}^{\pm\mathrm{i}(\omega-\Delta)t}$. The interference of these processes entails oscillatory contributions to the transient current whose individual frequencies thus scale with the energy difference between a given electron in the lead and the dot level.

Displacement current and dot occupation

Another quantity to mention is the displacement current which is defined as the derivative of the dot occupancy with respect to time. This type of current reflects charge conservation in the system fulfilling (Langreth and Nordlander [1991])

$$I_{\mathrm{disp}}(V,t) = \frac{\partial n_d(t)}{\partial t} = -\frac{\partial n_L(t)}{\partial t} - \frac{\partial n_R(t)}{\partial t} = I_L(V,t) + I_R(V,t) = I_L(V,t) + I_L(-V,t) \tag{3.10}$$

and is connected to previously calculated quantities as

$$I_{L/R}(V,t) = \frac{I_{\mathrm{disp}}(V,t)}{2} \pm I_{\mathrm{tot}}(V,t). \tag{3.11}$$

In fact, we can check if the dot Green's function was calculated correctly as it is related to the transient dot occupation $n(t) = -\mathrm{i}D^{-+}(t,t)$. Setting $t = t'$ in the above formula for $D^{-+}(t,t')$ yields

$$n(t) = \frac{\Gamma}{2\pi}\int d\omega \frac{[n_L(\omega)+n_R(\omega)]}{(\omega-\Delta)^2+\Gamma^2}\left(1 - e^{(\mathrm{i}(\omega-\Delta)-\Gamma)t} - e^{(-\mathrm{i}(\omega-\Delta)-\Gamma)t} + e^{-2\Gamma t}\right), \tag{3.12}$$

which has already been established previously in Schmidt et al. [2008]. In this formula, we can identify similar terms as for the total current, which means that the damping is characterized by the tunneling coupling Γ and the oscillations at zero temperature are determined by the frequencies $\Delta \pm V/2$.

3.2.2 Transient current in the MRLM

The transient evolution of the current with restriction to the case of symmetric coupling to both leads was calculated in an earlier work (Komnik [2009]). Instead of repeating the individual steps here, we would like to present the main results in comparison to the conventional resonant level model. In addition, this serves as a precursor of our discussion about noise below. First, there are two distinct regimes – one of *strong* detuning and one of *weak* detuning, characterized by $|\Delta| > \Gamma/2$ and $|\Delta| < \Gamma/2$, respectively. In the former case, a beating pattern with the frequencies $|V \pm \Omega'|$ can be observed during the transient regime which is absent in the latter. To find an intuitive picture to contrast this result with the RLM case, we split the tunneling operator given by Eq. (2.25) for symmetric coupling into conventional fermions to obtain

$$\hat{I} \propto d\psi_-^\dagger + d^\dagger\psi_- - d^\dagger\psi_-^\dagger - d\psi_-. \tag{3.13}$$

We recognize that the last two terms, which are not present in the RLM tunneling operator, are reminiscent of superconducting correlations describing Josephson-type tunneling processes. We speculate that the interference between these and the conventional tunneling processes alters the resonant level physics at strong detuning and is thus responsible for the beating.

3.3 Current noise

In contrast to the intuitive nature of current flowing through a conductor, one has a certain degree of freedom in defining the time-dependent current noise spectrum $S(\Omega)$ in a full quantum treatment of a transient problem. We use the following, rather general definition which is directly related to the conventional noise definition in the steady state (Blanter and Büttiker [2000])

$$S(\Omega) = \int_\Sigma d(t-t')\,\mathrm{e}^{\mathrm{i}\Omega(t-t')}S(t,t'), \tag{3.14}$$

with the irreducible current-current correlation function

$$S(t,t') = \left\langle \hat{I}(t)\hat{I}(t')\right\rangle - \left\langle \hat{I}(t)\right\rangle\left\langle \hat{I}(t')\right\rangle, \tag{3.15}$$

which quantifies the fluctuations accompanying the current flow. Σ denotes the domain in the space of time differences $t - t'$ in which information about the current correlations is available. In the most obvious case of the stationary state $\Sigma = (-\infty, \infty)$ and the current correlation function depends on $t - t'$ only. Therefore the noise as defined in Eq. (3.14) is time independent. In general $S(\Omega)$ is a time-dependent quantity though, as we shall see later. We can express Eq. (3.15) in terms of current cross correlators between different leads α and β

$$S_{\alpha\beta}(t,t') = \left\langle \hat{I}_\alpha(t)\hat{I}_\beta(t') \right\rangle - \left\langle \hat{I}_\alpha(t) \right\rangle \left\langle \hat{I}_\beta(t') \right\rangle \tag{3.16}$$

so that we obtain the decomposition

$$S(t,t') = \frac{1}{4} \sum_{\alpha,\beta=L,R=\pm} (\alpha\beta)\, S_{\alpha\beta}(t,t'). \tag{3.17}$$

Throughout this thesis, we consider the sudden switching on of the tunneling of the form $\gamma(t) = \gamma\theta(t)$, where $\theta(t)$ is the Heaviside step function. The substitution of new variables $\tau \equiv t - t'$ and $T \equiv t + t'$, measured in units of Γ^{-1}, effectively restricts the integration range from $-T$ to T and finally leads to the *transient* noise formula emphasizing the explicit time dependence,

$$S(\Omega, T) = \int_{-T}^{+T} d\tau\, \mathrm{e}^{\mathrm{i}\Omega\tau} S(\tau, T)\,, \tag{3.18}$$

which has to be evaluated for our two cases. The unit of current noise is given by $\pi^2\Gamma G_0^2$, where $G_0 = 2e^2/h$ is the conductance quantum. In a steady state, all Green's functions only exhibit a dependence on the time difference τ. Thus, we can immediately carry out the τ integration to access the stationary solution, which has to be equal to the transient noise in the limit of infinite time T,

$$S^{\mathrm{stat}}(\Omega) = \lim_{T\to\infty} \int_{-T}^{+T} d\tau\, \mathrm{e}^{\mathrm{i}\Omega\tau} S(\tau, T). \tag{3.19}$$

This relation serves as a consistency check of our results. One particular advantage of the definition (3.18) is that it can be easily applied to the experimental data in the form of time-dependent current traces as presented in Gustavsson et al. [2006]. Nonetheless, the solution of the transient problem as shown below can be very efficiently adopted to any other definition of the transient current as well.

3.4 Noise in the RLM

3.4.1 Adiabatic noise and transient current evolution

Before approaching the problem rigorously, we attempt an approximate calculation of the zero temperature current noise by assuming that it follows the transient current adiabatically. This *ad hoc* approach can only work well when the corresponding switch-on time τ_{sw} is much larger than the typical time scale of the current evolution, which is proportional to $1/\Gamma$. Nonetheless, we would like to look into the sudden switching case $\tau_{\mathrm{sw}} = 0$ to obtain a qualitative picture of what might happen to the transient noise. To achieve our goal, we insert the effective *time-dependent* transmission coefficient for the initially empty dot from the transient current formula, given by Eq. (3.9) into the generalization of the Schottky formula (Schottky [1918])

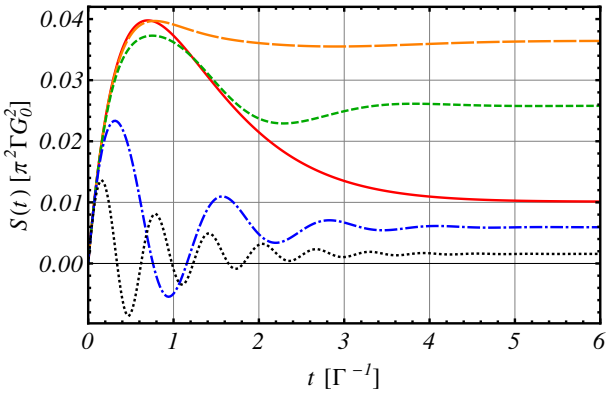

Figure 3.1: Adiabatic noise evolution at fixed voltage $V/\Gamma = 1$ and zero frequency $\Omega/\Gamma = 0$ for varying $|\Delta|/\Gamma = 0, 1, 2, 5, 10$ (red solid, orange long-dashed, green short-dashed, blue dot-dashed, and black dotted curves), computed with formula (3.20).

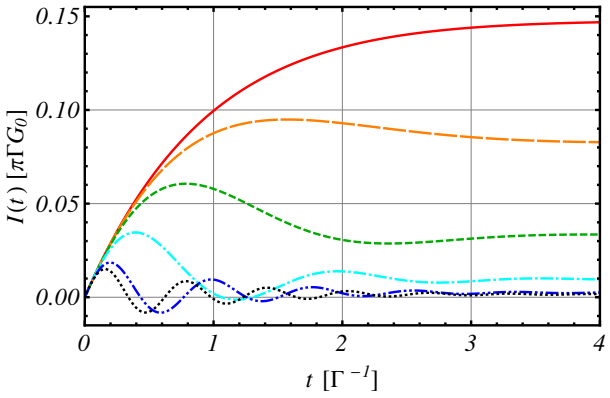

Figure 3.2: Transient current at voltage $V/\Gamma = 1$ for various detunings $|\Delta|/\Gamma = 0, 1, 2, 4, 8, 10$ (red solid, orange long-dashed, green short-dashed, cyan dot-dashed, blue double-dot-dashed, and black dotted curves), calculated with formula (3.8).

for zero-temperature, zero-frequency (shot) noise in a steady state with an energy-dependent transmission coefficient (Khlus [1987], Lesovik [1989]), which is nothing more than the second cumulant of the corresponding charge transfer probability distribution. Then, we obtain the adiabatic noise evolution as

$$S^{\mathrm{adia}}(\Omega = 0, t) = \int_{-V/2}^{+V/2} \frac{d\omega}{2\pi} \mathcal{T}(\omega, t) \left[1 - \mathcal{T}(\omega, t)\right] . \tag{3.20}$$

The function $S^{\mathrm{adia}}(t)$ is symmetric with respect to both voltage and dot level energy Δ and contains only the difference between the left and right Fermi functions. In general, the time dependence shows up oscillatory behavior with frequencies $V/2 \pm \Delta$. On the contrary, the envelope is exponential in time so that the stationary value is reached after a time proportional to $1/\Gamma$. Of course, this might be just an artifact of our approximation. That is why we would like to attempt an exact analytical solution of the problem below. An important point is that for a large enough absolute value of the detuning $|\Delta|$, the current noise according to our definition becomes negative, which is depicted in Fig. 3.1. This peculiar feature, which persists for the transient case to be studied below, has not been reported in the literature so far.
We briefly want to turn our attention to the total transient current which shares this property, illustrated in Fig. 3.2. It is due to the fact that the effective transmission coefficient $\mathcal{T}(\omega, t)$ can become negative. Although a net charge backflow at intermediate times seems to be counter-intuitive at first sight, it can be made plausible since both Fermi levels appear to be almost at the same height in the case of strong detuning (i.e., when Δ represents the largest energy scale of all adjustable parameters). Of course, this property also applies individually to both the left and the right currents. Just after switching on of tunneling the electrons of both leads start to populate the initially empty dot and at the very beginning both I_L *and* I_R have the same sign. Due to the very high energy difference $|\Delta|$ on very short time scales an overpopulation occurs. After that the current signs change and a negative net current can be observed for a short time interval. *Negative transient current* has already been discussed by the authors of Zhu et al. [2005] and Maciejko et al. [2006], but in these works, it arises only if the bandwidth of the leads is small enough, whereas in our case, the bandwidth is taken to be infinite.
Other adiabatic schemes for the approximate computation of transient noise have already been

proposed previously (see, for example, Moskalets and Büttiker [2007] and references therein).

3.4.2 Transient noise evolution

We now want to study the transient behavior of current noise at finite frequency in its most general form. We compare our results with a steady state calculation at finite frequency corroborated by an FCS calculation at zero frequency (see Rothstein et al. [2009]). In addition, we provide compact formulas for various limiting cases at zero temperature. The method of choice is the non-equilibrium Keldysh Green's function technique introduced in Section 2.4 as it provides an intuitive physical picture for every single constituent of relevant equations. As a cross check we performed the same computation using the functional integration technique and obtained precisely the same results. The substitution of our current operator Eq. (2.6) into Eq. (3.16) leads to the expression

$$\begin{aligned} S_{\alpha\beta}(t,t') = \gamma(t)\gamma(t')\Big(&\left\langle d^\dagger(t)\psi_\alpha(t)\psi^\dagger_\beta(t')d(t')\right\rangle + \left\langle \psi^\dagger_\alpha(t)d(t)d^\dagger(t')\psi_\beta(t')\right\rangle \\ &- \left\langle d^\dagger(t)\psi_\alpha(t)d^\dagger(t')\psi_\beta(t')\right\rangle - \left\langle \psi^\dagger_\alpha(t)d(t)\psi^\dagger_\beta(t')d(t')\right\rangle - \left\langle I_\alpha(t)\right\rangle \left\langle I_\beta(t')\right\rangle \Big). \end{aligned} \tag{3.21}$$

A natural choice consists of assigning times t and t' to different branches of the Keldysh contour. The transformation of the operators to a diagonal basis and back, which is equivalent to the application of Wick's theorem, then yields (Rammer [2007], Langreth [1976])

$$\begin{aligned} S_{\alpha\beta}(t_+,t'_-) = \gamma(t)\gamma(t')\big[&G^{-+}_{dd}(t',t)G^{+-}_{\alpha\beta}(t,t') + G^{-+}_{\beta\alpha}(t',t)G^{+-}_{dd}(t,t') \\ &- G^{-+}_{d\alpha}(t',t)G^{+-}_{d\beta}(t,t') - G^{-+}_{\beta d}(t',t)G^{+-}_{\alpha d}(t,t')\big]. \end{aligned} \tag{3.22}$$

Combining the various cross correlators and collecting different contributions, the complete current correlation function reads

$$\begin{aligned} S(t,t') = \frac{\gamma(t)\gamma(t')}{4}\Big\{ &D^{-+}(t',t)\left[G^{+-}_{LL}(t,t') + G^{+-}_{RR}(t,t') - G^{+-}_{LR}(t,t') - G^{+-}_{RL}(t,t')\right] \\ &+ \left[G^{-+}_{LL}(t',t) + G^{-+}_{RR}(t',t) - G^{-+}_{LR}(t',t) - G^{-+}_{RL}(t',t)\right] D^{+-}(t,t') \\ &- \left[G^{-+}_{dL}(t',t) - G^{-+}_{dR}(t',t)\right]\left[G^{+-}_{dL}(t,t') - G^{+-}_{dR}(t,t')\right] \\ &- \left[G^{-+}_{Ld}(t',t) - G^{-+}_{Rd}(t',t)\right]\left[G^{+-}_{Ld}(t,t') - G^{+-}_{Rd}(t,t')\right]\Big\}. \end{aligned} \tag{3.23}$$

Using the relations between different Green's functions derived in Chapter 2, we finally obtain the irreducible current-current correlation function

$$S(t,t') = \frac{1}{4}\left[S_1(t,t') + S_2(t,t')\right], \tag{3.24}$$

where we defined

$$S_1(t,t') = D^{-+}(t',t)\Sigma_+^{+-}(t,t') + \Sigma_+^{-+}(t',t)D^{+-}(t,t') \tag{3.25}$$

and

$$S_2(t,t') = -2\cdot \mathrm{Re}\left[\int dt_1 D^R(t',t_1)\Sigma_-^{-+}(t_1,t)\int dt_2 D^R(t,t_2)\Sigma_-^{-+}(t_2,t')\right]. \tag{3.26}$$

It has to be noted that this formula splits into two major parts. $S_1(t,t')$ involves the *sums* of Fermi functions and depends on the initial dot occupation while $S_2(t,t')$ contains the *differences* of Fermi functions and is insensitive to the initial preparation of the system. In our noise calculations, we first evaluate the time integral to get a formula which explicitly contains the Fermi functions and thus applies at arbitrary temperatures. We then restrict ourselves to zero temperature and give the quite lengthy result in Appendix C. The energy integrals of the first part $S_1(\Omega,T)$ then have $-\infty$ as a lower boundary owing to the wide flat band limit, whereas the corresponding integrations in the second part $S_2(\Omega,T)$ are performed on compact supports. The complete finite temperature result is provided in Appendix D. As an initial condition, we choose an empty dot.

Steady state solution

We want to check our results by calculating the steady state noise independently and comparing it later with the limit $T\to\infty$ of the transient noise. In the following, we want to derive a formula for steady state noise explicitly starting from Eq. (3.14). Taking advantage of time-translation invariance and transforming to Fourier space leads to

$$S_{\alpha\beta}^{\mathrm{stat}}(\Omega) = \gamma^2\int\frac{d\omega}{2\pi}\int\frac{d\omega'}{2\pi}\int d\tau\,\mathrm{e}^{\mathrm{i}(\Omega+\omega-\omega')\tau}\Big[D^{-+}(\omega)G_{\alpha\beta}^{+-}(\omega') + G_{\beta\alpha}^{-+}(\omega)D^{+-}(\omega') - G_{d\alpha}^{-+}(\omega)G_{d\beta}^{+-}(\omega') - G_{\beta d}^{-+}(\omega)G_{\alpha d}^{+-}(\omega')\Big] \tag{3.27}$$

Using the identity

$$\int d\tau\, e^{i(\Omega+\omega-\omega')\tau} = 2\pi\,\delta(\Omega+\omega-\omega'), \tag{3.28}$$

we obtain the following analytical formula after carrying out one energy integral

$$S_{\alpha\beta}^{\mathrm{stat}}(\Omega) = \gamma^2\int\frac{d\omega}{2\pi}\Big[D^{-+}(\omega)G_{\alpha\beta}^{+-}(\omega+\Omega) + G_{\beta\alpha}^{-+}(\omega)D^{+-}(\omega+\Omega) - G_{d\alpha}^{-+}(\omega)G_{d\beta}^{+-}(\omega+\Omega) - G_{\beta d}^{-+}(\omega)G_{\alpha d}^{+-}(\omega+\Omega)\Big]. \tag{3.29}$$

Unlike in the time-dependent case, the Green's functions of Eq. (3.29) are easily accessible and are obtained by inverting the corresponding Dyson equation in matrix form. Using another

formalism, the steady state noise spectrum for the RLM has first been calculated in Rothstein et al. [2009] and Orth et al. [2012], which is in excellent agreement with our result. We note in passing that, in comparison to our graphs, the authors of the aforementioned references obtained mirrored noise spectra with respect to Ω on account of their slightly different definition of the Fourier transformation. Carrying out explicitly the remaining integral as has been done by Orth et al. [2012] for the case of zero temperature, we deduce

$$\begin{aligned} S^{\mathrm{stat}}(\Omega) =& \frac{\Gamma}{2\pi} \sum_{\sigma,\sigma'=\pm} \left\{ \frac{\Gamma}{\Omega} \ln \left[\frac{(V/2+\sigma'\Delta+\sigma\Omega)^2+\Gamma^2}{(V/2+\sigma'\Delta)^2+\Gamma^2} \right] \theta_-(\Omega,\sigma V) \right. \\ &\left. + \sigma \left[\arctan\left(\frac{V/2+\sigma'\Delta+\sigma\Omega}{\Gamma} \right) + \arctan\left(\frac{V/2+\sigma'\Delta}{\Gamma} \right) \right] \theta_+(\Omega,\sigma V) \right\}, \end{aligned} \tag{3.30}$$

with the definitions

$$\begin{aligned} \theta_-(x,y) &= \theta(x) - \theta(y+x), \\ \theta_+(x,y) &= \theta(x) + \theta(y+x). \end{aligned} \tag{3.31}$$

We observe that this function is non-differentiable at $\Omega = 0$. After a straightforward calculation, we arrive at the following discontinuity of its derivative

$$\begin{aligned} \delta S' &= \lim_{\Omega\to 0^+} \frac{\partial S^{\mathrm{stat}}(\Omega)}{\partial\Omega} - \lim_{\Omega\to 0^-} \frac{\partial S^{\mathrm{stat}}(\Omega)}{\partial\Omega} \\ &= \frac{1}{2\pi} \sum_{\sigma=\pm} \left(\frac{\Gamma^2}{(\Delta+\sigma V/2)^2+\Gamma^2} \right)^{2-\delta_{V,0}}, \end{aligned} \tag{3.32}$$

where we used the Kronecker symbol $\delta_{i,j}$. This formula will be helpful in our discussion about transient noise below. As an additional check, we then specialize to the case $\Omega = 0$, which indeed yields the same stationary result as an independent derivation from the cumulant generating function presented in Appendix F.

Limiting cases

For the zero-temperature shot noise, we give compact, analytical formulas for various limiting cases by holding all other quantities fixed. The only terms that contribute are those of $S_1(\Omega, T)$. For $V \to \pm\infty$, we obtain

$$\lim_{V\to\pm\infty} S(\Omega,T) = \frac{\Gamma}{4}, \tag{3.33}$$

which is accompanied by the saturation of the total current through the constriction at high voltage,

$$\lim_{V\to\pm\infty} \langle I(t)\rangle = \pm\frac{\Gamma}{2}. \tag{3.34}$$

These two limits do not display any time dependence. It should be mentioned that this is generally not expected in a model with finite bandwidth ϵ_c, where the short time scale behavior of the transient current is dominated by oscillations with a period of $1/\epsilon_c$ (Schmidt et al. [2008]). For $T \to 0$, we have an offset

$$\lim_{T\to 0} S(\Omega, T) = \frac{\Gamma}{4}. \tag{3.35}$$

This limit can be linked to the $V \to \pm\infty$ case, which is the same, and could thus be interpreted as tunneling into vacuum. It is interesting to investigate how the definite choice of the switch-on function affects the onset of noise at $T = 0$. For an arbitrary switching procedure $\gamma(t) = \gamma\theta(t)f(t)$, a detailed analysis shows that the offset is generated by a boundary term of the form $\propto f(0)f(T)$, which obviously disappears in case of a continuous switching function $f(0) = 0$. In the following, we want to argue that this is indeed the case. To this end, we take the term that generates the offset in the sudden switching scenario,

$$S_{\text{offset}}(t,t') = \frac{1}{4}\int_{-T}^{T} d(t-t')\,\gamma(t)\gamma(t')\mathrm{e}^{\mathrm{i}\Omega(t-t')} \sum_{\alpha=L,R} g^{-+}_{\alpha\alpha}(t'-t)\left[D^R(t,t') - D^A(t,t')\right]. \tag{3.36}$$

Inserting the general solution of the Dyson equation with an arbitrary switching function given by Eq. (2.55) entails

$$S_{\text{offset}}(t,t') = \frac{\Gamma}{4}\int_0^T d\tau\, \mathrm{e}^{\Gamma\int_{(T+\tau)/2}^{(T-\tau)/2} ds f^2(s)} f\left(\frac{T-\tau}{2}\right) f\left(\frac{T+\tau}{2}\right) \times \sum_{\sigma=\pm}\int_{-\infty}^{\sigma V/2} \frac{d\omega}{2\pi}\left[\mathrm{e}^{\mathrm{i}(\Omega-\Delta+\omega)\tau} + \mathrm{e}^{-\mathrm{i}(\Omega-\Delta+\omega)\tau}\right]. \tag{3.37}$$

Now, we use the general formula for partial integration with respect to τ

$$\int_0^T d\tau\, h(\tau)\, g'(\tau) = h(\tau)\, g(\tau)\Big|_0^T - \int_0^T d\tau\, h'(\tau)\, g(\tau) \tag{3.38}$$

with the identification

$$g'(\tau) = \sum_{\sigma=\pm}\int_{-\infty}^{\sigma V/2} \frac{d\omega}{2\pi}\left[\mathrm{e}^{\mathrm{i}(\Omega-\Delta+\omega)\tau} + \mathrm{e}^{-\mathrm{i}(\Omega-\Delta+\omega)\tau}\right] \tag{3.39}$$

and $h(\tau)$ summarizing the remaining terms. With the primitive of $g(\tau)$

$$g(\tau) = \frac{1}{2\pi}\sum_{\sigma=\pm}\int_{-\infty}^{\sigma V/2} d\omega\left[\frac{\mathrm{e}^{\mathrm{i}(\Omega-\Delta+\omega)\tau}}{\mathrm{i}(\Omega-\Delta+\omega)} + \frac{\mathrm{e}^{-\mathrm{i}(\Omega-\Delta+\omega)\tau}}{-\mathrm{i}(\Omega-\Delta+\omega)}\right], \tag{3.40}$$

we obtain the final result

$$\lim_{T\to 0} g(\tau)h(\tau)\Big|_0^T = \frac{\Gamma}{4}f^2(0). \tag{3.41}$$

This contribution disappears if the switching function is continuous, i.e. if it starts from zero at initial time. Since the second contribution $\propto \lim_{T\to 0}\int_0^T d\tau f'(\tau)g(\tau)$ is vanishing for sudden switch-on processes this holds even more if these are continuous. As a result, the instantaneous jump of the total noise at initial time $t = 0$ survives only for a discontinuous switching scenario. For $\Omega \to \pm\infty$, we have

$$\lim_{\Omega\to+\infty} S(\Omega, T) = \frac{\Gamma}{2}, \quad \lim_{\Omega\to-\infty} S(\Omega, T) = 0. \tag{3.42}$$

These are the usual limits of the unsymmetrized noise in the steady state. We note that the aforementioned cases are all independent of the initial dot occupation.
On the contrary, for $\Delta \to \pm\infty$, we have for an initially empty dot

$$\lim_{\Delta\to-\infty} S(\Omega, T) = \frac{\Gamma}{2}e^{-\Gamma T}, \quad \lim_{\Delta\to+\infty} S(\Omega, T) = 0, \tag{3.43}$$

whereas for an initially occupied dot, the limits are reversed. The remaining dynamics of noise is understandable since, in the former limit, a tunneling process is allowed only for an initially empty dot that can be populated by one lead electron, whereas in the latter, an electron on the dot can jump to one of the leads. This jump probability is equal for electrons on/to both leads, thus the time-dependent net current vanishes although zero temperature fluctuations are present. All formulas are clearly in excellent agreement with the steady state result.

Long-time asymptotics: Zero temperature case

Apart from the special limits above, we now analyze the general long-time behavior of transient noise at zero temperature. The most astonishing feature is the temporal decay as a power law for large times. At zero frequency ($\Omega = 0$), we obtain in case of an initially occupied dot

$$\begin{aligned} S(\Omega = 0, T) = &+ \frac{\Gamma^2}{(2\pi)^2}\sum_{m,n=\pm}\int_{-\infty}^{mV/2} d\omega \frac{\mathrm{Si}\left[(\omega + nV/2)T\right]}{(\omega-\Delta)^2+\Gamma^2} + \frac{\Gamma^2}{4\pi}\sum_{m=\pm}\int_{-\infty}^{mV/2} d\omega \frac{1}{(\omega-\Delta)^2+\Gamma^2} \\ &- \frac{\Gamma^2}{(2\pi)^2}\int_{-V/2}^{V/2} d\omega \int_{-V/2}^{V/2} d\omega' \frac{\left[\Gamma^2 - (\omega-\Delta)(\omega'-\Delta)\right] T\mathrm{sinc}\left[(\omega'-\omega)T\right]}{\left[(\omega-\Delta)^2+\Gamma^2\right]\left[(\omega'-\Delta)^2+\Gamma^2\right]} + g(T), \end{aligned} \tag{3.44}$$

where $\mathrm{Si}(x)$ is the sine-integral function, $\mathrm{sinc}(x)$ is the cardinal sine function as defined in Gradshteyn and Ryzhik [1975] and $g(T)$ comprises all terms which decay exponentially and are thus subleading in T. For zero voltage at resonance ($\Delta = 0$), this simplifies to produce

$$S(\Omega = 0, T) = \frac{\Gamma^2}{2\pi}\int_{-\infty}^{0} d\omega \frac{1 + \mathrm{Si}\left(\omega T\right)/(2\pi)}{\omega^2+\Gamma^2} + g(T). \tag{3.45}$$

To leading order in $1/T$, we find that the transient noise evolution for large times is dominated by a power law

$$S(\Omega = 0, T\Gamma \gg 1) \approx \frac{1}{\pi^2 T}. \tag{3.46}$$

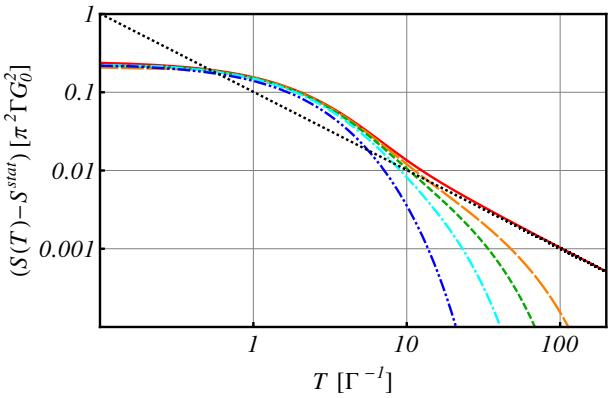

Figure 3.3: Difference between transient noise and its steady state at $V/\Gamma = \Delta/\Gamma = \Omega/\Gamma = 0$ for zero temperature (red solid curve) and finite inverse temperature $\beta\Gamma = 200, 100, 50, 20$ (orange long-dashed, green short-dashed, cyan dot-dashed, and blue double-dot-dashed curves). We include the reference function $1/(\pi^2 T)$ (black dotted curve). Note the double-logarithmic scale.

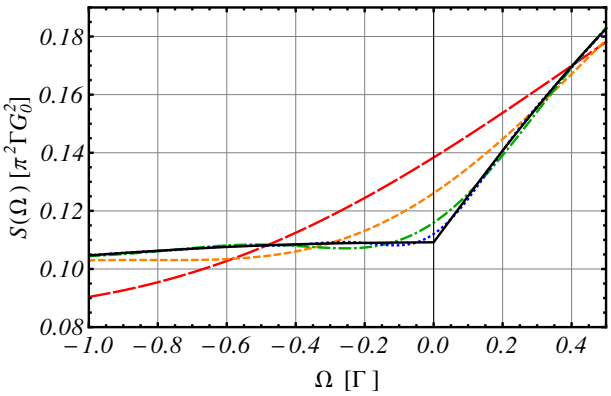

Figure 3.4: Transient noise at times $T\Gamma = 2.5, 5, 10, 20$ (red long-dashed, orange short-dashed, green dot-dashed, and blue dotted curves) and steady state noise (black solid curve) at $V/\Gamma = 2\Delta/\Gamma = 10$ as a function of frequency Ω/Γ.

For increasing voltage, this distinctive feature gradually disappears until, at infinite voltage, we attain the limit of Eq. (3.33). It can only be retained by adjusting the detuning Δ in such a way that the Lorentzian peak in the integrand of the first term in Eq. (3.44) is shifted to the zero of one of the sine integrals (i.e., to the position of one of the lead Fermi levels $-V/2$ or $V/2$). This tendency is illustrated in Fig. 3.3. Moreover, the feature is only dominant if the frequency fulfills the condition $\Omega/\Gamma \ll 1$, which can be seen in Fig. 3.4 where we depict the transient noise spectrum at different times. As expected, we note the pronounced discrepancy to the steady state noise spectrum around $\Omega/\Gamma = 0$ in this graph. Apart from that region, the curves are almost indistinguishable for $T\Gamma = 20$ on the plotted scale. In Figs. 3.5-3.7, we display the effects of tuning the various parameters of the model, namely voltage, dot level energy and frequency for the case of an initially unoccupied dot. Obviously, one recognizes the gradual approach to the limits calculated before. We stress that, using our definition of noise, we still observe *negative transient noise* in two important cases: large negative frequency or large positive/negative detuning for an initially empty/occupied dot, although the steady state noise is always strictly positive. This is consistent with very small overall noise levels in the corresponding limiting cases ($\Delta \to \pm\infty$ and $\Omega \to -\infty$). Since at finite values of these parameters, shortly before approaching the extreme cases, we always have oscillatory behavior, we expect and indeed observe an undershooting below the zero line.

Connection of the long-time asymptotics to the steady state

We want to present evidence of a relation between the long-time asymptotics and a feature of the steady state solution. Indeed, it is striking that the algebraic decay of the transient noise is dominant at zero frequency, where the stationary noise spectrum is non-differentiable, its first derivative having a discontinuity $\delta S'$ given by Eq. (3.32). Inspired by the plots of Fig. 3.8, it is tempting to suggest the following generalization of our transient noise formula to arbitrary

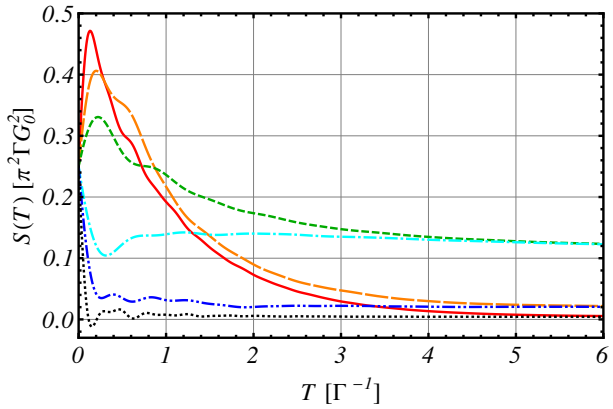

Figure 3.5: Zero-frequency transient noise at fixed voltage $V/\Gamma = 10$ for various detunings $\Delta/\Gamma = -20, -10, -5, 5, 10, 20$ (red solid, orange long-dashed, green short-dashed, cyan dot-dashed, blue double-dot-dashed, and black dotted curves). Note the dominance of the algebraic decay of the green and cyan curves ($V = \pm 2\Delta$).

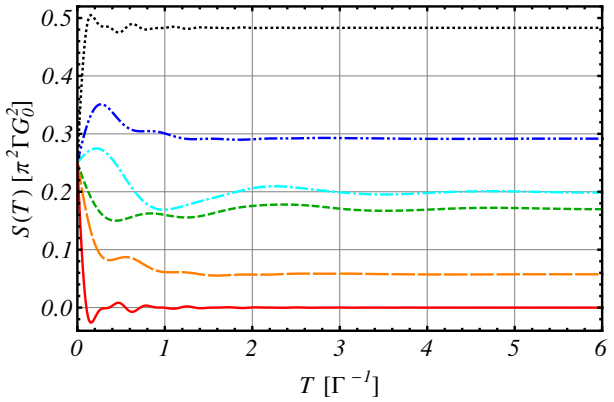

Figure 3.6: Transient noise at resonance ($\Delta/\Gamma = 0$) and fixed voltage $V/\Gamma = 10$ for various frequencies $\Omega/\Gamma = -20, -5, -2, 2, 5, 20$ (red solid, orange long-dashed, green short-dashed, cyan dot-dashed, blue double-dot-dashed, and black dotted curves).

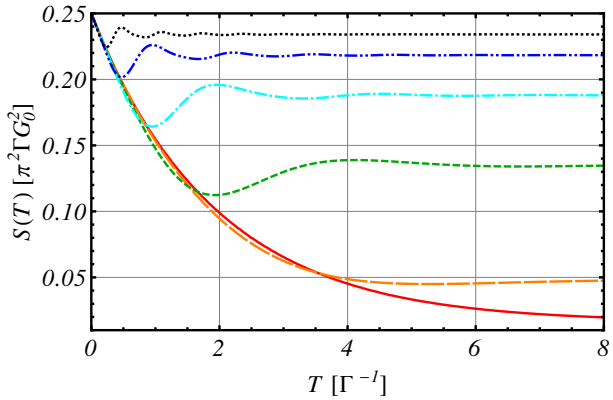

Figure 3.7: Zero-frequency transient noise at resonance ($\Delta/\Gamma = 0$) for various voltages $|V|/\Gamma = 1, 2, 5, 10, 20, 40$ (red solid, orange long-dashed, green short-dashed, cyan dot-dashed, blue double-dot-dashed, and black dotted curves). Note the increasing dominance of the algebraic decay by lowering the voltage.

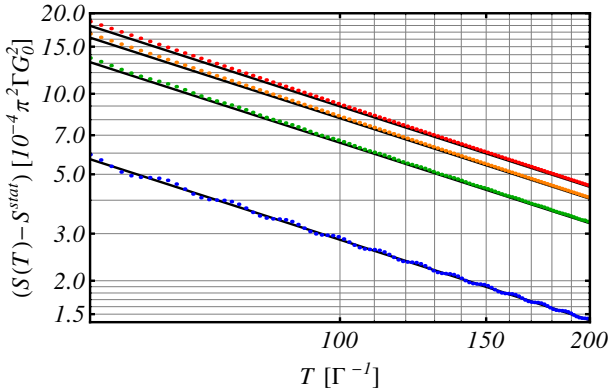

Figure 3.8: Difference between zero-frequency transient noise and its steady state value for parameter pairs $(V/\Gamma, \Delta/\Gamma) = (0.5, 0), (0, 0.5), (0.5, 0.5), (0.5, 1)$ (red, orange, green, and blue dotted curves from top to bottom) compared with the respective reference curves calculated according to the function $\delta S'/(\pi T)$ (black solid curves) with $\delta S'$ given by Eq. (3.32). Note the double-logarithmic scale.

values of V and Δ,

$$S(\Omega = 0, T\Gamma \gg 1) = S^{\text{stat}}(\Omega = 0) + \frac{\delta S'}{\pi T} + r(T)\,, \tag{3.47}$$

where the function $r(T)$ incorporates all terms of subleading order (i.e., algebraic terms of higher order $\propto 1/T^{\alpha}$ with $\alpha > 1$ and exponentially decaying functions). Our conjecture Eq. (3.47) obviously reproduces our analytical result from Eq. (3.46) and hence the dominance of the algebraic decay for such parameter constellations in which the dot level coincides with a Fermi level of the electrodes and its gradual disappearance for growing detuning of the dot level away from a Fermi edge. This is supported by our calculations as well as numerical evaluation, especially by the limiting cases $V \to \pm\infty$ and $\Delta \to \pm\infty$, where this feature is absent. At this point, we would like to address the similarities and differences to the calculation from Feng et al. [2008], which addresses transient equal time current-current fluctuations in an RLM setup. There the calculated quantity is

$$S(\tau = 0, T) = \int_{-\infty}^{+\infty} d\Omega\; S(\Omega, T)\,, \tag{3.48}$$

that is, Eq. (3.15) taken at $t = t'$. Moreover, the t of Feng et al. [2008] is related to our parameter by $t = T/2$. The procedure presented there consists of taking a time-dependent bias voltage and assuming its dynamics to be sufficiently slow so that an adiabatic approximation can be applied. On the contrary, in our case the tunneling coupling is switched on instantaneously and thus infinitely fast and anti-adiabatic.

Long-time asymptotics: Finite temperature case

We now want to address the calculation of transient noise for finite temperature. The result obtained after a cumbersome calculation is provided in Appendix D. We here concentrate on the salient feature which consists of a modification of the temporal decay compared to zero temperature, which is now exponential. Indeed, we observe that the presence of thermal fluctuations introduces a new energy scale to the problem on which the new damping constant is linearly dependent. In Fig. 3.3, we contrast these two types of decay. We point out that in these plots, we have subtracted the respective steady state values due to thermal Johnson-Nyquist noise. An estimation of the finite-temperature damping constant is provided by $\Gamma' = \pi/\beta$ so that the envelope of the plotted functions for large times is cut off by a function proportional to $\mathrm{e}^{-\pi T/\beta}$, where β is the inverse temperature. For more details, see Appendix D. This behavior is not unexpected as the transition from algebraic decay at zero temperature to exponential decay at finite temperature is a quite general phenomenon, which occurs in various systems and is not restricted to temporal evolution. As an example, we cite the spatial decay of Friedel oscillations, which follows a similar pattern. Furthermore, our result has a dramatic consequence for eventual numerical simulations, which depend sensitively on the approach to steady state. We thus conclude that, in order to get the steady state result fast, these should be performed at finite temperature to reduce computational effort (Branschädel et al. [2010], Carr et al. [2011], Andergassen et al. [2011], Schmitt and Anders [2010], Schmidt et al. [2008]). From an experimental point of view, it should be an observable effect, at least at sufficiently low temperature where the Fermi functions are not much smeared out so that one can detect the decrease of the damping constant as a function of temperature in different parameter regimes. Indeed, typical parameters taken from state-of-the-art experiments provide for $\Gamma \sim meV$ and $\Gamma' \sim \mu eV$, so that the condition $\Gamma' \ll \Gamma$ can be fulfilled.

Correlation function for dot occupation

We want to mention an interesting similarity to the Fourier transform of the correlation function for the dot occupation,

$$\mathrm{F}(\Omega, T) = \int_{-T}^{+T} d(t-t')\, \mathrm{e}^{\mathrm{i}\Omega(t-t')} \langle \hat{n}_d(t) \hat{n}_d(t') \rangle. \tag{3.49}$$

In an analogous calculation as before it can be shown that this function already displays an algebraic long-time asymptotics. For the special case $V = \Delta = \Omega = 0$, we find to leading order

$$\mathrm{F}(\Omega, T\Gamma \gg 1) \approx \frac{2}{\pi^2 T}. \tag{3.50}$$

However, it has to be stated that the charge susceptibility $\chi(\Omega, T)$ exhibits a purely exponential decay in time already at zero temperature as it is related to a retarded Green's function and thus involves a commutator. Its definition reads

$$\chi(\Omega, T) = \int_{-T}^{+T} d(t-t')\, \chi(t, t'), \tag{3.51}$$

where $\chi(t, t')$ is a retarded Green's function given by

$$\chi(t, t') = \mathrm{i}\theta(t-t') \langle [\hat{n}_d(t), \hat{n}_d(t')] \rangle. \tag{3.52}$$

This behavior is not surprising though. The charge susceptibility represents the response function to external fields. One particular realization of such fields is a finite voltage across the constriction. The response is then the current through the system which, as we know, has an exponential behavior. We speculate that the drastic qualitative difference in the decay of the two quantities defined in Eqs. (3.49) and (3.51) can be explained by the fact that the former one shows no explicit time-ordering whereas in the latter one, time-ordering is implemented by a Heavidside step function. Thus, it is presumably the common feature of that absence of real time-ordering in the definition of the current-current correlator and the dot occupancy correlator which is responsible for the algebraic decay of their Fourier transforms.

3.5 Noise in the MRLM

3.5.1 Transient noise evolution

We proceed along the lines of the previous section to evaluate the transient behavior of current noise in the MRLM in order to test if the qualitative conclusions from the RLM calculation remain true in case of the inclusion of electron-electron interactions. Carrying out similar steps as before one obtains the irreducible current-current correlation function

$$\begin{aligned} S(t_+, t'_-) &= \frac{\gamma(t)\gamma(t')}{4} \left[\langle b(t_+)\eta(t_+) \rangle \left\langle b(t'_-)\eta(t'_-) \right\rangle - \left\langle b(t_+)\eta(t_+)b(t'_-)\eta(t'_-) \right\rangle \right] \\ &= \frac{\gamma(t)\gamma(t')}{4} \left[G^{+-}_{b\eta}(t, t') G^{+-}_{\eta b}(t, t') - D^{+-}_{bb}(t, t') G^{+-}_{\eta\eta}(t, t') \right] \\ &= \frac{\gamma(t)\gamma(t')}{4} \left[G^{-+}_{b\eta}(t, t') G^{-+}_{\eta b}(t, t') - D^{+-}_{bb}(t, t') g^{+-}_{\eta\eta}(t, t') \right], \end{aligned} \tag{3.53}$$

where the $-/+$ sign again denotes the forward/backward branch of the Keldysh contour. In the last line, we used the facts that the retarded mixed Green's function vanishes and that the η-Majoranas decouple from the transport process for symmetric coupling. As a result, we find a similar structure of the irreducible current-current correlation function as in the RLM,

$$S(t,t') = \frac{1}{4}\left[S_1(t,t') + S_2(t,t')\right], \tag{3.54}$$

where we defined

$$S_1(t,t') = -D^{+-}_{bb}(t,t')\Xi^{+-}_{+}(t,t') \tag{3.55}$$

and

$$S_2(t,t') = \int dt_1\, D^{R}_{bb}(t,t_1)\Xi^{-+}_{-}(t_1,t') \int dt_2\, \Xi^{-+}_{-}(t,t_2) D^{A}_{bb}(t_2,t'). \tag{3.56}$$

The functions $\Xi_\pm$ represent tunneling self-energies and are defined in Fourier-Keldysh space as

$$\hat{\Xi}_{+}(\omega) = \gamma^2 \hat{g}_{\eta\eta}(\omega) = \gamma^2 \hat{g}_{\xi\xi}(\omega) \tag{3.57}$$

and

$$\hat{\Xi}_{-}(\omega) = \gamma^2 \hat{g}_{\xi\eta}(\omega) = -\gamma^2 \hat{g}_{\eta\xi}(\omega). \tag{3.58}$$

Steady state noise spectrum

In the steady state, all Green's functions are only dependent on the time difference $\tau = t - t'$, so that we can easily use the Fourier representation

$$G^{ij}(\tau) = \int_{-\infty}^{\infty} \frac{d\omega}{2\pi} e^{-\mathrm{i}\omega\tau} G^{ij}(\omega) \tag{3.59}$$

to arrive at

$$S^{\mathrm{stat}}(\Omega) = \frac{\gamma^2}{4} \int_{-\infty}^{\infty} \frac{d\omega}{2\pi} \left[G^{+-}_{b\eta}(\omega) G^{+-}_{\eta b}(\Omega-\omega) - D^{+-}_{bb}(\omega) G^{+-}_{\eta\eta}(\Omega-\omega)\right]. \tag{3.60}$$

As expected, we recover the stationary results of the authors of Schiller and Hershfield [1998] and Komnik and Gogolin [2003a]. Such a calculation can directly be performed numerically in a straightforward manner.

Limiting cases

As for the RLM calculation, we give compact formulas for various limiting cases at zero temperature by keeping all other quantities fixed. The contributions are due to terms of $S_1(\Omega, T)$, again containing only sums of Fermi functions. In the following, we list them in the same order as before, see Section 3.4.
For $V \to \pm\infty$, we obtain

$$\lim_{V\to\pm\infty} S(\Omega,T) = \frac{\Gamma}{8}(1 + 2e^{-\Gamma T}), \tag{3.61}$$

which is accompanied by the saturation of the total current through the constriction at high voltage,

$$\lim_{V\to\pm\infty}\langle I(t)\rangle = \pm\frac{\Gamma}{4}. \tag{3.62}$$

At $T \to 0$, we again have an offset

$$\lim_{T\to 0} S(\Omega, T) = \frac{3\Gamma}{8}. \tag{3.63}$$

At this point, we would like to mention that the discrepancy of the latter result with Eq. (3.35) is due to a non-vanishing contribution from the first part of Eq. (2.61) which is absent in the RLM case. For $\Omega \to \pm\infty$, we have

$$\lim_{\Omega\to+\infty} S(\Omega, T) = \frac{\Gamma}{4}(1 + 2e^{-\Gamma T}), \quad \lim_{\Omega\to-\infty} S(\Omega, T) = 0. \tag{3.64}$$

However, for $\Delta \to \pm\infty$, we have for an initially empty dot

$$\lim_{\Delta\to-\infty} S(\Omega, T) = \frac{5\Gamma}{8}e^{-\frac{\Gamma T}{2}}, \quad \lim_{\Delta\to+\infty} S(\Omega, T) = 0, \tag{3.65}$$

whereas for an initially occupied dot the limits are reversed. In relation to the RLM case, we state the qualitative difference that we have a temporal dynamics in the case of limits $\Omega \to \pm\infty$ and $V \to \pm\infty$ for the MRLM. We speculate that, at least in the IRLM case, the feature is due to the Coulomb interaction term in the Hamiltonian, which is absent in the RLM case. The seemingly slower exponential decay in the limits $\Delta \to \pm\infty$ with $\Gamma/2$ is not directly comparable to the RLM due to a different definition of Γ in both models. Of course, letting $T \to \infty$ in the above formulas, we find an approach to the expected steady state values.

Long-time asymptotics: Zero temperature case

Since we only want to concentrate on the discussion of the main results, we provide the exact analytical formula for the transient noise in the MRLM in Appendix E. In analogy to the RLM case, we identify a term with a similar structure involving sine integrals. For $\Omega = 0$, it is given by

$$S_1(\Omega = 0, T) = -\frac{\Gamma}{16\pi}\Bigg\{\sum_{m,n=\pm}\int_{-V}^{+V} d\omega \int_{-V}^{+V} d\omega' \frac{T\Gamma\,(m\Omega' + \Gamma/2)(n\Omega' + \Gamma/2)\,\mathrm{sinc}\,[(\omega+\omega')T]}{\pi\Omega'^2\,[\Omega' + m\,(\Gamma/2 - \mathrm{i}\omega)]\,[\Omega' + n\,(\Gamma/2 + \mathrm{i}\omega')]}$$

$$+ \sum_{m,n,p=\pm}\int_{-\infty}^{pV} d\omega \left[\frac{(\Omega' - n\Gamma/2)}{\Omega'\,[\mathrm{i}m(\Omega+\omega) + (n\Omega' - \Gamma/2)]} - \frac{\Gamma\omega^2\,(\mathrm{Si}\,[(\omega - mV)T] - \pi/2)}{\pi\,[(\omega^2+\Delta^2)^2 + \omega^2(\Gamma^2 - 4\Delta^2)]}\right] + h(T)\Bigg\}, \tag{3.66}$$

where the function $h(T)$ summarizes all terms that are exponentially decaying and thus subleading in $1/T$. Note that here, the voltage is doubled with respect to the RLM, a peculiarity due to the transformation steps from the original models (Komnik and Gogolin [2003a]). For

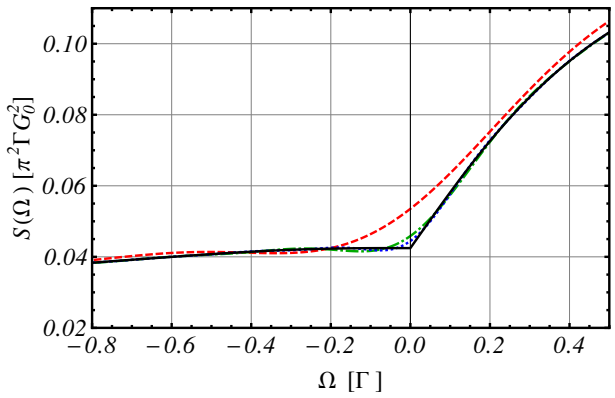

Figure 3.9: Transient noise at times $T\Gamma = 10, 20, 30$ (red dashed, green dot-dashed, and blue dotted curves) and steady state noise (black solid curve) at $V/\Gamma = \Delta/\Gamma = 5$ as a function of frequency Ω/Γ. Around $\Omega = 0$, the discrepancy of the transient noise to the steady state result is dominant, which mirrors its pronounced algebraic decay in time in that region.

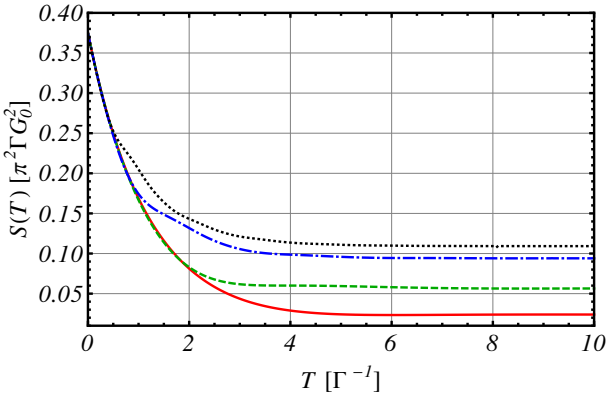

Figure 3.10: Zero-frequency transient noise at resonance ($\Delta/\Gamma = 0$) for various voltages $|V|/\Gamma = 1, 2, 5, 10$ (red solid, green dashed, blue dot-dashed, and black dotted curves). Note that decreasing the voltage enhances the dominance of the algebraic decay.

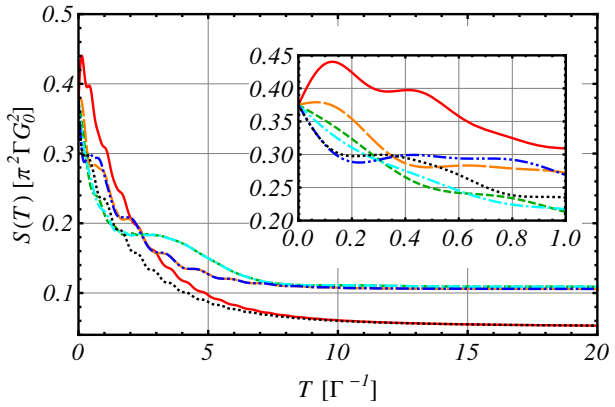

Figure 3.11: Zero-frequency transient noise at fixed voltage $V/\Gamma = 10$ for detunings $\Delta/\Gamma = -10, -5, -1, 1, 5, 10$ (red solid, orange long-dashed, green short-dashed, cyan dot-dashed, blue double-dot-dashed, and black dotted curves). Note the dominance of the algebraic decay of the red and black curves ($V = \pm\Delta$). The inset shows the same plot magnified in the range $[0, 1]$ in order to demonstrate the differences of the curves at early times.

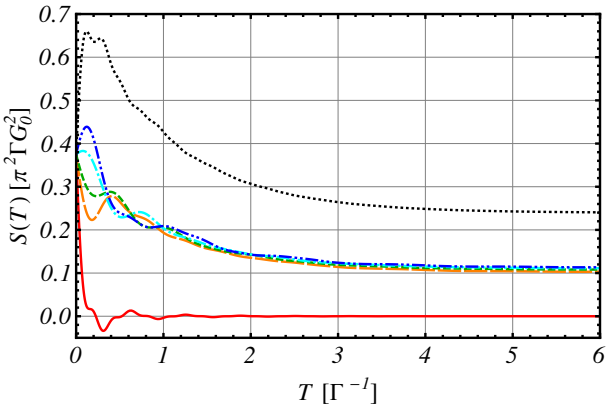

Figure 3.12: Transient noise at resonance ($\Delta/\Gamma = 0$) and fixed voltage $V/\Gamma = 10$ for various frequencies $\Omega/\Gamma = -20, -5, -2, 2, 5, 20$ (red solid, orange long-dashed, green short-dashed, cyan dot-dashed, blue double-dot-dashed, and black dotted curves).

$V = \Delta = 0$, we come to the same conclusion as the one drawn from Eq. (3.46) and again obtain an algebraic decay, namely to leading order

$$S(\Omega = 0, \Gamma T \gg 1) \approx \frac{1}{2\pi^2 T}. \tag{3.67}$$

In general, instead of one Lorentzian peak as for the RLM, the second term of Eq. (3.66) shows a two-peak structure with maxima at $\omega = \pm\Delta$. However, this does not modify our conclusion. Obviously, the term has an appreciable effect only if $V \approx \pm\Delta$ (i.e., if the dot level almost coincides with one of the 'dressed' lead Fermi levels). If the dot and Fermi levels move away from each other, the two peaks are no longer situated at the respective zeros of the sine integrals. For increasing Ω, we also observe the gradual disappearance of this distinctive feature as shown in Fig. 3.9. Moreover, we emphasize that the transient noise as well as the current can also become negative in the MRLM. The transient noise evolution for various parameters in the case of an initially empty dot is shown in Figs. 3.10-3.12.

3.6 Heat current in the RLM

Apart from the electronic transport characteristics of our models, a significant issue resides in the heat carried by the electrons tunneling through the quantum dot. Another channel of heat transfer can be associated with phononic degrees of freedom which are absent in our models and are therefore neglected also in this part of the thesis. A major motivation to investigate transport quantities related to the heat flow is that the amount of heat released in a nanostructure can even result in its complete destruction, especially when the quantum dot is composed of a fragile molecule attached to macroscopic electrodes, see Schulze et al.. From a theoretical point of view, the investigation of the statistics of heat transfer has revealed the existence of a heat conductance quantum in analogy with the conventional conductance quantization associated with charge transport through perfect transmission channels in quantum point contacts, see Kindermann and Pilgram [2004]. There exists a direct relationship between the electric current operator and the operator of the heat current between the dot and lead α, which can be deduced by the general equilibrium thermodynamic relation $dQ_\alpha = dE_\alpha - \mu_\alpha dN_\alpha$. Here, Q_α, E_α and N_α determine the heat, energy and particle number in lead α, respectively. This formula, which is applicable for our setup since the reservoirs are supposed to be at equilibrium, leads to the heat current operator

$$\hat{I}^{\mathrm{h}}_\alpha = \hat{I}^{\mathrm{E}}_\alpha - \mu_\alpha \hat{I}^{\mathrm{e}}_\alpha. \tag{3.68}$$

In this equation, $\hat{I}^{\mathrm{e}}$ and $\hat{I}^{\mathrm{E}}$ denote the operators for the electric and energy currents, respectively. In contrast to the former operator, already introduced in previous sections, the latter can be deduced analogously, starting from the Heisenberg equation of motion for the energy operator, yielding

$$\hat{I}^{\mathrm{E}}_\alpha = \mathrm{i} \sum_k \epsilon_{\alpha k} \left(\gamma_{\alpha k} c^\dagger_{\alpha k} d - \mathrm{H.c.} \right). \tag{3.69}$$

To access the heat current, we use Eq. (3.68) with the same simplifications as those taken for the electric current and its associated noise in previous sections where we set $\gamma_{\alpha k} = \gamma$ and switched to a continuum description. We thus arrive at the formula for the total heat current

$$I^{\mathrm{h}}(V,t) = \frac{1}{2}\left[I^{\mathrm{h}}_L(V,t) - I^{\mathrm{h}}_R(V,t) \right] = I^{\mathrm{E}}(V,t) - \frac{V}{4}\left[I^{\mathrm{e}}_L(V,t) + I^{\mathrm{e}}_R(V,t) \right], \tag{3.70}$$

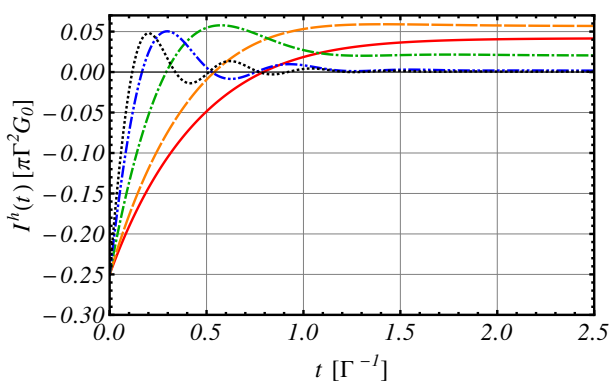

Figure 3.13: Transient heat current at temperature $\beta_L\Gamma = \beta_R\Gamma = 1$ and chemical potentials of the left and right reservoirs $\mu_L = 0.5$ and $\mu_R = -0.5$ for detunings $|\Delta|/\Gamma = 1, 2, 5, 10, 15$ (red solid, orange dashed, green dot-dashed, blue double-dot-dashed, and black dotted curves).

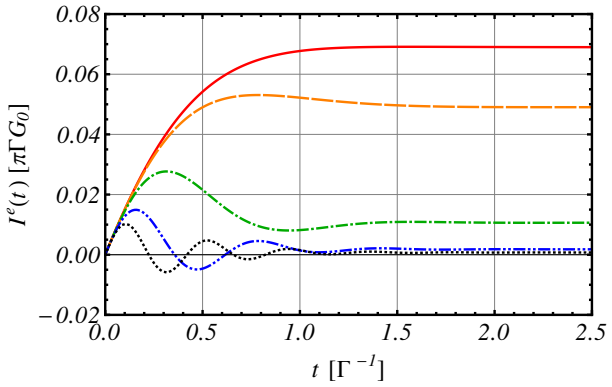

Figure 3.14: Transient electric current at temperature $\beta_L\Gamma = \beta_R\Gamma = 1$ and chemical potentials of the left and right reservoirs $\mu_L = 0.5$ and $\mu_R = -0.5$ for detunings $|\Delta|/\Gamma = 1, 2, 5, 10, 15$ (red solid, orange dashed, green dot-dashed, blue double-dot-dashed, and black dotted curves).

where $V = \mu_L - \mu_R$ is the voltage across the quantum dot. In Eq. (3.70), the electric current for lead α is given by formula (3.4) and the total energy current reads

$$I^{\mathrm{E}}(V,t) = \frac{1}{2}\left[I_L^{\mathrm{E}}(V,t) - I_R^{\mathrm{E}}(V,t)\right] = \frac{1}{2\pi}\int d\omega\,[n_L(\omega) - n_R(\omega)]\,\omega\,\mathcal{T}(\omega,t), \tag{3.71}$$

where we have the same transmission coefficient as the one for the total electric current defined in Eq. (3.9).

3.7 Thermoelectric effects in the RLM

Generally speaking, transport processes are characterized by currents (a.k.a. fluxes) which are associated with thermodynamic forces (a.k.a. affinities). As famous examples one can enumerate Fick's law, Ohm's law and Fourier law, which describe the response of a system to gradients of concentration, chemical potential and temperature manifesting themselves in particle, electric and heat currents. Besides the aforementioned laws describing direct effects, one can raise the question about their interdependence. Indeed, there generally exists a coupling between these processes, e.g. a concentration gradient can result in an effective heat transport. In this section, we would like to concentrate on the mutual influence of the electric and heat currents. These thermoelectric effects have a variety of technical applications the most prominent being cooling devices like refrigerators. Their study could even be profitable for engineers searching for a means of optimizing the reconversion into electric energy of a part of the heat produced by electric currents in a sample. Having both the heat and electric current operators at hand, we can calculate the Peltier coefficient defined as the ratio

$$\Pi(t) = \left.\frac{\langle\hat{I}_L^{\mathrm{h}}\rangle(t) - \langle\hat{I}_R^{\mathrm{h}}\rangle(t)}{\langle\hat{I}_L^{\mathrm{e}}\rangle(t) - \langle\hat{I}_R^{\mathrm{e}}\rangle(t)}\right|_{T_L=T_R}, \tag{3.72}$$

taken at equal temperatures of both leads. This quantity measures the heat current induced by the electric current across a junction which is the quantum dot in our case. Due to the fact that

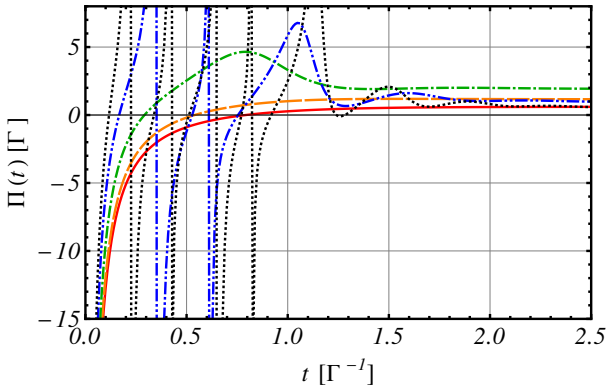

Figure 3.15: Peltier coefficient at temperature $\beta_L\Gamma = \beta_R\Gamma = 1$ and chemical potentials of the left and right reservoirs $\mu_L = 0.5$ and $\mu_R = -0.5$ for detunings $|\Delta|/\Gamma = 1, 2, 5, 10, 15$ (red solid, orange dashed, green dot-dashed, blue double-dot-dashed, and black dotted curves). Notice the increase of the number of pronounced maxima and singularities with increasing detuning. The singularities are indicated by vertical lines in the same color as the corresponding function.

the microscopic laws of physics are time-reversal invariant, this coefficient obeys a relation first established by Onsager which can be useful in certain calculations. Thermoelectric effects in the transient regime have already been analyzed recently for a time-dependent dot level energy in the RLM (Crépieux et al. [2011]). However, in this paper, which puts its main focus on the Seebeck coefficient only an analytical formula for the Peltier coefficient was given without any plots. So we can adapt the procedure for our case of the switching-on of the tunneling to check if the main features persist and if additional ones are present. The transient behavior of the Peltier coefficient for various values of the detuning of the dot level energy is plotted in Fig. 3.15. We recognize that an increasing detuning leads to an increase of the number of maxima becoming more and more pronounced finally ending up as singularities. This observation can be explained by the fact that a singularity always occurs when a further zero-crossing of the transient electric current appears in the course of the detuning. For comparison, plots of the transient heat and electric currents are shown in Figs. 3.13 and 3.14 This peculiar feature for large detuning has not been addressed in Crépieux et al. [2011]

3.8 Towards transient heat noise in the RLM

We now turn to the heat noise spectrum. It is defined analogously to the current noise spectrum, with the electric current operators replaced by the heat current operators. To simplify calculations, we assume different temperatures $\Theta_L \neq \Theta_R$ but equal chemical potentials $\mu_L = \mu_R$ for the leads. This allows us to distill possible effects without any influence from voltage. The heat current correlator is then only determined by the energy current correlator,

$$S^{\mathrm{h}}(t,t') = \left\langle \hat{I}^E(t)\hat{I}^E(t') \right\rangle - \left\langle \hat{I}^E(t) \right\rangle \left\langle \hat{I}^E(t') \right\rangle . \tag{3.73}$$

Assuming again no k dependence of $\gamma_{\alpha k} = \gamma$, we obtain

$$S_{\alpha\beta}(t_+, t'_-) = \gamma(t)\gamma(t') \sum_k \sum_{k'} \epsilon_{k\alpha}\epsilon_{k'\beta} \big[G^{-+}_{dd}(t',t) G^{+-}_{\alpha\beta}(t,t') + G^{-+}_{\beta\alpha}(t',t) G^{+-}_{dd}(t,t') \\ - G^{-+}_{d\alpha}(t',t) G^{+-}_{d\beta}(t,t') - G^{-+}_{\beta d}(t',t) G^{+-}_{\alpha d}(t,t') \big]. \quad (3.74)$$

The evaluation proceeds along the lines of the current noise leading to an expression in terms of Green's functions. We only have to take care of the additional energy factors ω and ω'. As an example, we evaluate explicitly one term of the numerous terms containing free lead Green's functions after the application of Wick's theorem has been carried out,

$$\begin{aligned} & \mathrm{i} \sum_k \sum_{k'} \epsilon_{k\alpha}\epsilon_{k'\alpha} \langle c^\dagger_{k\alpha}(t') c_{k'\alpha}(t) \rangle_0 \, d(t,t') \\ & = \mathrm{i} \sum_k \sum_{k'} \epsilon_{k\alpha}\epsilon_{k'\alpha} \mathrm{e}^{-\mathrm{i}\epsilon_k t} \mathrm{e}^{+\mathrm{i}\epsilon_{k'} t'} \underbrace{\langle c^\dagger_{k\alpha}(0) c_{k'\alpha}(0) \rangle_0}_{\delta_{kk'} n_F(\epsilon_k)} \, d(t,t') \\ & = \mathrm{i} \sum_k \epsilon^2_{k\alpha} \mathrm{e}^{-\mathrm{i}\epsilon_k (t-t')} n_F(\epsilon_k) \, d(t,t') \\ & = \mathrm{i} \int d\omega \, \rho(\omega) \, \omega^2 \mathrm{e}^{-\mathrm{i}\omega(t-t')} n_F(\omega) \, d(t,t') \\ & = \int \frac{d\omega}{2\pi} \underbrace{2\pi\mathrm{i}\rho(\omega) n_F(\omega)}_{=g^{-+}(\omega)} \omega^2 \mathrm{e}^{-\mathrm{i}\omega(t-t')} \, d(t,t') \end{aligned} \quad (3.75)$$

where $d(t,t')$ is a full dot Green's function which is only a spectator since only the energies of lead electrons are involved and, additionally, we switched over to a continuum description using the common replacement

$$\sum_k (...) \longrightarrow \int d\omega \, \rho(\omega) (...). \quad (3.76)$$

Thus, we have to multiply all free lead Green's functions with a factor of ω before carrying out the integration. This harmless looking manipulation indeed constitutes a major complication as the convergence deteriorates in the full time-dependent case. A possible way out would be a complete calculation with a cutoff right from the beginning, which is beyond the scope of this thesis. Rather, we want to discuss the adiabatic heat noise evolution only, since we have discussed its relevance before for current noise in Section 3.4.

3.8.1 Steady state spectrum and adiabatic noise evolution

Since the steady state noise spectrum is easily accessible (Zhan et al. [2011]), we can take it as a starting point to apply an adiabatic approach first. Adapting the steps from the current

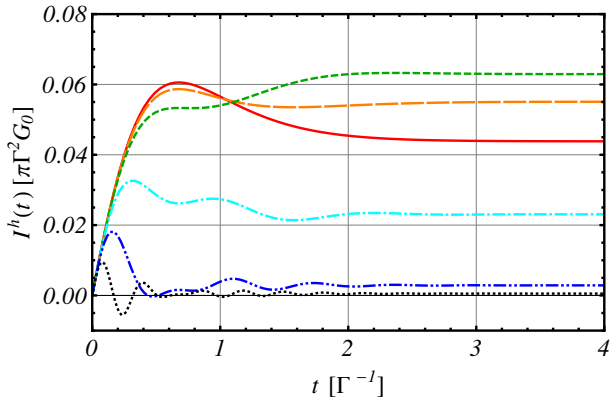

Figure 3.16: Transient heat current at fixed temperatures of left and right reservoirs $\beta_L\Gamma = 1$ and $\beta_R\Gamma = 2$ for zero voltage and detunings $|\Delta|/\Gamma = 0, 1, 2, 5, 10, 20$ (red solid, orange long-dashed, green short-dashed, cyan dot-dashed, blue double-dot-dashed, and black dotted curves).

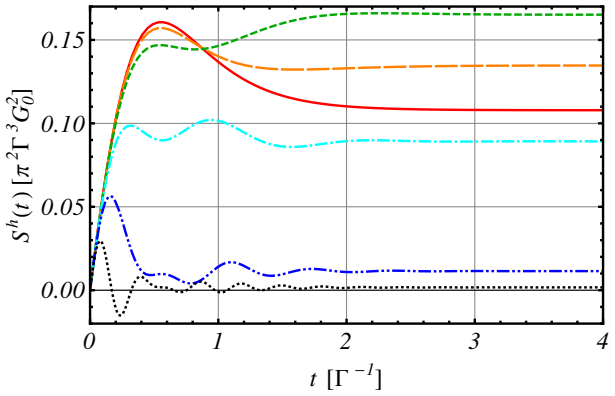

Figure 3.17: Adiabatic heat noise at fixed temperatures of left and right reservoirs $\beta_L\Gamma = 1$ and $\beta_R\Gamma = 2$ for zero voltage and detunings $|\Delta|/\Gamma = 0, 1, 2, 5, 10, 20$ (red solid, orange long-dashed, green short-dashed, cyan dot-dashed, blue double-dot-dashed, and black dotted curves).

noise, we arrive at

$$S^{\mathrm{h,stat}}_{\alpha\beta}(\Omega) = \gamma^2 \int \frac{d\omega}{2\pi} \int \frac{d\omega'}{2\pi} \int d\tau\, \mathrm{e}^{\mathrm{i}(\Omega+\omega-\omega')\tau} \Big[D^{-+}(\omega)\,\omega'^2\, G^{+-}_{\alpha\beta}(\omega') + \omega^2\, G^{-+}_{\beta\alpha}(\omega)\, D^{+-}(\omega') - \omega\, G^{-+}_{d\alpha}(\omega)\,\omega'\, G^{+-}_{d\beta}(\omega') - \omega\, G^{-+}_{\beta d}(\omega)\,\omega'\, G^{+-}_{\alpha d}(\omega') \Big]$$

$$= \gamma^2 \int \frac{d\omega}{2\pi} \Big[(\omega+\Omega)^2\ D^{-+}(\omega)\, G^{+-}_{\alpha\beta}(\omega+\Omega) + \omega^2\, G^{-+}_{\beta\alpha}(\omega)\, D^{+-}(\omega+\Omega) - \omega\,(\omega+\Omega) \Big(G^{-+}_{d\alpha}(\omega) G^{+-}_{d\beta}(\omega+\Omega) - G^{-+}_{\beta d}(\omega) G^{+-}_{\alpha d}(\omega+\Omega) \Big) \Big]. \quad (3.77)$$

Specializing to zero frequency $\Omega = 0$ we end up with a formula which is similar to Eq. (F.8), but with an additional factor of ω^2 under the integral.

$$\Big\langle \Big\langle \Big(\hat{I}^E\Big)^2 \Big\rangle \Big\rangle = \Big\langle \Big(\hat{I}^E\Big)^2 \Big\rangle - \Big\langle \hat{I}^E \Big\rangle^2$$

$$= \int \frac{d\omega}{2\pi}\, \omega^2 \Big\{ \mathcal{T}(\omega)\,[n_L(1-n_R) + n_R(1-n_L)] - \mathcal{T}^2(\omega)\,[n_L(1-n_R) - n_R(1-n_L)]^2 \Big\}$$

$$= \int \frac{d\omega}{2\pi}\, \omega^2 \Big\{ \mathcal{T}(\omega)\,[n_L(1-n_L) + n_R(1-n_R)] + \mathcal{T}(\omega)\,[1-\mathcal{T}(\omega)]\,[n_L - n_R]^2 \Big\}. \quad (3.78)$$

We can now replace the static transmission coefficient by the time-dependent transmission coefficient from Eq. (3.9) to access the adiabatic heat noise dynamics, which is depicted in

Fig. 3.17. It possesses analogous features as the adiabatic current noise dynamics, especially that it becomes negative for a strong detuning of the dot level.

Chapter 4

Discussion and Outlook

In the present work, we have studied quantum transport through nanostructures. In contrast to previous research which focused on steady-state properties, the monitoring of the temporal evolution of such quantum systems as a reaction to an external perturbation is still in its infancy. The only transport quantity the time-dependence of which has been extensively investigated and is by now well understood is the electric current, which usually approaches its steady state exponentially fast. Since the noise in electronic nanostructures is dominated by quantum fluctuations it is worthwhile to ask whether the noise transients show up qualitatively new effects. The aim of this thesis was to fill this gap and extend the noise analysis to the transient regime after the sudden switching on of the tunneling coupling in characteristic models of mesoscopic physics.

We found a parameter window in which the transient current noise temporarily becomes negative, a property it shares with the transient current. Furthermore, we analyzed the adiabatic heat noise evolution, which shows similar tendencies as the adiabatic current noise evolution for corresponding parameter changes. For increasing absolute value of the detuning it can also temporarily become negative. It will be exciting to see if negative noise – be it current or heat noise – can be measured and how this can be interpreted in practice.
However, the most striking feature that distinguishes the zero temperature transient current noise from the evolution of the current itself and dot population in both a non-interacting model (the resonant level model) and an interacting model (the Majorana resonant level model) is its algebraic temporal decay dominant for certain parameter sets. It reaches its maximum magnitude if one of the (dressed in the case of resonant tunneling between Luttinger liquids) Fermi levels matches the dot energy at $\Omega = 0$ and is suppressed if one of the model parameters Δ and V becomes significantly larger than the hybridization constant Γ. With increasing frequency Ω, the feature also becomes less pronounced. In both cases of the conventional as well as the Majorana resonant level model, this remarkable effect can be traced back to contributions involving energy integrals over sinc functions, which, in turn, are a result of resonances in involved Green's functions.

We expect this effect to survive in the case of realistic band structures beyond the adopted wide flat band limit since a finite bandwidth can only affect the transient behavior on short time scales. It is also independent of the detailed switching mechanism as it is an effect at large times. However, we find that finite temperature destroys this effect by introducing a new energy scale determining the damping constant of the exponential decay. Thus, we expect the

results to be observable at sufficiently low, but finite temperature in experimental setups like those described in this thesis.

Its interpretation in terms of an appealing physical picture is yet far from clear. On the one hand, the current dynamics is not affected qualitatively at the coincidence of the dot level and one of the lead Fermi levels, on the other hand, the noise dynamics is inhibited, which suggests that non-trivial temporal correlations arise. As a result, the noise has by far a better 'memory' about the switch-on process than the current. Thus, a measurement of the time dependence of the noise allows for a retrieval of important information about the transients at far later times than the electric current. We conclude that our result has also severe implications for the approach to the steady state in numerical real-time simulations, which should thus preferably be carried out at finite temperature for the discussed setups.

With these results in mind, it would be rewarding to verify if a similar pattern as the observed algebraic decay of transient noise persists in other models which take into account interactions in a different way from those treated in this thesis. The possible avenues for further progress could then be a detailed analysis of the impact of the on-dot interactions within the framework of the conventional Anderson impurity model, or a discussion of transient noise in Kondo systems beyond the Toulouse point. To summarize, our work lays the foundation toward a more comprehensive understanding of switch-on processes in future nanoscale devices, where it is important to know how external perturbations affect transport properties even beyond noise.

Peer reviewed Publications

Large parts of this thesis have already been published.

- K. Joho, S. Maier, and A. Komnik. Transient noise spectra in resonant tunneling setups: Exactly solvable models. *Phys. Rev. B*, 86:155304, 2012

Appendix A

Dyson equations

For completeness, we would like to indicate the various Dyson equations for the full Green's functions explicity.

$$\hat{D} = \hat{D}_0 + \gamma \hat{D}_0 \hat{\sigma}_3 (\hat{G}_{Rd} + \hat{G}_{Ld}), \tag{A.1}$$

$$\hat{D} = \hat{D}_0 + \gamma (\hat{G}_{dR} + \hat{G}_{dL}) \hat{\sigma}_3 \hat{D}_0, \tag{A.2}$$

$$\hat{G}_{\alpha\alpha} = \hat{g}_{\alpha\alpha} + \gamma \hat{g}_{\alpha\alpha} \hat{\sigma}_3 \hat{G}_{d\alpha}, \tag{A.3}$$

$$\hat{G}_{\alpha\alpha} = \hat{g}_{\alpha\alpha} + \gamma \hat{G}_{\alpha d} \hat{\sigma}_3 \hat{g}_{\alpha\alpha}, \tag{A.4}$$

$$\hat{G}_{d\alpha} = \gamma \hat{D} \hat{\sigma}_3 \hat{g}_{\alpha\alpha} = \gamma \hat{D}_0 \hat{\sigma}_3 \hat{G}_{\alpha\alpha}, \tag{A.5}$$

$$\hat{G}_{\alpha d} = \gamma \hat{g}_{\alpha\alpha} \hat{\sigma}_3 \hat{D} = \gamma \hat{G}_{\alpha\alpha} \hat{\sigma}_3 \hat{D}_0, \tag{A.6}$$

$$\hat{G}_{\alpha\alpha'} = \gamma \hat{g}_{\alpha\alpha} \hat{\sigma}_3 \hat{G}_{d\alpha'} = \gamma \hat{G}_{\alpha d} \hat{\sigma}_3 \hat{g}_{\alpha'\alpha'}, \tag{A.7}$$

where α and α' represent different leads. A part of these equations is used in calculations presented in the main text.

Appendix B

General relations for Green's functions

This appendix introduces the triagonal representation a.k.a. RAK notation which is obtained by carrying out a $\pi/4$ rotation in Keldysh space of the matrix Green's function $\hat{G}$ in conventional representation,

$$\tilde{G} = L\hat{G}L^{\dagger}, \tag{B.1}$$

where we introduced the orthogonal matrix L which can be rewritten in terms of the second Pauli matrix $\hat{\sigma}_2 = \begin{pmatrix} 0 & -\mathrm{i} \\ \mathrm{i} & 0 \end{pmatrix}$, so that $L = \frac{1}{\sqrt{2}}(1 - \mathrm{i}\hat{\sigma}_2) = \frac{1}{\sqrt{2}} \begin{pmatrix} 1 & -1 \\ 1 & 1 \end{pmatrix}$. The result for the Green's function is

$$\tilde{G} = L\hat{G}L^{\dagger} = \frac{1}{\sqrt{2}} \begin{pmatrix} 1 & -1 \\ 1 & 1 \end{pmatrix} \begin{pmatrix} G^{--} & G^{-+} \\ G^{+-} & G^{++} \end{pmatrix} \frac{1}{\sqrt{2}} \begin{pmatrix} 1 & 1 \\ -1 & 1 \end{pmatrix} \tag{B.2}$$

$$= \frac{1}{2} \begin{pmatrix} 1 & -1 \\ 1 & 1 \end{pmatrix} \begin{pmatrix} G^{--} - G^{-+} & G^{--} + G^{-+} \\ G^{+-} - G^{++} & G^{+-} + G^{++} \end{pmatrix} \tag{B.3}$$

$$= \frac{1}{2} \begin{pmatrix} G^{--} - G^{-+} - (G^{+-} - G^{++}) & G^{--} + G^{-+} - (G^{+-} + G^{++}) \\ G^{--} - G^{-+} + G^{+-} - G^{++} & G^{--} + G^{-+} + G^{+-} + G^{++} \end{pmatrix} \tag{B.4}$$

$$= \begin{pmatrix} 0 & G^{A} \\ G^{R} & G^{K} \end{pmatrix}, \tag{B.5}$$

where we defined the retarded, advanced and Keldysh Green's functions

$$\begin{aligned} G^{R} &= G^{+-} - G^{++} = G^{--} - G^{-+}, \\ G^{A} &= G^{-+} - G^{++} = G^{--} - G^{+-}, \\ G^{K} &= G^{--} + G^{++} = G^{-+} + G^{+-}, \end{aligned} \tag{B.6}$$

fulfilling the relation

$$G^{-+} - G^{+-} = G^{A} - G^{R}. \tag{B.7}$$

Thus, we can reformulate the Dyson equation in the form $\hat{G} = \hat{G}_0 + \hat{G}_0\hat{\sigma}_3\hat{\Sigma}\hat{\sigma}_3\hat{G}$ by applying the L and $L^\dagger$ operators, resulting in

$$L\hat{G}L^\dagger = L\hat{G}_0L^\dagger + L\hat{G}_0L^\dagger L\hat{\sigma}_3\hat{\Sigma}\hat{\sigma}_3L^\dagger L\hat{G}L^\dagger, \tag{B.8}$$

so that we arrive at the following Dyson equation in triagonal representation

$$\tilde{G} = \tilde{G}_0 + \tilde{G}_0\tilde{\Sigma}\tilde{G}, \tag{B.9}$$

where[1]

$$\tilde{\Sigma} = L\hat{\sigma}_3\hat{\Sigma}\hat{\sigma}_3L^\dagger \tag{B.11}$$

$$= \frac{1}{\sqrt{2}}\begin{pmatrix}1 & 1\\ 1 & -1\end{pmatrix}\begin{pmatrix}\Sigma^{--} & \Sigma^{-+}\\ \Sigma^{+-} & \Sigma^{++}\end{pmatrix}\frac{1}{\sqrt{2}}\begin{pmatrix}1 & 1\\ 1 & -1\end{pmatrix} \tag{B.12}$$

$$= \frac{1}{2}\begin{pmatrix}1 & 1\\ 1 & -1\end{pmatrix}\begin{pmatrix}\Sigma^{--}+\Sigma^{-+} & \Sigma^{--}-\Sigma^{-+}\\ \Sigma^{+-}+\Sigma^{++} & \Sigma^{+-}-\Sigma^{++}\end{pmatrix} \tag{B.13}$$

$$= \frac{1}{2}\begin{pmatrix}\Sigma^{--}+\Sigma^{-+}+\Sigma^{+-}+\Sigma^{++} & \Sigma^{--}-\Sigma^{-+}+\Sigma^{+-}-\Sigma^{++}\\ \Sigma^{--}+\Sigma^{-+}-(\Sigma^{+-}+\Sigma^{++}) & \Sigma^{--}-\Sigma^{-+}-(\Sigma^{+-}-\Sigma^{++})\end{pmatrix} \tag{B.14}$$

$$= \begin{pmatrix}\Sigma^K & \Sigma^R\\ \Sigma^A & 0\end{pmatrix}, \tag{B.15}$$

where we have used the definitions of retarded, advanced and Keldysh self-energies

$$\begin{aligned}\Sigma^R &= \Sigma^{+-} - \Sigma^{++} = \Sigma^{--} - \Sigma^{-+},\\ \Sigma^A &= \Sigma^{-+} - \Sigma^{++} = \Sigma^{--} - \Sigma^{+-},\\ \Sigma^K &= \Sigma^{--} + \Sigma^{++} = \Sigma^{-+} + \Sigma^{+-},\end{aligned} \tag{B.16}$$

implying the relation

$$\Sigma^{-+} - \Sigma^{+-} = \Sigma^A - \Sigma^R. \tag{B.17}$$

To sum up, we can now write the Dyson equation in RAK notation,

$$\tilde{G} = \tilde{G}_0 + \tilde{G}_0\tilde{\Sigma}\tilde{G} \tag{B.18}$$

$$= \begin{pmatrix}0 & G_0^A\\ G_0^R & G_0^K\end{pmatrix} + \begin{pmatrix}0 & G_0^A\\ G_0^R & G_0^K\end{pmatrix}\begin{pmatrix}\Sigma^K & \Sigma^R\\ \Sigma^A & 0\end{pmatrix}\begin{pmatrix}0 & G^A\\ G^R & G^K\end{pmatrix} \tag{B.19}$$

$$= \begin{pmatrix}0 & G_0^A\\ G_0^R & G_0^K\end{pmatrix} + \begin{pmatrix}0 & G_0^A\Sigma^AG^A\\ G_0^R\Sigma^RG^R & G_0^R\Sigma^KG^A + G_0^R\Sigma^RG^K + G_0^K\Sigma^AG^A\end{pmatrix}. \tag{B.20}$$

[1]Explicitly, we have

$$L\hat{\sigma}_3 = \frac{1}{\sqrt{2}}\begin{pmatrix}1 & -1\\ 1 & 1\end{pmatrix}\begin{pmatrix}1 & 0\\ 0 & -1\end{pmatrix} = \frac{1}{\sqrt{2}}\begin{pmatrix}1 & 1\\ 1 & -1\end{pmatrix} = (L\hat{\sigma}_3)^\dagger = \hat{\sigma}_3L^\dagger \tag{B.10}$$

Thus, we can easily read off the following relations

$$G^R = G_0^R + G_0^R \Sigma^R G^R, \tag{B.21}$$

$$G^A = G_0^A + G_0^A \Sigma^A G^A, \tag{B.22}$$

$$G^K = G_0^K + G_0^R \Sigma^K G^A + G_0^R \Sigma^R G^K + G_0^K \Sigma^A G^A, \tag{B.23}$$

which are solved for our specific problems.

Appendix C

Exact analytical expression for transient current noise in the RLM: Zero temperature case

Below, we give an exact expression for the transient noise in the RLM at zero temperature for an initially unoccupied dot. The first part involves single integrals on the non-compact supports $[-\infty, \pm V/2]$ and reads

$$S_1(\Omega, T) = \sum_{\sigma=\pm} \int_{-\infty}^{\sigma V/2} d\omega \left(\frac{s_{1,1}(\omega, \Omega, T)}{(\omega - \Delta + \Omega)^2 + \Gamma^2} + \sum_{i=2}^{3} \frac{s_{1,i}(\omega, \Omega, T)}{(\omega - \Delta)^2 + \Gamma^2} \right) \tag{C.1}$$

with

$$\begin{aligned}
s_{1,1} &= \frac{\Gamma}{4\pi} \left(\Gamma - \mathrm{e}^{-\Gamma T} \Gamma \cos\left[(\Delta - \omega - \Omega)T\right] + e^{-\Gamma T} (\Delta - \omega - \Omega) \sin\left[(\Delta - \omega - \Omega)T\right] \right), \\
s_{1,2} &= \frac{\Gamma^2}{8\pi^2} \sum_{p,q=\pm} q \cdot \left(\mathrm{Si}\left[(pV/2 + q\omega - \Omega)T\right] + \mathrm{Si}\left[(pV/2 + q\Delta - \Omega)T\right] \mathrm{e}^{-\Gamma T} \right), \\
s_{1,3} &= \frac{\Gamma^2}{8\pi^2} \sum_{p,q,s=\pm} q \cdot \mathrm{Si}\left[\left((pV - q(\omega + \Delta) - 2\Omega) + \mathrm{i}qs\Gamma\right) T/2\right] \mathrm{e}^{(\mathrm{i}s(\omega - \Delta) - \Gamma)T/2}.
\end{aligned} \tag{C.2}$$

The second part consisting of double integrals, both on the compact support $[-V/2, +V/2]$, is given by

$$S_2(\Omega, T) = \sum_{\sigma=\pm} \int_{-V/2}^{V/2} d\omega \int_{-V/2}^{V/2} d\omega' \sum_{i=1}^{4} \frac{\Gamma^2}{4\pi^2} \frac{s_{2,i}(\omega, \omega', \Omega, T)}{\left[(\omega - \Delta)^2 + \Gamma^2\right] \left[(\omega' - \Delta)^2 + \Gamma^2\right]} \tag{C.3}$$

with

$$
\begin{aligned}
s_{2,1} &= \left[(\omega-\Delta)(\omega'-\Delta)-\Gamma^2\right] T\,\mathrm{sinc}\left[(\omega'-\omega-\Omega)T\right], \\
s_{2,2} &= \left[(\omega-\Delta)(\omega'-\Delta)-\Gamma^2\right] \mathrm{e}^{-\Gamma T}\cos\left[(\omega+\omega'-2\Delta)T/2\right] T\,\mathrm{sinc}\left[(\omega'-\omega-2\Omega)T/2\right], \\
s_{2,3} &= (\omega+\omega'-2\Delta)\Gamma\,\mathrm{e}^{-\Gamma T}\sin\left[(\omega+\omega'-2\Delta)T/2\right] T\,\mathrm{sinc}\left[(\omega'-\omega-2\Omega)T/2\right], \\
s_{2,4} &= \mathrm{Re}\left[\frac{(\omega-\Delta)(\omega'-\Delta)+\mathrm{i}\Gamma(\omega-\Delta)(\omega'-\Delta)-\Gamma^2}{\mathrm{i}(2\omega-\omega'+\Delta-2\Omega\sigma)+\Gamma}\left(\mathrm{e}^{(\mathrm{i}(\Delta-\omega+\sigma\Omega)-\Gamma)T}-\mathrm{e}^{\mathrm{i}(\omega-\omega'-\sigma\Omega)T}\right)\right].
\end{aligned}
\tag{C.4}
$$

This result is taken to generate the plots shown in this section.

Appendix D

Exact analytical expression for transient current noise in the RLM: Finite temperature case

In the case of finite temperature, the caclculation is much more involved. We begin with the analog contribution to S_1 in case of zero temperature. It splits into two parts, one, where all integrals are performed,

$$S_{1,1} = \frac{\Gamma}{8\pi}\frac{1}{4\beta\Gamma}\sum_{\sigma}\Bigg\{4\mathrm{i}\pi\left[\mathfrak{B}_1\left(z,x_{1\sigma}\right)-\mathfrak{B}_1\left(z,-\bar{x}_{1\sigma}\right)\right]+4\mathrm{i}\pi\mathrm{e}^{-2\Gamma T}\left[\mathfrak{B}_1\left(z,-x_{1\sigma}\right)-\mathfrak{B}_1\left(z,\bar{x}_{1\sigma}\right)\right]$$

$$+\left(2\mathrm{i}\pi-x_{1\sigma}\right)\left[\mathfrak{B}_0\left(z,-\bar{x}_{1\sigma}\right)-\mathrm{e}^{-2\Gamma T}\mathfrak{B}_0\left(z,-x_{1\sigma}\right)\right]-\left(2\mathrm{i}\pi+\bar{x}_{1\sigma}\right)\left[\mathfrak{B}_0\left(z,x_{1\sigma}\right)-\mathrm{e}^{-2\Gamma T}\mathfrak{B}_0\left(z,\bar{x}_{1\sigma}\right)\right]$$

$$+4\beta\Gamma\left[\pi-\mathrm{i}\psi\left(\frac{1}{2}+\frac{\mathrm{i}x_{1\sigma}}{4\pi}\right)+\mathrm{i}\psi\left(\frac{1}{2}-\frac{\mathrm{i}\bar{x}_{1\sigma}}{4\pi}\right)\right]\Bigg\}, \tag{D.1}$$

and a second one where one frequency integration is left over,

$$S_{1,2} = -\frac{\Gamma^2}{4}\sum_{\sigma,\tau=\pm}\sigma\int\frac{d\omega}{\left(2\pi\right)^2}\frac{n_{\mathrm{L}}\left(\omega\right)+n_{\mathrm{R}}\left(\omega\right)}{\left(\omega-\Delta\right)^2+\Gamma^2}\Bigg\{2\pi n_{\mathrm{S}}\left(\frac{x_{2\sigma\tau}}{2}\right)$$

$$+\mathrm{i}\mathfrak{B}_0\left(z,-x_{2\sigma\tau}\right)-\mathrm{i}\mathfrak{B}_0\left(z,x_{2\sigma\tau}\right)+\mathrm{e}^{-\Gamma T}\left[2\pi n_{\mathrm{S}}\left(\frac{x_{3\sigma\tau}}{2}\right)+\mathrm{i}\mathfrak{B}_0\left(z,-x_{3\sigma\tau}\right)-\mathrm{i}\mathfrak{B}_0\left(z,x_{3\sigma\tau}\right)\right]$$

$$-\mathrm{e}^{-\Gamma T/2}\mathrm{e}^{-\mathrm{i}T(\omega-\Delta)/2}\left[2\pi n_{\mathrm{S}}\left(\frac{x_{4\sigma\tau}}{2}\right)+\mathrm{i}\mathfrak{B}_0\left(z,-x_{4\sigma\tau}\right)-\mathrm{i}\mathfrak{B}_0\left(z,x_{4\sigma\tau}\right)\right] \tag{D.2}$$

$$-\mathrm{e}^{-\Gamma T/2}\mathrm{e}^{\mathrm{i}T(\omega-\Delta)/2}\left[2\pi n_{\mathrm{S}}\left(\frac{\bar{x}_{4\sigma\tau}}{2}\right)+\mathrm{i}\mathfrak{B}_0\left(z,-\bar{x}_{4\sigma\tau}\right)-\mathrm{i}\mathfrak{B}_0\left(z,\bar{x}_{4\sigma\tau}\right)\right]\Bigg\}.$$

$\mathfrak{B}_i\left(z,a\right)=B_z\left(\frac{1}{2}+\frac{\mathrm{i}a}{4\pi},-i\right)$ with B denoting the incomplete Beta function (Abramowitz and Stegun [1964]), $x_{1\sigma}=\beta\left(\sigma V-2\left(\Delta+\Omega\right)-2\mathrm{i}\Gamma\right)$, $x_{2\sigma\tau}=\beta\left(\tau V-2\Omega-2\sigma\omega\right)$, $x_{3\sigma\tau}=\beta\left(\tau V-2\Omega-2\sigma\Delta\right)$,

$x_{4\sigma\tau} = \beta(\tau V - 2\Omega - \sigma\omega - \sigma\Delta - \mathrm{i}\sigma\Gamma)$, and $z = \mathrm{e}^{-2\pi T/\beta}$. $n_{\mathrm{S}}(x) = n_{\mathrm{F}}(-x/\beta)$ is the Sigmoid function (Abramowitz and Stegun [1964]). The analog contribution to S_2 is given by

$$\begin{aligned}
S_2 = -\frac{\Gamma^2}{4}\mathrm{Re}\sum_{\sigma,\tau=\pm}\tau\int\frac{d\omega}{(2\pi)^2}\frac{n_{\mathrm{L}}(\omega)-n_{\mathrm{R}}(\omega)}{\mathrm{i}(\omega-\Delta)+\Gamma}\Bigg\{\frac{\beta}{y_{1\sigma\tau}-y'_{1,\tau}}\Big[\mathfrak{B}_0(z,y_{1\sigma\tau})-\mathfrak{B}_0(z,-y_{1\sigma\tau})\\
-\mathrm{e}^{\frac{-\mathrm{i}(y_{1\sigma\tau}-y_\tau)T}{2\beta}}\mathfrak{B}_0(z,y_\tau)+\mathrm{e}^{\frac{\mathrm{i}(y_{1\sigma\tau}-y_\tau)T}{2\beta}}\mathfrak{B}_0(z,-y_\tau)+2\mathrm{i}\pi n_{\mathrm{S}}\left(\frac{y_{1\tau}}{2}\right)-2\mathrm{i}\pi n_{\mathrm{S}}\left(\frac{y_\tau}{2}\right)\mathrm{e}^{\frac{\mathrm{i}(y_{1\sigma\tau}-y_\tau)T}{2\beta}}\Big]\\
-\frac{2\beta\mathrm{e}^{\mathrm{i}\sigma\Omega T}}{y_{2\sigma\tau}-y_\tau}\Big[\mathfrak{B}_0(z,y_\tau)-\mathrm{e}^{\frac{\mathrm{i}T(y_{2\sigma\tau}-y_\tau)}{2\beta}}\left(\mathfrak{B}_0(z,y_{2\sigma\tau})+\psi\left(\frac{1}{2}+\frac{\mathrm{i}y_{2\sigma\tau}}{4\pi}\right)-\psi\left(\frac{1}{2}+\frac{\mathrm{i}y_\tau}{4\pi}\right)\right)\Big]\\
-\frac{2\beta\mathrm{e}^{\mathrm{i}\sigma\Omega T}}{y_{3\sigma\tau}-y_\tau}\Big[\mathrm{e}^{\frac{\mathrm{i}(y_{3\sigma\tau}-y_\tau)T}{2\beta}}\left(\mathfrak{B}_0(z,y_{3\sigma\tau})+\mathfrak{B}_0(z,-y_{3\sigma\tau})-2\mathrm{i}\pi n_{\mathrm{S}}\left(\frac{y_{3\sigma\tau}}{2}\right)\right)\\
-\mathfrak{B}_0(z,y_\tau)+\mathrm{e}^{\frac{\mathrm{i}(y_{3\sigma\tau}-y_\tau)T}{\beta}}\left(-\mathfrak{B}_0(z,-y_\tau)+2\mathrm{i}\pi n_{\mathrm{S}}\left(\frac{y_\tau}{2}\right)\right)\Big]\Bigg\}
\end{aligned} \tag{D.3}$$

where $y_\tau = \beta(\tau V - 2\Delta - 2\mathrm{i}\Gamma)$, $y_{1\sigma\tau} = \beta(\tau V - 2\omega - 2\sigma\Omega)$, $y_{2\sigma\tau} = \beta(\tau V - 2\omega - 4\sigma\Omega)$ and $y_{3\sigma\tau} = \beta(\tau V - \omega - \Delta - 2\sigma\Omega - \mathrm{i}\Gamma)$. To find the decay law of the noise correlation with time, one has to investigate term by term. First, we notice that all the remaining integrals are convergent even without the Beta functions (all the Beta functions are at most constant or decaying as a function of ω). This is because of the overall Lorentzian-like prefactors. To estimate the asymptotics due to the Beta functions, the following power series representations turn out to be extremely useful ($|z| < 1$),

$$B_z(a,b) = z^a\sum_{n=0}^{\infty}\frac{(1-b)_n}{n!\,(a+n)}z^n \tag{D.4}$$

where $(x)_n = \Gamma(x+n)/\Gamma(x)$ is the Pochhammer symbol. In our case, we only need $(1)_n = n!$ in the case of $x = 0$ and $(2)_n = (n+1)!$ in the case of $x = -1$. We introduce the following notation $z' = \beta(\eta_\omega + \mathrm{i}\xi\Gamma)$ where η_ω is a real function of ω and ξ is a real constant. With g_ω we denote an arbitrary complex function of the variable ω. Then one obtains

$$\begin{aligned}
g_\omega B_z\left(\frac{1}{2}+\frac{\mathrm{i}z'}{4\pi},0\right) &= g_\omega\mathrm{e}^{-\pi T/\beta}\mathrm{e}^{\frac{\xi\Gamma T}{2}}\mathrm{e}^{\frac{-\mathrm{i}\eta_\omega T}{2}}\sum_{n=0}^{\infty}\frac{\mathrm{e}^{-2\pi nT/\beta}}{1/2+n-\xi\Gamma\beta/(4\pi)+\mathrm{i}\eta_\omega\beta/(4\pi)}\\
&= g_\omega\mathrm{e}^{-\pi T/\beta}\mathrm{e}^{\frac{\xi\Gamma T}{2}}\mathrm{e}^{\frac{-\mathrm{i}\eta_\omega T}{2}}\sum_{n=0}^{\infty}\frac{1/2+n-\xi\Gamma\beta/(4\pi)-\mathrm{i}\eta_\omega\beta/(4\pi)}{(1/2+n-\xi\Gamma\beta/(4\pi))^2+(\eta_\omega\beta/(4\pi))^2}\mathrm{e}^{-2\pi nT/\beta}\\
&= g_\omega\mathrm{e}^{-\pi T/\beta}\mathrm{e}^{\frac{\xi\Gamma T}{2}}\mathrm{e}^{\frac{-\mathrm{i}\eta_\omega T}{2}}\sum_{n=0}^{\infty}(a_n+\mathrm{i}b_n)\,\mathrm{e}^{-2\pi nT/\beta}.
\end{aligned} \tag{D.5}$$

Now, it is crucial that for every β there exists a positive integer N_β so that the modulus of the real part a_n or the imaginary parts b_n is majorized by 1 for $n \geq N_\beta$. Hence, the real or imaginary part of the whole expression can be estimated by a combination of finite polynomial $p_{N_\beta}\left(\mathrm{e}^{-2\pi T/\beta}\right)$ and $\mathrm{e}^{-2\pi N_\beta T/\beta}/\left(1-\mathrm{e}^{-2\pi T/\beta}\right)$. It is important to notice that the prefactor $\mathrm{e}^{\xi\Gamma T/2}$ does not lead to an exponential increase in any case. The function g_ω always suppresses this tendency. Although our result is valid for arbitrary temperature, we emphasize that the zero temperature limit (i.e., $\beta \to \infty$) is far from being trivial.

Appendix E

Exact analytical expression for transient current noise in the MRLM: Zero temperature case

We provide the result for $\Delta \neq \Gamma/2$ in the zero temperature case. Here, $\kappa = \pm$ specifies the initially occupied/empty dot. As mentioned above, there are two main contributions given on the following pages.

$$S_1(\Omega,T) = \sum_{i=1}^{2} s_{1,i}(\Omega,T) + \sum_{\sigma=\pm}\int_{\sigma V}^{\infty} d\omega s_{1,3}(\omega,\Omega,T) + \sum_{\sigma=\pm}\int_{-\infty}^{\sigma V} d\omega \sum_{i=4}^{7} s_{1,i}(\omega,\Omega,T) \tag{E.1}$$

with

$$s_{1,1} = \frac{\Gamma^3}{32\Omega'^2\pi}\sum_{m,n=\pm}\frac{(\Omega'+n\Gamma/2)^2 \mathrm{e}^{(-n\Omega'-\Gamma/2)T}}{(\Omega'+n\Gamma/2)^2+\Delta^2}\left(\frac{\pi}{2}+\mathrm{Si}\left[(\Omega+mV)T\right]\right),$$

$$s_{1,2} = \frac{\Gamma^3}{32\Omega'^2\pi}\sum_{m,n=\pm}\frac{\Delta^2 \mathrm{e}^{-\Gamma T/2}}{-2\Delta^2+2\mathrm{i}\kappa\Delta n\Omega'}\left(\frac{\pi}{2}+\mathrm{Si}\left[((\Omega+mV)+\mathrm{i}n\Omega')\,T\right]\right),$$

$$s_{1,3} = \frac{\Gamma}{16\Omega'\pi}\sum_{m,n=\pm}\frac{(\Omega'-n\Gamma/2)}{\mathrm{i}m(\Omega-\omega)+(n\Omega'-\Gamma/2)}\left(\mathrm{e}^{(\mathrm{i}m(\Omega-\omega)+n\Omega'-\Gamma/2)T}-1\right), \tag{E.2}$$

$$s_{1,4} = \frac{\Gamma^2}{32\Omega'^2\pi^2}\sum_{m,n=\pm}\frac{-(\Omega'+n\Gamma/2)^2 \mathrm{e}^{(-n\Omega'-\Gamma/2)T}}{(\Omega'+n\Gamma/2)^2+\omega^2}\left(\frac{\pi}{2}+\mathrm{Si}\left[(\Omega+mV)T\right]\right),$$

$$s_{1,5} = \frac{\Gamma^2}{8\pi^2}\sum_{m=\pm}\frac{\omega^2}{(\omega^2+\Delta^2)^2+\omega^2(\Gamma^2-4\Delta^2)}\left(\mathrm{Si}\left[(\omega-mV-\Omega)T\right]-\frac{\pi}{2}\right),$$

$$s_{1,6} = \frac{\Gamma^2}{32\Omega'^2\pi^2} \sum_{k,m,n,p=\pm} \frac{m(\Omega' + n\Gamma/2)(m\Omega' + n\Gamma/2)}{[\Omega' + n\,(\Gamma/2 - \mathrm{i}k\omega)]\,[m\Omega' + n\,(\Gamma/2 + \mathrm{i}k\omega)]} \mathrm{e}^{(\mathrm{i}k\omega - n\Omega' - \Gamma/2)T/2}$$

$$\times \left(\frac{\pi}{2} + \mathrm{Si}\left[((2\Omega + pV - \omega) + \mathrm{i}k\,(n\Omega' + \Gamma/2))\,T/2 \right] \right),$$

$$s_{1,7} = \frac{\Gamma^2}{32\Omega'^2\pi^2} \sum_{m,n=\pm} \frac{(\Omega' - \Gamma/2)(\Omega' + \Gamma/2)\mathrm{e}^{-\Gamma T/2}}{[\Omega' - n\,(\Gamma/2 - \mathrm{i}\omega)]\,[\Omega' + n\,(\Gamma/2 + \mathrm{i}\omega)]} \left(\frac{\pi}{2} + \mathrm{Si}\left[((\Omega + mV) - \mathrm{i}n\Omega')\,T \right] \right), \tag{E.3}$$

and

$$S_2(\Omega, T) = -\frac{\Gamma^2}{64\Omega'^2\pi^2} \sum_{\sigma=\pm} \int_{-V}^{+V} d\omega \int_{-V}^{+V} d\omega' \sum_{i=1}^{4} s_{2,i}(\omega, \omega', \Omega, T) \tag{E.4}$$

with

$$s_{2,1} = \sum_{k,m=\pm} \frac{(k\Omega' + \Gamma/2)(m\Omega' + \Gamma/2)}{[\Omega' + k\,(\Gamma/2 - \mathrm{i}\omega)]\,[\Omega' + m\,(\Gamma/2 + \mathrm{i}\omega')]} 2T\mathrm{sinc}\left[(\Omega - \omega - \omega')T \right],$$

$$s_{2,2} = \sum_{k,m,n=\pm} \frac{-m\,(\Omega' + n\Gamma/2)\,(m\Omega' + n\Gamma/2)}{[\Omega' + n\,(\Gamma/2 - \mathrm{i}k\omega)]\,[m\Omega' + n\,(\Gamma/2 + \mathrm{i}k\omega')]} \mathrm{e}^{(\mathrm{i}k\omega - n\Omega' - \Gamma/2)T/2}$$

$$\times 2T\mathrm{sinc}\left[((2\Omega - 2\omega' - \omega) + \mathrm{i}k\,(n\Omega' + \Gamma/2))\,T/2 \right],$$

$$s_{2,3} = \sum_{m=\pm} \frac{(\Omega' + m\Gamma/2)^2}{[\Omega' + m\,(\Gamma/2 - \mathrm{i}\omega)]\,[\Omega' + m\,(\Gamma/2 + \mathrm{i}\omega')]} \mathrm{e}^{(\mathrm{i}(\omega - \omega') - 2m\Omega' - \Gamma)T/2} \tag{E.5}$$

$$\times 2T\mathrm{sinc}\left[(2\Omega - \omega' - \omega)T/2 \right],$$

$$s_{2,4} = \sum_{m=\pm} \frac{-(\Omega' + \Gamma/2)(\Omega' - \Gamma/2)}{[\Omega' + m\,(\Gamma/2 - \mathrm{i}\omega)]\,[\Omega' - m\,(\Gamma/2 + \mathrm{i}\omega')]} \mathrm{e}^{(\mathrm{i}(\omega - \omega') - \Gamma)T/2}$$

$$\times 2T\mathrm{sinc}\left[(2\Omega - \omega - \omega' + \mathrm{i}2m\Omega')\,T/2 \right].$$

This result is taken to generate the plots shown in this section.

Appendix F

Zero-frequency steady state current noise in the RLM from FCS formalism

To check our calculation of the steady state current noise spectrum, we compare its zero-frequency limit, which is nothing else than the second cumulant of the probability distribution, with the result obtained from Full Counting Statistics (FCS). The cumulant generating function (CGF) of the two-terminal resonant level model reads (de Jong [1996], Gogolin and Komnik [2006])

$$\ln \chi_0(\lambda) = T_m \int \frac{d\omega}{2\pi} \ln \left\{ 1 + \mathcal{T}(\omega) \left[n_L(1-n_R)(\mathrm{e}^{\mathrm{i}\lambda} - 1) + n_R(1-n_L)(\mathrm{e}^{-\mathrm{i}\lambda} - 1) \right] \right\} \tag{F.1}$$

with T_m being the measuring time in that section and the transmission function $\mathcal{T}(\omega)$ of the constriction which is given by a Lorentzian function,

$$\mathcal{T}(\omega) = \frac{\Gamma^2}{(\omega - \Delta)^2 + \Gamma^2}. \tag{F.2}$$

As indicated in the main text, we neglect the spin degrees of freedom. We obtain the cumulants by successively differentiating this function with respect to λ and setting $\lambda = 0$ in the end. The first cumulant which corresponds to the mean value of the probability distribution is obtained as

$$\langle\langle I \rangle\rangle = \langle I \rangle = \frac{(-\mathrm{i})}{T_m} \frac{\partial \ln \chi_0(\lambda)}{\partial \lambda}\bigg|_{\lambda=0}. \tag{F.3}$$

The second cumulant which corresponds to the variance of the probability distribution is then

$$\left\langle\left\langle I^2 \right\rangle\right\rangle = \left\langle I^2 \right\rangle - \langle I \rangle^2 = \frac{(-\mathrm{i})^2}{T_m} \frac{\partial^2 \ln \chi_0(\lambda)}{\partial \lambda^2}\bigg|_{\lambda=0}. \tag{F.4}$$

The derivatives are

$$\frac{\partial \ln \chi_0(\lambda)}{\partial \lambda} = T_m \int \frac{d\omega}{2\pi} \frac{\mathcal{T}(\omega) \left[n_L(1-n_R)\mathrm{i}\mathrm{e}^{\mathrm{i}\lambda} + n_R(1-n_L)(-\mathrm{i})\mathrm{e}^{-\mathrm{i}\lambda} \right]}{1 + \mathcal{T}(\omega) \left[n_L(1-n_R)(\mathrm{e}^{\mathrm{i}\lambda} - 1) + n_R(1-n_L)(\mathrm{e}^{-\mathrm{i}\lambda} - 1) \right]}, \tag{F.5}$$

$$\frac{\partial^2 \ln \chi_0(\lambda)}{\partial \lambda^2} = T_m \int \frac{d\omega}{2\pi} \Bigg\{ - \frac{\mathcal{T}(\omega) \left[n_L(1-n_R) \mathrm{e}^{\mathrm{i}\lambda} + n_R(1-n_L) \mathrm{e}^{-\mathrm{i}\lambda} \right]}{1 + \mathcal{T}(\omega) \left[n_L(1-n_R)(\mathrm{e}^{\mathrm{i}\lambda}-1) + n_R(1-n_L)(\mathrm{e}^{-\mathrm{i}\lambda}-1) \right]} + (-1) \frac{\left(\mathcal{T}(\omega) \left[n_L(1-n_R) \mathrm{i}\mathrm{e}^{\mathrm{i}\lambda} + n_R(1-n_L)(-\mathrm{i})\mathrm{e}^{-\mathrm{i}\lambda} \right] \right)^2}{\left(1 + \mathcal{T}(\omega) \left[n_L(1-n_R) \left(\mathrm{e}^{\mathrm{i}\lambda} - 1 \right) + n_R(1-n_L)(\mathrm{e}^{-\mathrm{i}\lambda}-1) \right] \right)^2} \Bigg\}. \tag{F.6}$$

In the next step, we set $\lambda = 0$

$$\left. \frac{\partial^2 \ln \chi_0(\lambda)}{\partial \lambda^2} \right|_{\lambda=0} = T_m \int \frac{d\omega}{2\pi} \Big\{ - \mathcal{T}(\omega) \left[n_L(1-n_R) + n_R(1-n_L) \right] + \mathcal{T}^2(\omega) \left[n_L(1-n_R) - n_R(1-n_L) \right]^2 \Big\}. \tag{F.7}$$

We finally arrive at the compact formula

$$\begin{aligned} \left\langle\left\langle I^2 \right\rangle\right\rangle = \left\langle I^2 \right\rangle - \left\langle I \right\rangle^2 &= \frac{(-\mathrm{i})^2}{T_m} \left. \frac{\partial^2 \ln \chi_0(\lambda)}{\partial \lambda^2} \right|_{\lambda=0} \\ &= \int \frac{d\omega}{2\pi} \Big\{ \mathcal{T}(\omega) \left[n_L(1-n_R) + n_R(1-n_L) \right] - \mathcal{T}^2(\omega) \left[n_L(1-n_R) - n_R(1-n_L) \right]^2 \Big\} \\ &= \int \frac{d\omega}{2\pi} \Big\{ \mathcal{T}(\omega) \left[n_L(1-n_L) + n_R(1-n_R) \right] + \mathcal{T}(\omega) \left[1 - \mathcal{T}(\omega) \right] \left[n_L(\omega) - n_R(\omega) \right]^2 \Big\}. \end{aligned} \tag{F.8}$$

It can be directly verified that this result is identical to $\lim_{\Omega \to 0} S^{\mathrm{stat}}(\Omega)$ of Eq. (3.29). The last line of Eq. (F.8) is easily interpretable. The first summand is the Johnson-Nyquist contribution absent at zero temperature, whereas the second summand corresponds to shot noise that disappears if the temperatures and chemical potentials are equal in both leads. Specializing to vanishing temperatures $\Theta_L = \Theta_R = 0$, we can set $n_R^2 = n_R$, $n_L^2 = n_L$ and $n_L n_R = n_R$, provided that the left lead is at a higher chemical potential compared to the right one. We then immediately get the expected zero temperature shot noise result

$$S(\Omega = 0, \Theta_L = \Theta_R = 0) = \int_{-V/2}^{V/2} \frac{d\omega}{2\pi} \, \mathcal{T}(\omega) \left[1 - \mathcal{T}(\omega) \right]. \tag{F.9}$$

Bibliography

M. Abramowitz and I. A. Stegun. *Handbook of Mathematical Functions with Formulas, Graphs, and Mathematical Tables*. Dover, New York, 1964.

S. Andergassen, M. Pletyukhov, D. Schuricht, H. Schoeller, and L. Borda. Renormalization group analysis of the interacting resonant-level model at finite bias: Generic analytic study of static properties and quench dynamics. *Phys. Rev. B*, 83:205103, 2011.

P. W. Anderson. Localized magnetic states in metals. *Phys. Rev.*, 124:41, 1961.

J. Basset, A. Yu. Kasumov, C. P. Moca, G. Zaránd, P. Simon, H. Bouchiat, and R. Deblock. Measurement of Quantum Noise in a Carbon Nanotube Quantum Dot in the Kondo Regime. *Phys. Rev. Lett.*, 108:046802, 2012.

Ya. M. Blanter and M. Büttiker. Shot noise in mesoscopic conductors. *Phys. Rep.*, 336:1, 2000.

M. Bockrath, D. H. Cobden, J. Lu, A. G. Rinzler, R. E. Smalley, L. Balents, and P. L. McEuen. Luttinger-liquid behaviour in carbon nanotubes. *Nature (London)*, 397:598, 1999.

A. Branschädel, E. Boulat, H. Saleur, and P. Schmitteckert. Numerical evaluation of shot noise using real-time simulations. *Phys. Rev. B*, 82:205414, 2010.

C. Caroli, R. Combescot, P. Nozières, and D. Saint-James. Direct calculation of the tunneling current. *J. Phys. C*, 4:916, 1971.

S. T. Carr, D. A. Bagrets, and P. Schmitteckert. Full counting statistics in the self-dual interacting resonant level model. *Phys. Rev. Lett.*, 107:206801, 2011.

A. Crépieux, F. Šimkovic, B. Cambon, and F. Michelini. Enhanced thermopower under a time-dependent gate voltage. *Phys. Rev. B*, 83:153417, 2011.

S. M. Cronenwett, T. H. Oosterkamp, and L. P. Kouwenhoven. A tunable Kondo effect in quantum dots. *Science*, 281:540, 1998.

M. J. M. de Jong. Distribution of transmitted charge through a double-barrier junction. *Phys. Rev. B*, 54:8144–8149, 1996.

R. de Picciotto, M. Reznikov, M. Heiblum, V. Umansky, G. Bunin, and D. Mahalu. Direct observation of a fractional charge. *Nature (London)*, 389:162, 1997.

R. Egger and A. O. Gogolin. Effective low-energy theory for correlated carbon nanotubes. *Phys. Rev. Lett.*, 79:5082–5085, 1997.

V. J. Emery and S. Kivelson. Mapping of the two-channel Kondo problem to a resonant-level model. *Phys. Rev. B*, 46:10812, 1992.

Z. Feng, J. Maciejko, J. Wang, and H. Guo. Current fluctuations in the transient regime: An exact formulation for mesoscopic systems. *Phys. Rev. B*, 77:075302, 2008.

L. I. Glazman. Mesoscopic fluctuations of co-tunneling and Kondo effect in quantum dots. In I. O. Kulik and R. Ellialtioglu, editors, *Quantum Mesoscopic Phenomena and Mesoscopic Devices in Microelectronics*, NATO ASI, Dordrecht, The Netherlands, 2000. Kluwer.

A. O. Gogolin and A. Komnik. Towards full counting statistics for the anderson impurity model. *Phys. Rev. B*, 73:195301, 2006.

A. O. Gogolin, A. A. Nersesyan, and A. M. Tsvelik. *Bosonization and Strongly Correlated Systems*. Cambridge University Press, Cambridge, 1998.

D. Goldhaber-Gordon, H. Shtrikman, D. Mahalu, D. Abusch-Magder, U. Meirav, and M. A. Kastner. Kondo effect in a single-electron transistor. *Nature (London)*, 391:156, 1998.

I. Gradshteyn and I. Ryzhik. *Table of Integrals, Series and Products*. Academic Press, New York, 1975.

S. Gustavsson, R. Leturcq, B. Simovič, R. Schleser, T. Ihn, P. Studerus, K. Ensslin, D. C. Driscoll, and A. C. Gossard. Counting statistics of single electron transport in a quantum dot. *Phys. Rev. Lett.*, 96:076605, 2006.

N. Hamada, S.-I. Sawada, and A. Oshiyama. New one-dimensional conductors: Graphitic microtubules. *Phys. Rev. Lett.*, 68:1579–1581, 1992.

A.-P. Jauho, N. S. Wingreen, and Y. Meir. Time-dependent transport in interacting and non-interacting resonant-tunneling systems. *Phys. Rev. B*, 50:5528, 1994.

X. Jehl, M. Sanquer, R. Calemczuk, and D. Mailly. Detection of doubled shot noise in short normal-metal/superconductor junctions. *Nature (London)*, 405:50, 2000.

K. Joho, S. Maier, and A. Komnik. Transient noise spectra in resonant tunneling setups: Exactly solvable models. *Phys. Rev. B*, 86:155304, 2012.

V. A. Khlus. Current and voltage fluctuations in microjunctions of normal and superconducting metals. *Sov. Phys. JETP*, 66:1243, 1987.

M. Kindermann and S. Pilgram. Statistics of heat transfer in mesoscopic circuits. *Phys. Rev. B*, 69:155334, 2004.

A. Komnik. Transient dynamics of the nonequilibrium Majorana resonant level model. *Phys. Rev. B*, 79:245102, 2009.

A. Komnik and A. O. Gogolin. Transport, optical properties, and quantum ratchet effects for quantum dots and molecules coupled to Luttinger liquids. *Phys. Rev. B*, 68:235323, 2003a.

A. Komnik and A. O. Gogolin. Resonant Tunneling between Luttinger Liquids: A Solvable Case. *Phys. Rev. Lett.*, 90:246403, 2003b.

J. Kondo. Resistance Minimum in Dilute Magnetic Alloys. *Prog. Theor. Phys.*, 32:37–49, 1964.

D. C. Langreth. Linear and nonlinear response theory with applications. In J. J. Devreese and V. E. van Doren, editors, *Linear and nonlinear electron transport in solids*, volume 17 of *NATO ASI, Series B*. Plenum, New York, 1976.

D. C. Langreth and P. Nordlander. Derivation of a master equation for charge-transfer processes in atom-surface collisions. *Phys. Rev. B*, 43:2541–2557, 1991.

G. B. Lesovik. Excess quantum shot noise in 2D ballistic point contacts. *JETP Lett.*, 49:592, 1989.

L. S. Levitov and G. B. Lesovik. Charge distribution in quantum shot noise. *JETP Lett.*, 58: 230–235, 1993.

L. S. Levitov, H. W. Lee, and G. B. Lesovik. Electron Counting Statistics and Coherent States of Electric Current. *J. Math. Phys.*, 37:4845–4866, 1996.

A. W. W. Ludwig and I. Affleck. Exact conformal-field-theory results on the multi-channel Kondo effect: Asymptotic three-dimensional space- and time-dependent multi-point and many-particle Green's functions. *Nuclear Physics B*, 428(3):545 – 611, 1994.

J. Maciejko, J. Wang, and H. Guo. Time-dependent quantum transport far from equilibrium: An exact nonlinear response theory. *Phys. Rev. B*, 74:085324, 2006.

G. D. Mahan. *Many-Particle Physics*. Plenum, New York, 1990.

Y. Meir and N. S. Wingreen. Landauer formula for the current through an interacting electron region. *Phys. Rev. Lett.*, 68:2512, 1992.

J. W. Mintmire, B. I. Dunlap, G. Dresselhaus, and C. T. White. Are fullerene tubules metallic? *Phys. Rev. Lett.*, 68:631–634, 1992.

L. G. Molinari. Another proof of Gell-Mann and Low's theorem. *J. Math. Phys.*, 48:052113, 2007.

M. Moskalets and M. Büttiker. Time-resolved noise of adiabatic quantum pumps. *Phys. Rev. B*, 75:035315, 2007.

Yu. V. Nazarov. Universalities of weak localization. *Ann. Phys. (Leipzig)*, 8 (SI-193):507, 1999.

T. W. Odom, J.-L. Huang, P. Kim, and C. M. Lieber. Atomic structure and electronic properties of single-walled carbon nanotubes. *Nature (London)*, 391:62, 1998.

C. P. Orth, D. F. Urban, and A. Komnik. Finite-frequency noise properties of the nonequilibrium Anderson impurity model. *Phys. Rev. B*, 86:125324, 2012.

J. Rammer. *Quantum Field Theory of Non-Equilibrium States*. Cambridge University Press, Cambridge, England, 2007.

E. A. Rothstein, O. Entin-Wohlman, and A. Aharony. Noise spectra of a biased quantum dot. *Phys. Rev. B*, 79:075307, 2009.

R. Saito, M. Fujita, G. Dresselhaus, and M. G. Dresselhaus. Electronic structure of chiral graphene tubules. *Appl. Phys. Lett.*, 60:2204–2206, 1992.

L. Saminadayar, D. C. Glattli, Y. Jin, and B. Etienne. Observation of the $e/3$ Fractionally Charged Laughlin Quasiparticle. *Phys. Rev. Lett.*, 79:2526–2529, 1997.

A. Schiller and S. Hershfield. Solution of an ac Kondo model. *Phys. Rev. Lett.*, 77:1821, 1996.

A. Schiller and S. Hershfield. Toulouse limit for the nonequilibrium Kondo impurity: Currents, noise spectra, and magnetic properties. *Phys. Rev. B*, 58:14978, 1998.

T. L. Schmidt, P. Werner, L. Mühlbacher, and A. Komnik. Transient dynamics of the Anderson impurity model out of equilibrium. *Phys. Rev. B*, 78(23):235110, 2008.

S. Schmitt and F. B. Anders. Comparison between scattering-states numerical renormalization group and the Kadanoff-Baym-Keldysh approach to quantum transport: Crossover from weak to strong correlations. *Phys. Rev. B*, 81:165106, 2010.

W. Schottky. Über spontane Stromschwankungen in verschiedenen Elektrizitätsleitern. *Ann. Physik (Lepizig)*, 362:541, 1918.

G. Schulze, K. J. Franke, A. Gagliardi, G. Romano, C. S. Lin, A. L. Rosa, T. A. Niehaus, Th. Frauenheim, A. Di Carlo, A. Pecchia, and J. I. Pascual. Resonant Electron Heating and Molecular Phonon Cooling in Single C_{60} Junctions. *Phys. Rev. Lett.*, 100:136801.

D. Sénéchal. An introduction to bosonization. *arXiv:cond-mat/9908262v1*, 1999.

G. Toulouse. Expression exacte de l'énergie de l'état de base de l'hamiltonien de Kondo pour une valeur particulière de J_z. *C. R. Séances Acad. Sci., Sér. B*, 268:1200, 1969.

N. Ubbelohde, C. Fricke, C. Flindt, F. Hohls, and R. J. Haug. Measurement of finite-frequency current statistics in a single-electron transistor. *Nat. Commun.*, 3:612, 2012.

J. von Delft and H. Schoeller. Bosonization for beginners — refermionization for experts. *Annalen der Physik*, 7(4):225–305, 1998.

J. W. G. Wildöer, L. C. Venema, Andrew G. Rinzler, R. E. Smalley, and C. Dekker. Electronic structure of atomically resolved carbon nanotubes. *Nature (London)*, 391:59, 1998.

N. S. Wingreen, A.-P. Jauho, and Y. Meir. Time-dependent transport through a mesoscopic structure. *Phys. Rev. B*, 48:8487, 1993.

F. Zhan, S. Denisov, and P. Hänggi. Electronic heat transport across a molecular wire: Power spectrum of heat fluctuations. *Phys. Rev. B*, 84:195117, 2011.

Y. Zhu, J. Maciejko, T. Ji, H. Guo, and J. Wang. Time-dependent quantum transport: Direct analysis in the time domain. *Phys. Rev. B*, 71:075317, 2005.

Acknowledgment

At the end of this thesis, there are many people I have to thank. I would like to express my gratitude especially to ...

- Prof. Dr. Andreas Komnik for giving me the opportunity of working in his research group. His human qualities such as his guidance as an advisor, his patience and his constant optimism significantly contributed to the success of this thesis.
- Prof. Dr. Matthias Weidemüller and Dr. Boris Fine for being my co-advisors.
- Prof. Dr. Andreas Mielke for accepting the time-consuming task of assessing this thesis as a second referee.
- Prof. Dr. Rüdiger Klingeler and Prof. Dr. Werner Aeschbach-Hertig for taking part in the examination committee representing the branches of experimental and applied physics, respectively.
- the secretaries Sonja Bartsch, Cornelia Merkel and Melanie Steiert for guaranteeing that everything concering administrative matter goes smoothly.
- my colleagues of the research group Stefan Maier, Henning Soller and David Breyel for making life at the institute such a great time and personal gain. In particular, concerning my thesis, Stefan was a permanent source of inspiration in endless discussions of the subject. Henning's advice especially as proofreader of this thesis proved to be invaluable.
- my parents who constantly support me throughout my life.